

**STUDIES ON THE EVALUATION OF PHOTODYNAMIC EFFICACY
OF CHLOROPHYLL DERIVATIVES IN CANCER CELLS AND
ANIMAL TUMOR MODEL**

By

ARPANA PARIHAR

Enrolment No. -LIFE03200704001

RAJA RAMANNA CENTRE FOR ADVANCED TECHNOLOGY, INDORE

*A thesis submitted to the
Board of Studies in Life Sciences
In partial fulfillment of requirements
For the degree of*

DOCTOR OF PHILOSOPHY

of

HOMI BHABHA NATIONAL INSTITUTE



August, 2013

Homi Bhabha National Institute

Recommendations of the Viva Voce Board

As members of the Viva Voce Board, we certify that we have read the dissertation prepared by Arpana Parihar entitled "Studies on the Evaluation of Photodynamic Efficacy of Chlorophyll Derivatives in Cancer Cells and Animal Tumor Model" and recommend that it may be accepted as fulfilling the dissertation requirement for the Degree of Doctor of Philosophy.



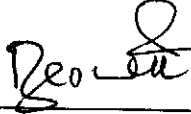
Date: 7/8/14

Chairman- Dr. S. K. Apte



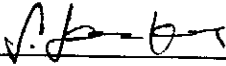
Date: 7/8/14

Guide/ Convener - Dr. Alok Dube



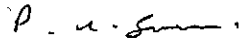
Date: 7/8/14

External Examiner -



Date: 7/8/14

Member 1 - Dr. Santosh S. Kumar

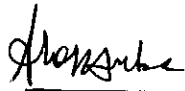


Date: 7/8/14

Co-Guide/Member 2 - Dr. P K Gupta

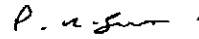
Final approval and acceptance of this dissertation is contingent upon the candidate's submission of the final copies of the dissertation to HBNI.

I hereby certify that I have read this dissertation prepared under my direction and recommend that it may be accepted as fulfilling the dissertation requirement.



Date: 07/8/14

Guide
(Dr Alok Dube)



Co-Guide
(Dr. P K Gupta)

Place: RRAT

STATEMENT BY AUTHOR

This dissertation has been submitted in partial fulfillment of requirements for an advanced degree at Homi Bhabha National Institute (HBNI) and is deposited in the Library to be made available to borrowers under rules of the HBNI.

Brief quotations from this dissertation are allowable without special permission, provided that accurate acknowledgement of source is made. Requests for permission for extended quotation from or reproduction of this manuscript in whole or in part may be granted by the Competent Authority of HBNI when in his or her judgment the proposed use of the material is in the interests of scholarship. In all other instances, however, permission must be obtained from the author.

Arpana
15/08/14
Arpana Parihar

DECLARATION

I, hereby declare that the investigation presented in the thesis has been carried out by me.

The work is original and has not been submitted earlier as a whole or in part for a degree / diploma at this or any other Institution / University.

Arpana
15/08/14
Arpana Parihar

LIST OF PUBLICATIONS

Journals

1. Conjugation of Chlorin p_6 to histamine enhances its cellular uptake and phototoxicity in oral cancer cells. Parihar A, Dube A, Gupta PK. *Cancer Chemothe. Pharmacol.* 2011, 68:359-369.
2. Photodynamic treatment of oral squamous cell carcinoma in hamster cheek pouch model using chlorin p_6 -histamine conjugate. Parihar A, Dube A, Gupta PK. *Photodiagnosis and Photodynamic Therapy*, 2013, 10:79-86.
3. Interaction of chlorin p_6 -histamine conjugate with serum albumin and mouse liver microsomes and its comparison with free chlorin p_6 . Parihar A, Dube A, Gupta PK. Under revision.
4. Characterization of organelle damage induced by photodynamic treatment with chlorin p_6 -histamine conjugate in human oral carcinoma cells by 3D fluorescence microscopy. Parihar A, Dube A, Patel H S, Gupta PK. Under revision.

Conference

1. Evaluation of photodynamic efficacy of Chlorin p_6 -histamine conjugate in oral cancer cell lines. A. Parihar, A. Dube, P.K. Gupta. "National Symposium on Frontiers in Photobiology" (24-26 Aug., 2009) Bhabha Atomic Research Centre, India.
2. Conjugation of Chlorin p_6 to histamine enhances efficacy of photodynamic treatment in human breast cancer cells. A. Parihar, A. Dube and P. K. Gupta. "8th

International Symposium on Photodynamic Therapy and Photodiagnosis in Clinical Practice” (05-09 Oct., 2010) University of Padova, Brixen, Italy.

3. Tumor selectivity and Photodynamic treatment efficacy of chlorin p_6 - histamine conjugate in Hamster cheek pouch tumor model. A. Parihar, A. Dube and P. K. Gupta. “13th IPA World Congress International Photodynamic Association” (10-14 May, 2011) Innsbruck, Austria.

Arpana
15/08/14
Arpana Parihar

DEDICATED

TO

MY

LOVED ONES

ACKNOWLEDGEMENTS

I thank Almighty GOD, whose blessings have made me who I am today. He showered upon me the strength and good health all throughout these years that gave me endurance to successfully complete the PhD work in spite of many challenges faced. With His blessings and kind support, I came across all those who helped me in this endeavor and it's a priceless opportunity for me to thank each and every one who contributed during my PhD work.

I am greatly indebted and would like to express my sincere gratitude to Dr P.K Gupta, Distinguished Scientist and Head, Laser Biomedical Application and Instrumentation Division, Raja Ramanna Centre for Advanced Technology, for giving me an opportunity to work in this eminent research group and for providing the necessary facilities. His constant encouragement and positive support was a source of great motivation for me during the course of my PhD work. Despite of his enormous professional responsibilities, being my co-guide he gave his valuable time and significant suggestions time to time for which I am extremely thankful to him.

I take my great pride and privilege to say undoubtedly, that as a true guide, I owe my deepest gratitude to Dr Alok Dube, Scientific officer G, Laser Biomedical Application and Instrumentation Division, Raja Ramanna Centre for Advanced Technology, for his peerless guidance, expert planning, untiring and bountiful help and support. While there have been many ups and downs during my research, his constant faith and confidence in me motivated me to work with renewed zest.

I wish to express my deep sense of gratitude to Dr. S. K. Apte, chairman of doctoral committee for his positive questions, suggestions and appreciation during the course of my research work. I am also extremely thankful to Dr. T.P.A. Devasagayam, member of my doctoral committee, for his useful suggestions and encouragement.

I feel great pleasure to express my heartfelt thanks to members of the group specially Dr Mrinalini Sharma, Khageshwar Sahu, Shri. H.S. Patel, Mr. Mahesh Swami, Dr Biplab

Bose, Dr Shovan Majumdar, Dr Kaustuv Das, Dr Abha Uppal, Smt. Beena Jain, Mrs. Harsha Bansal for their help and suggestions.

I would like to express my sincere thanks to Dr. B. N. Pandey, Radiation Biology and Health Science Division BARC for providing Laser Scanning Confocal Microscope facility in his lab. Technical help extended by Mr. Manjoor Ali and Ms. Vasumati in use of confocal microscope is duly acknowledged.

I feel highly obliged and have immense pleasure in expressing my heartfelt thanks to my senior Dr. Sulbha Sharma for her help and valuable suggestion in experimental work. She has always been a source of constant support and encouragement whenever I faced problems. I acknowledge my sincere and heartfelt thanks to Mrs. Parul Arora for good company and moral support.

I would like to express my sincere thanks to Mr. Deshpande and Mr. Gyansingh for their assistance in a number of ways specially in performing all the animal experiments.

I owe my thanks to all my batch mates (51st batch BARC) especially Nazir, C. Vijay, Mrityunjay, Ravindra, Pooja, Nidhi, Kirti, for their loving support during the training period. I am thankful to Sam, for her love, selfless help, affection and support during my stay at BARC Training School.

I express my sincere thanks to wonderful friend and brother, Dipesh Singh Parihar for his utmost help. It was a great pleasure to remember the time spent with you brother and the way you handle my problems with your imaginative thoughts, support and appreciation. I am highly indebted for all the things you did for me. A healthy conversation with you had been my biggest stress buster and source of inspiration. Discussions with you induced new gush of energy in me whenever I felt low and perturbed. Without your support and understanding I could have never reached my goal.

The unconditional love, care, support and faith showered upon me by my dear ones could never be acknowledged by any means. I am overwhelmed when it comes to express my gratitude towards my family members. I thank my parents, for their supreme moral

support and boundless love they have showered upon me. My special thanks to my Papa who instilled in me the undying spirit to fight and never give up. I thank my mother for her blessings. Her modesty, calm and cool nature, intelligence, and the way to handle tuff situations, have been a constant source of inspiration for me.

Words fail me to express the love and admiration to my husband Dr. Ashish Singh Kushwah, whose supportive and friendly nature, dedication, immense faith on me, improved my self-confidence and ability to do several works. Due to his support and reassurance I was never alone with my problems. His help during the tough times of my research will be indelible from my mind. I owe my every achievement to my parents, husband and my family members.

I would also like to thank my siblings Mragendra, Dipesh, Munendra, Kamna, Bhabhi Komal, Pradeep jijaji, Pratima Bua for their constant support, care and encouragement and cheering me up whenever I felt low.

My in-laws, especially mother-in-law, father-in-law and sister-in-laws Alpana, Archana and Anjana deserve special thanks for their constant encouragement, understandings, faith and patience during the time of thesis writing.

Financial assistance provided by DAE is duly acknowledged.

Finally, to err is human!! All those whose mention might have slipped from my mind, deserve my sincere gratitude for their direct or indirect help in this pursuit.

Arpana Parihar

CONTENTS

	Page No.
SYNOPSIS	1-10
LIST OF SCHEMES	11
LIST OF TABLES	12
LIST OF FIGURES	13-15
LIST OF ABBREVIATIONS	16-17
CHAPTER 1: INTRODUCTION AND REVIEW OF LITERATURE	18-67
1.1 Basics of Photodynamic Therapy	
1.2 Photophysics and photochemistry of PDT	
1.3 Basic components of PDT	
1.3.1 Photosensitizer types and ideal properties	
1.3.2 Light sources	
1.4 Mechanism of Tumor Destruction by PDT	
1.4.1 Direct Killing of Tumor cells	
1.4.2 Tumor Vasculature damage	
1.4.3 Immune Response	
1.5 Brief History of PDT	
1.6 Status of Photosensitizer in the development of PDT	
1.6.1 First Generation of Photosensitizers	
1.6.2 Second Generation of Photosensitizers	
1.6.2.1 Chlorophyll Derivatives as a Potential PDT agents	
1.6.2.2 Pheophorbide and its Derivatives	
1.6.2.3 Chlorin <i>e</i> ₆ and its Derivatives	
1.6.2.4 Chlorin <i>p</i> ₆ and its Derivatives	
1.6.3 Third Generation of Photosensitizers	
1.6.3.1 LDL receptor based targeting	
1.6.3.2 EGF receptor based targeting	
1.6.3.3 Carbohydrate receptor based targeting	
1.6.3.4 Folic acid receptor based targeting	
1.6.3.5 Insulin and other receptor based targeting	
1.6.3.6 Transferin receptor based targeting	
1.6.3.7 Histamine receptors can be exploited as a potential Therapeutic targets	

1.7 Aims of the Present Study

CHAPTER 2: MATERIALS AND METHODS

68-92

2.1 Materials

2.2 Procedures and methods

- 2.2.1 Cell culture
- 2.2.2 Animal model
- 2.2.3 Preparation of Cp_6 and Cp_6 -his
- 2.2.4 Absorption and fluorescence spectra
- 2.2.5 Photosensitizer treatment
- 2.2.6 Extraction and estimation of photosensitizer content in cells
- 2.2.7 Photodynamic Treatment
- 2.2.8 Measurements on phototoxicity
- 2.2.9 Western blot for detection of histamine H2 receptor
- 2.2.10 Intracellular localization of photosensitizer
- 2.2.11 Monitoring of cellular and nuclear morphology
- 2.2.12 DNA fragmentation by gel electrophoresis
- 2.2.13 Assessment of apoptosis and necrosis
- 2.2.14 Mitochondrial membrane potential in cells
- 2.2.15 Confocal fluorescence imaging of Cp_6 -his localization in cells
- 2.2.16 3D fluorescence imaging of cells
- 2.2.17 Photosensitizer administration in hamsters
- 2.2.18 *In vivo* fluorescence measurements
- 2.2.19 Photodynamic Treatment of tumors
- 2.2.20 Tumor volume measurements
- 2.2.21 Tissue Histology
- 2.2.22 Immunohistochemistry
- 2.2.23 Western blot for detection of histamine H2 receptors
- 2.2.24 Isolation of liver microsomes
- 2.2.25 Measurement of binding parameters
- 2.2.26 Spectroscopic measurements
- 2.2.27 Irradiation Procedure
- 2.2.28 Assay of singlet oxygen yield
- 2.2.29 Octanol/ water partition coefficient
- 2.2.30 Protein carbonyl estimation
- 2.2.31 Assay for lipid peroxidation
- 2.2.32 Fluorescence quenching by potassium iodide
- 2.2.33 Effect of Cp_6 and Cp_6 -his on activity of microsomal enzymes
- 2.2.34 Statistics

CHAPTER 3: UPTAKE AND PHOTOTOXICITY OF *Cp6*-his IN
CANCER CELLS

93-119

3.1 Results

- 3.1.1 Characterization of the *Cp6*-his
- 3.1.2 Intracellular uptake of *Cp6* and *Cp6*-his
- 3.1.3 Detection of histamine receptors in cells
- 3.1.4 Intracellular localization of photosensitizers
- 3.1.5 Phototoxicity
- 3.1.6 Mode of cell death induced by *Cp6*-his

3.2 Discussion

3.3 Conclusion

CHAPTER 4: INTRACELLULAR SITE OF *Cp6*-his LOCALIZATION
AND PDT-INDUCED CELL ORGANELLE DAMAGE

120-140

4.1 Results

- 4.1.1 Intracellular localization of *Cp6*-his
- 4.1.2 Phototoxicity
- 4.1.3 Alterations in ER morphology due to PDT
- 4.1.4 Alterations in the morphology of Golgi due to PDT
- 4.1.5 PDT induced damage to lysosomes

4.2 Discussion

- 4.2.1 Intracellular localization of *Cp6*-his
- 4.2.2 PDT-induced ER damage
- 4.2.3 PDT induced Indirect damage to Golgi apparatus
- 4.2.4 PDT induced damage to lysosomes

4.3 Conclusion

CHAPTER 5: EVALUATION OF PDT EFFICACY OF *Cp6*-his IN
HAMSTER CHEEK POUCH MODEL

141-158

5.1 Results

- 5.1.1 Tumor selectivity of *Cp6*-his
- 5.1.2 Pharmacokinetics of *Cp6*-his in Hamster cheek

- Pouch Model
- 5.1.3 Histamine receptors Expression
- 5.1.4 PDT induced tumor damage and regression
- 5.2 Discussion
- 5.3 Conclusion

CHAPTER 6: INTERACTION OF *Cp₆*-his AND *Cp₆* WITH
BSA AND LIVER MICROSOMES

159-178

- 6.1 Results
 - 6.1.1 Interaction of *Cp₆* and *Cp₆*-his with BSA and liver microsomes
 - 6.1.2 Measurement of binding Parameters
 - 6.1.3 Effect of *Cp₆* and *Cp₆*-his on microsomal enzymes
 - 6.1.4 Quenching of tryptophan fluorescence with potassium Iodide
 - 6.1.5 Protein damage induced by PDT with *Cp₆* and *Cp₆*-his
 - 6.1.6 Photodynamic lipid damage induced by PDT with *Cp₆* and *Cp₆*-his
 - 6.1.7 Octanol/Water partition coefficient
- 6.2 Discussion
 - 6.2.1 Interaction of *Cp₆* and *Cp₆*-his with BSA
 - 6.2.2 Interaction of *Cp₆* and *Cp₆*-his with liver microsomes
 - 6.2.3 Photodynamic damage to protein and lipids
- 6.3 Conclusion

CHAPTER 7: SUMMARY AND FUTURE PROSPECTIVES

179-185

REFERENCES

186-219

SYNOPSIS

Photodynamic therapy (PDT) is an attractive clinical modality for the treatment of various types of cancer because compared to radiation and chemo therapy it produces better tumor selectivity and fewer side effects [1]. The anticancer effect of PDT is based on the activation of a photosensitive drug referred as 'photosensitizer' using light of appropriate wavelength to generate cytotoxic reactive oxygen species [2]. Currently, clinical approval exists in USA and Europe for photosensitizers such as Photofrin (Hematoporphyrin derivative), 5-aminolevulinic acid (ALA), a porphyrin precursor and its methylester derivative and Methyl-tetrahydroxyphenylchlorin (Temoporfin) [1]. Several second generation photosensitizers that belong to porphyrin, chlorin and phthalocyanine groups have been evaluated for PDT and some of these such as Visudyne, Lutetium texaphyrin (Lutrin) palladium bacteriopheophorbide a (Tookad), Tin etiopurpurin (Purlytin), Mono-l-aspartylchlorin-e6 (Laserphyrin), and Sulfonated aluminum phthalocyanine (Photosens) are under clinical trials for the treatment of various types of cancer [3].

Among second generation photosensitizers the derivatives prepared from plant pigment 'chlorophyll-a' have received considerable attention because they possess significantly higher absorption in the longer wavelength region (660-800 nm) which leads to a higher depth of treatment due to reduced tissue absorption and scattering at these wavelengths [4]. Chlorin₆ (Cp₆), a hydrophilic chlorophyll derivative has been explored for PDT application at Raja Ramanna Centre for Advanced Technology (RRCAT) and detailed studies carried out on its photophysical and photochemical properties have shown

that the hydrophobicity of Cp_6 increases at pH lower than physiological [5] which also leads to its higher incorporation in lipid bilayer [6]. Since the microenvironment within solid tumors is often acidic this property of Cp_6 was considered important for its preferential accumulation in tumors. Cp_6 also showed good photodynamic activity at micromolar concentration without having significant dark toxicity in cancer cells [7]. Based on these results the use of Cp_6 was investigated for PDT of tumors in hamster cheek pouch model of oral carcinoma and it was observed that Cp_6 accumulated preferentially in tumors showed rapid clearance from skin and led to complete tumor regression after PDT for the tumors of the size $\sim 130 \text{ mm}^3$ [8, 9]. However, for relatively large tumors its uptake was poor which compromised the PDT efficacy.

A promising approach to enhance the tumor uptake and selectivity of photosensitizer is to couple it with a suitable molecule which can interact specifically with receptors on cancer cells. This approach utilizes the fact that tumor cells typically have increased expression of cell surface receptors for various growth factors or regulatory biomolecules [10, 11]. In this context, the use of photosensitizers coupled to molecules such as folic acid, steroids, epidermal growth factor (EGF), and antibodies against some cell surface receptors have been investigated [11-12]. However, since the type and level of receptor expression can differ in different types of malignancies there is a need to explore new targets and targeting molecules.

There exist reports in literature which suggest interesting role of histamine, a biogenic amine in tumor growth and development [13-15]. It has been reported that

various types of cancer cells produce high levels of histamine to regulate their cell proliferation via histamine receptors. The over-expression of histamine receptors in malignant tissue (almost 2–5 times higher than normal tissue) has been reported in several types of malignancies e.g., breast carcinoma, melanoma and adrenocortical cancer [16-18]. However, the use of histamine or its receptors for targeting the photosensitizer for PDT of cancer has not yet been investigated. As part of the thesis we have investigated the uptake, tumor selectivity and PDT efficacy of chlorin p6 (Cp_6) histamine conjugate in cancer cell lines and animal tumor model.

The thesis is organized as follows:

Chapter 1: It deals with introduction to PDT, provides details basics components of PDT (photosensitizer, light and oxygen), as well as photophysics photochemistry and photobiological aspects of PDT. Literature on the development of PDT with second generation photosensitizer including chlorophyll derivatives and targeted approach using third generation photosensitisers has also been reviewed. The chapter also provides review of relevant literature on role of histamine and its receptors in tumor growth in context of possibility to exploiting over expression of histamine receptors for targeted PDT.

Chapter 2: It describes methods used for cell culture, preparation of Cp_6 -histamine conjugate, monitoring cellular uptake and site of intracellular localization of the photosensitizers, expression of histamine receptors, photodynamic treatment of cells, phototoxicity, cell organelle damage, mode of cell death, induction of tumors in hamster

cheek pouch, accumulation of photosensitizer in tumor and normal tissue, photodynamic treatment of tumor, assessment of tumor regression, binding affinity of photosensitizers with serum and microsomal proteins and their relative singlet oxygen yield, photodynamic damage to protein and lipids etc.

Chapter 3: Here we provide results of studies carried out on the cellular uptake and phototoxicity of Cp_6 -his in two oral cancer cell lines Nt8e and 4451. Results showed that the uptake of chlorin-p6 histamine conjugate in these cell lines was ~10 times higher than free Cp_6 and that this led to significant enhancement in phototoxicity of the conjugate. The presence of histamine receptors and receptor mediated uptake of the conjugate was confirmed in both the cell lines. Results also showed that there was no significant difference in the mode of cell death induced by free Cp_6 and Cp_6 -his. Since the expression of histamine receptors is well documented in human breast carcinoma cell line MCF-7, studies were also done using this cell line and higher uptake of Cp_6 -his and enhancement in phototoxicity has been observed. It is concluded that conjugating Cp_6 with histamine can help to improve the effectiveness of PDT in oral and breast cancer cells by enhancing its intracellular delivery.

Chapter 4: Photosensitizer often exhibit selective specificity for different organelles depending on their physicochemical properties, and the subsequent structural alteration/damage induced by PDT in these organelles plays a very crucial role in cell death after PDT [1]. To explore this aspect for Cp_6 histamine conjugate, studies have been carried out to identify the sites of its intracellular localization and to characterize the

structural damage in cell organelles using fluorescence probes and confocal microscopy. The results of these studies are presented and discussed in this chapter. Observations by wide-field fluorescence microscopy showed that Cp_6 -his conjugate localizes initially at cell membrane and then internalized in the endosome like compartments beyond 1hr interval. At longer time interval (3 h) the fluorescence of conjugate was seen at the periphery of cell nucleus. These results suggested that the uptake of the conjugate is mediated by endocytosis. Results of colocalization studies using confocal microscope revealed that the conjugate localizes mainly in endoplasmic reticulum and lysosomes but not in Golgi and mitochondria. To characterize the PDT-induced damage to cell organelles, confocal fluorescence imaging and 3D reconstruction of images of cellular structures have been carried out. It was observed that PDT led to fragmentation of ER due to damage in the tubular regions of ER and PDT-induced structural alterations in ER were distinctly different in apoptotic and necrotic cells. In spite of the fact that the Cp_6 -his did not localize in Golgi apparatus, PDT led to alterations of Golgi structure such as displacement and swelling. The results show that damage to ER structure could be the possible reason for alteration in the structure.

Chapter 5: Our *in-vitro* results motivated us to extend this study in *in-vivo* model system. Studies have been carried out to explore the tumor selectivity and photodynamic efficacy of Cp_6 -his in Hamster cheek pouch model of oral cancer after establishing that histamine receptor is over-expressed in tumors. These results are presented and discussed in this chapter. Cp_6 -his (3 mg/kg body weight) was injected intra-peritoneally and its accumulation in tumor, surrounding tissue, normal mucosa and abdominal skin was

monitored non-invasively by fluorescence spectroscopy. Results show significant accumulation of Cp_6 -his in tumors and rapid clearance from the skin showing ~ 80% decreases within 48 h from its peak level at 4 h after drug injection. The tumor selectivity of Cp_6 -histamine was significantly higher as compared to the free Cp_6 . For PDT, tumors at 4 h after Cp_6 -his administration were exposed to red light (660 ± 25 nm, 100 J/cm²). Histology at 48 h after PDT revealed extensive cellular damage in the treated tumor. Further using conjugate complete regression of tumors of size ≤ 1000 mm³ was observed one week after PDT while with free Cp_6 tumors of volume of only up to 130 mm³ could be treated. Higher tumor selectivity of Cp_6 -his and complete regression of bigger tumors after PDT suggest that conjugating Cp_6 to histamine is a promising approach to improve PDT efficacy.

Chapter 6: The coupling of Cp_6 to histamine is expected to lead to change in physical properties of Cp_6 such as charge and hydrophobicity which could also play a role in the pharmacokinetics and clearance. To investigate this aspect the interaction of Cp_6 -his with serum albumin and liver microsomes has been investigated and the results are presented and discussed in this chapter. The quenching of intrinsic tryptophan fluorescence of BSA and microsomal proteins by Cp_6 and Cp_6 -his is measured and plotted as Stern–Volmer plot to determine the binding parameters such as binding constant and number of binding sites. Results showed that the binding constant of Cp_6 -his with BSA was lower by ~ 4 orders as compared to that of Cp_6 and the number of binding sites was decreased to nearly half. These results correlated with the extent of photodynamic damage to BSA induced by the conjugate and free Cp_6 as determined by estimation of protein carbonyls formation. With

microsomal proteins the binding constant of Cp_6 -his was lower by ~2 orders than that of Cp_6 and the amount of PDT-induced protein carbonyl formation was consistent with their relative binding affinity. Measurements on the activity of microsomal enzymes cytochrome P-450 reductase and NADH cytochrome b5 reductase showed that both Cp_6 -his and Cp_6 did not affect the activity of these enzymes. The two photosensitizers can also bind to microsomes due to lipophilic/hydrophobic interaction with membrane lipids. Measurements on PDT induced lipid peroxidation however showed no difference for Cp_6 -his and Cp_6 indicating that their non-specific binding is also similar. These results led to the understanding that serum albumin is less likely to play a role in the transport of Cp_6 conjugate as compared to free Cp_6 whereas, its recognition by microsomal proteins for further metabolism and clearance is not altered which are desirable features for its *in vivo* PDT efficacy.

Chapter 7: Here we provide summary of the various studies carried out as part of this thesis work and discuss scope of future work to translate the results obtained with hamster oral cancer model to human oral cancer.

References

- [1] Agostinis P, Berg K, Cengel KA, Foster TH, Girotti AW, Gollnick SO, Hahn SM, Hamblin MR, Juzeniene A, Kessel D, Korbelik M, Moan J, Mroz P, Nowis D, Piette J, Wilson BC, Golab J. Photodynamic therapy of cancer: an update. *CA Cancer J Clin.* 2011; 61:250-281.

- [2] Wilson BC, Patterson MS. The physics, biophysics and technology of photodynamic therapy. *Phys Med Biol*. 2008; 53:R61–R109.
- [3] Yano S, Hirohara S, Obata M, Hagiya Y, Ogura S, Ikeda A, Kataoka H, Tanaka M, Joh T. Current status and future views in photodynamic therapy. *J. Photochem. Photobiol. C: Photochemistry Reviews*. 2011 ;12 : 46– 67
- [4] Spikes JD, BommerTC. Chlorophylls and related pigments as photosensitizers in biology and medicine, in: H. Scheer (Ed.), *Chlorophylls*, CRC press, Boca Raton, FL, 1991, pp. 145–157.
- [5] Datta A, Dube A, Jain B, Tiwari A, Gupta PK. The effect of pH and surfactant on the aggregation behavior of chlorin p6: A fluorescence spectroscopic study. *PhotochemPhotobiol*. 2002; 75:488-494.
- [6] Das K, Jain B, Dube A, Gupta PK. pH dependent binding of chlorin-p6 with phosphatidyl choline liposomes. *Chemical Physics Letters*. 2005, 401:185-188.
- [7] Sharma M, Dube A, Bansal H, Kumar Gupta PK. Effect of pH on uptake and photodynamic action of chlorin p6 on human colon and breast adenocarcinoma cell lines. *PhotochemPhotobiol Sci*. 2004; 3:231-235.
- [8] Dube A, Sharma S, Gupta PK. Evaluation of chlorin p6 for photodynamic treatment of squamous cell carcinoma in the hamster cheek pouch model. *Oral Oncol*. 2006; 42:77–82.
- [9] Dube A, Sharma S, Gupta PK. Tumor regression induced by photodynamic treatment with chlorin p6 in hamster cheek pouch model of oral carcinogenesis: Dependence of mode of tumor cell death on the applied drug dose. *Oral Oncol*. 2011; 47: 467–471.

- [10] Sharman WM, van Lier JE, Allen CM. Targeted photodynamic therapy via receptor mediated delivery systems. *Adv Drug Dev Rev* 2004; 56:53–76.
- [11] Chen B, Pogue BW, Hoopes PJ, Hasan T. Vascular and cellular targeting for photodynamic therapy. *Crit Rev Eukaryot Gene Expr.* 2006; 16:279–305.
- [12] Soukos NS, Hamblin MR, Keel S, Fabian RL, Deutsch TF, Hasan T. Epidermal growth factor receptor-targeted immunophotodiagnosis and photoimmunotherapy of oral precancer in vivo. *Cancer Res.* 2001; 61:4490-4496.
- [13] Bartholeyns J, Fozard JR. Role of histamine in tumor development. *Trends PharmacolSci* 1985; 6:123–125.
- [14] Medina MA, Quesada AR, de Núñez Castro I, Sánchez-Jiménez F. Histamine, polyamines, and cancer. *BiochemPharmacol* 1999; 57:1341–1344.
- [15] Rivera ES, Cricco GP, Engel NI, Fitzsimons CP, Martín GA, Bergoc RM. Histamine as an autocrine growth factor: an unusual role for a widespread mediator. *Semin Cancer Biol.* 2000; 10:15–23.
- [16] Pós Z, Sáfrány G, Müller K, Tóth S, Falus A, Hegyesi H. Phenotypic profiling of engineered mouse melanomas with manipulated histamine production identifies histamine H2 receptor and rho-C as histamine-regulated melanoma progression markers. *Cancer Res* 2005; 65: 4458–4466.
- [17] Medina VA, Rivera ES. Histamine receptors and cancer pharmacology. *Br J Pharmacol* 2010; 161:755–767.
- [18] Szabó PM, Wiener Z, Tömböl Z, Kovács A, Pócza P, Horányi J, Kulka J, Riesz P, Tóth M, Patócs A, Gaillard RC, Falus A, Rác K, Igaz P Differences in the

expression of histamine-related genes and proteins in normal human adrenal cortex and adrenocortical tumors. *Virchows Arch.* 2009; 455:133–142.

LIST OF SCHEMES

Scheme No.	Page No.
Scheme1.1: Synthesis of Chlorin _{p6} from Chlorophyll-A.	45
Scheme1.2: Autocrine loop of Histamine.	65
Scheme2.1: Chemical reaction showing synthesis of Cp ₆ -his from purpurin-18	72

LIST OF TABLES

Table No.	Page No.
1.1: Current status of Clinically Applied Photosensitizers.	38
1.2: Different types of histamine receptors, their location and functions	60
1.3: Expression of histamine receptor, intracellular histamine content and Effect of histamine on cell proliferation in various types of carcinoma	61
3.1: The effect of histamine receptor antagonist ranitidine, pheniramine, low temperature and histamine on the cellular uptake of Cp_6 and Cp_6 -his.	103
3.2: Percentage of apoptotic and necrotic cells in MCF-7 cells after 18 hr of Photodynamic treatment with Cp_6 -his.	114
5.1: Fluorescence intensity of Cp_6 -his and Cp_6 in tumor and normal mucosa at 4 h after the administration of photosensitizer.	145
5.2: Tumor volume before and one week after photodynamic treatment using Cp_6 -his.	154
6.1: Binding parameters.	165
6.2. Effect of Cp_6 and Cp_6 -his on the reduction of cytochrome c by NADPH- cytochrome P-450 and NADH-cytochrome b5 reductase	165
6.3. Estimation of Protein carbonyl following PDT with Cp_6 -his and Cp_6 .	169
6.4. Lipid peroxidation in microsomes following PDT with Cp_6 -his and Cp_6 .	170

LIST OF FIGURES

Figure No.	Page No.
1.1: Photodynamic therapy of cancer.	21
1.3: Jablonski energy level diagram for photodynamic therapy	23
1.2: Optical absorption spectra of various tissue components in the ultraviolet to infrared wavelength range.	26
1.4: Historical development of PDT	35
1.5: CIM inhibitory effect on tumor growth. CIM blocks the cell growth-promoting activity of histamine.	64
2.1: Microphotographs of 4451 and Nt8e and MCF-7 cells showing nuclear morphology.	79
3.1: Photograph of TLC plate showing mobility of Cp_6 and Cp_6 -his after Chromatography using 90% methanol as mobile phase.	96
3.2: Absorption spectra of Cp_6 and Cp_6 -his in Ethanol: PEG: Water system.	97
3.3: Time dependent cellular uptake of Cp_6 and Cp_6 -his Conjugate.	100
3.4: The effect of histamine (a) and histamine receptor antagonist (b) on the cellular uptake of Cp_6 and Cp_6 -his conjugate.	101
3.5: The effect of temperature on the cellular uptake of Cp_6 and Cp_6 -his conjugate.	102
3.6: Image of nitrocellulose membrane showing presence of H2 receptor in 4451, Nt8e and MCF-7 cells after Western blot	104
3.7: Microphotographs of 4451, Nt8e, MCF-7 cells incubated with 5.0 μ M Cp_6 or Cp_6 -his in growth medium.	106
3.8: Percent phototoxicity induced by Cp_6 -his at varying concentration from 1-5 μ M and fixed light dose at 28 kJ/m ²	108
3.9: Microphotographs of 4451, Nt8e and MCF-7 cells showing changes in the cellular morphology after PDT with Cp_6 -his.	111
3.10: DNA gel electrophoresis.	112
3.11: Percentage of apoptotic and necrotic cells in 4451 and Nt8e cells	113

following PDT with Cp_6 or Cp_6 -his.	
4.1: Microphotographs of Nt8e cells showing subcellular localization Of Cp_6 -his.	124
4.2: Microphotographs of Nt8e cells showing subcellular localization of Cp_6 .	125
4.3: Bright field and fluorescence images of Nt8e cells after PDT with Cp_6 -his showing changes in morphology and mitochondrial membrane potential.	126
4.4: 3D reconstructions of z-stacked images of Nt8e cells stained with ER-tracker green.	129
4.5: 3D reconstructions of z-stacked images of Nt8e cells stained With Golgi specific bodipy ceramide green.	131
4.6: 3D reconstructions of z-stacked images of Nt8e cells stained With lysotracker green.	134
5.1: Fluorescence emission spectra collected from a tumor and normal pouch	144
5.2: The level of Cp_6 -his and Cp_6 in the abdominal skin of the hamster at different time interval after i.p injection	146
5.3: Fluorescence emission spectra collected from a tumor at different time interwalafter administration of Cp_6 -his	147
5.4: Immunohistochemical detection of H2R receptor in tumor, mucosa adjoining tumor, and normal mucosa.	148
5.5: Image of nitrocellulose membrane showing presence of H2 receptor in tumor,mucosa adjoining tumor and normal mucosa of the hamster after Western blot	150
5.6: Photomicrographs showing histology of untreated tumor tissue and tumor tissue subjected to PDT using Cp_6 -his.	152
5.7: Photographs showing PDT-induced tumor regression in hamster.	153
6.1: Absorption spectra of Cp_6 and Cp_6 -hisand in presence of either BSA or microsome.	162
6.2: (a) Double logarithm plot of $\log (F_0-F)/F$ vs. $\log [Cp_6/ Cp_6$ -his] for BSA/Microsomes.	164

6.3: Stern–Volmer quenching plots of Cp_6/ Cp_6 -his fluorescence:	168
6.4: Cp_6/Cp_6 -his mediated photodynamic RNO bleaching vs.irradiation time.	175
7.1: H2R receptor expression in Human OSCC biopsy samples.	182-185

LIST OF ABBREVIATIONS

μl	Microleter
μM	Micromolar
ALA	5-aminolevulinic acid
BSA	Bovine Serum Albumin
BCA	Bicinchoninic acid
Ce_6	Chlorin e_6
Cp_6	Chlorin p_6
Cp_6 -His	Chlorin p_6 -Histamine conjugate
Chl	Chlorophyll
Chl- <i>a</i>	Chlorophyll- <i>a</i>
Chl- <i>b</i>	Chlorophyll- <i>b</i>
Chlide- <i>a</i>	Chlorophyllide- <i>a</i>
DMBA	7,12-Dimethyl- benz (a) anthracene
DMEM	Dulbecco's modified essential media
DMSO	Dimethyl sulfoxide
EDTA	Ethylene diamine tetra acetate
ER	Endoplasmic reticulum
FBS	Foetal bovine serum
FCS	Foetal calf serum
HEPES	N-2-hydroxyethylpiperazine- N'-2- ethanesulphonic acid
HpD	Hematoporphyrin derivative
HPPH	2-(1-hexyloxyethyl)-2-devinyl Pyropheophorbide- <i>a</i>
JC-1	5, 5, 6, 6-tetrachloro-1,1,3,3-

	Tetraethylbenzimidazolylcarbo cyanine Iodide
LDL	Low density lipoproteins
mM	Milimolar
MMP	Mitochondrial membrane potential
MTT	3(4,5-dimethylthiazol-2-yl)2,5 diphenyltetrazolium bromide
NaOH	Sodium Hydroxide
NPe6	Mono-L-aspartylchlorin e6
OSCC cells	Oral squamous cell carcinoma
PAGE	Polyacrylamide gel
PBS	Phosphate buffer saline
PDT	Photodynamic therapy
PF	Photofrin®
Pheid- <i>a</i>	Pheophorbide- <i>a</i>
<i>Pp-18</i>	Pupurin-18
PpIX	Protoporphyrin IX
PS	Photosensitizer
PI	Propidium Iodide
ROS	Reactive oxygen species
SDS	Sodium dodecyl sulphate
TBS	Tris buffered saline
TNF- α	Tumor Necrosis Factor- α
mTHPC chlorine	Tetra(m-hydroxyphenyl) (temophrin)
VEGF	Vascular endothelial growth Factor

CHAPTER 1

INTRODUCTION

AND

REVIEW OF LITERATURE

1.1 Basics of Photodynamic Therapy

Cancer remains leading cause of death globally. Almost 7.6 million deaths worldwide were estimated due to cancer with 12.7 million new cases per year being reported worldwide as per the recent report, prepared by the International Agency for Research on Cancer (IARC) [1]. Cancer is uncontrolled proliferation of cells that is manifested by loss of cell cycle control leading to serious adverse effects on the host through invasive growth and metastases [2-4]. Chemotherapy, surgery and radiotherapy either alone or in combination are currently the main treatments available for cancer. In chemotherapy the approach is based on the use of drug that can either inhibit or block the proliferation of rapidly dividing cancer cells [5]. However, such chemotherapeutic drugs also interfere with the proliferation of healthy rapidly dividing normal cells such as blood forming cells in the bone marrow, hair follicles, and epithelial cells of oral cavity skin, digestive tract, and reproductive system. Thus, chemotherapy leads to several severe side effects such as nausea, vomiting, pain, anemia, hair fall, loss of fertility etc [5]. Surgery is applicable only when tumor is confined to limited area in the body. Radiation therapy is more commonly used therapeutic modality for the treatment of cancer in which ionizing radiation (X-rays, gamma rays and charged proton beam) is used to destroy cancer cells [6-8]. Although, these therapeutic modalities can improve the life expectancy of patients from several months to years, the repeated use of these therapeutic modalities required for the complete eradication of cancer also leads to the development of resistance and tumor recurrence.

In past decade, significant advancement in cancer research led to development of some new promising strategies for the treatment of cancer such as gene therapy,

immunotherapy, hormone therapy, heat therapy (hyperthermia), stem cell transplantation etc [1]. Photodynamic therapy (PDT) is one of such promising options for the treatment of cancer in which visible light in combination with photoactive compound referred as photosensitizer (PS) is used. Light alone is a non toxic form of electromagnetic radiation, but in the presence of a photosensitive molecule referred here as photosensitizer can generate reactive oxygen species (ROS) which causes cellular destruction. Photodynamic therapy (PDT) is minimally invasive modality for the treatment of cancer which has been clinically approved and found effective for the treatment of various types of malignancies [8,10,11]. In PDT the photosensitizer is administered either topically or systemically and allowed to accumulate selectively in tumor tissue. In second step, a limited area where the tumor or cancerous tissue is located is irradiated with visible light of appropriate wavelength. The cytotoxic species such as singlet oxygen and free radicals generated via photochemical reactions leads to destruction of target tumor tissue (Fig. 1.1). Thus PDT offers dual selectivity with the use of a tumor selective photosensitizer and by limiting the light exposure to the diseased region [11]. The destruction of cancerous tissue with minimal effect on healthy tissues is one of the most advantageous features of PDT over the other established therapeutic modality of cancer. Hematoporphyrin derivative (HpD) was the first clinically approved PDT drug. Currently, the clinical approval for only few photosensitisers exists, which are Photofrin (porfimer sodium) for the treatment of oesophagus cancer and lung cancer (NSCLC), ALA for the treatment of skin cancer, Verteporfin (BPD, benzoporphyrin derivative) for the treatment of macular degeneration and Foscan (temporfin, meta-tetrahydroxyphenyl chlorin) for the treatment of advanced squamous cell cancer of the head and neck [12,13].

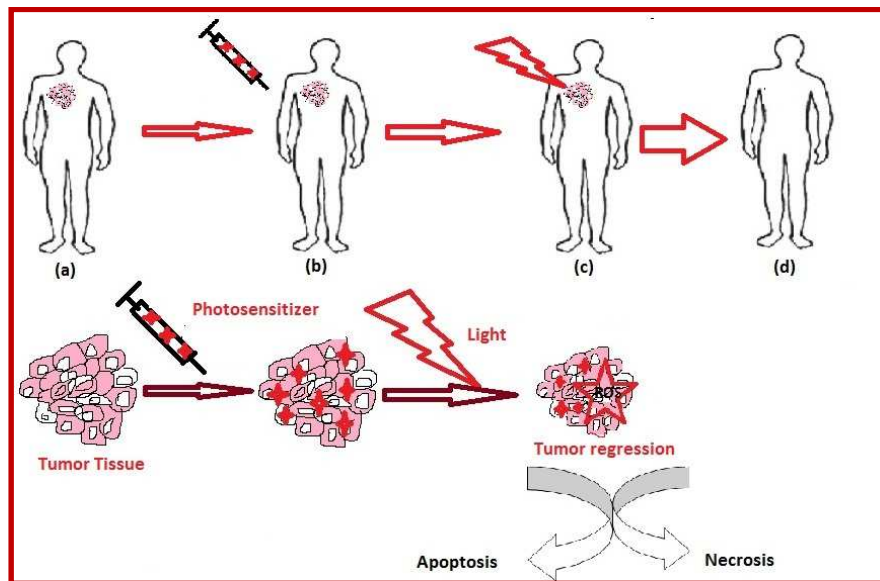


Figure 1.1 Photodynamic therapy of cancer. (a) The photosensitizer is injected systemically in the body (b) Preferential accumulation of photosensitizer in to the tumor tissue (c) Irradiation of the tumor area with light of appropriate wavelength to activate the photosensitizer (d) Generation of reactive oxygen species which destroys the tumor.

1.2 Photophysics and photochemistry of PDT

The reactions after the excitation of the photosensitizers i.e. Photochemical and photophysical principles of PDT have been extensively studied and can be depicted through a Jablonski diagram (Fig. 1.2). Briefly, upon illumination, the photosensitizer is excited from the ground state (S_0) to the first excited single state (S_1), followed by conversion to the triplet state (T_1) via intersystem crossing. The excited triplet state can react in two ways, defined as Type I and Type II mechanisms [13, 15]. A Type I mechanism involves hydrogen-atom abstraction or electron-transfer reactions between the excited state of the sensitizer and a neighboring substrate molecule which result in generation of free radicals and radical ions. These free radical species are generally highly reactive and can readily interact with molecular oxygen to either generate reactive oxygen species such as superoxide anions or hydroxyl radicals or can cause irreparable biological damage. These reactions produce oxidative damage that is eventually expressed as biological lesions. In contrast, a Type II mechanism results from an energy transfer between the excited triplet state of the sensitizer and the ground-state molecular oxygen, generating the singlet oxygen, which is extremely reactive and can interact with a large number of biological substrates, inducing oxidative damage and ultimately cell death [13, 15].

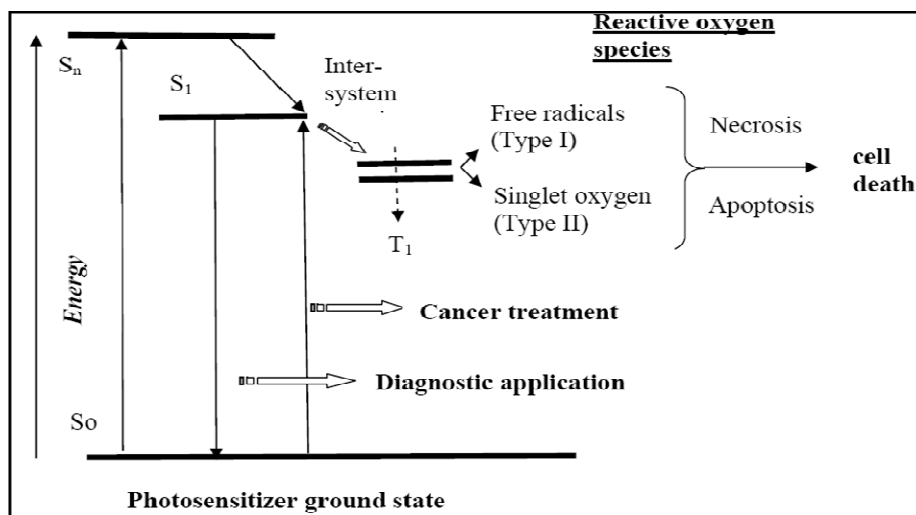


Figure 1.2: Jablonski energy level diagram for photodynamic therapy: The photosensitizer in its ground state (S_0) absorbs a photon, which gives rise to the short-lived excited singlet state (S_1). At this state it can either lose energy by fluorescence, or by intersystem crossing to the long-lived triplet state (T_1). This triplet state of photosensitizer either interact with neighboring bio-molecule or with molecular oxygen and produces Type I (hydroxyl radical) and Type II (singlet oxygen) reactive oxygen species.

1.3 Basic components of PDT

The three essential components of PDT i.e. photosensitizer (PS), light, and oxygen [16, 17] are described in details in the following paragraphs.

1.3.1 Photosensitizers

The majority of PDT photosensitizers comprise a heterocyclic ring structure similar to that of chlorophyll or heme in hemoglobin. Photosensitizers can be categorized by their chemical structures and can be divided into three broad families: the porphyrin-based photosensitizer (*e.g.*, Photofrin, ALA/PpIX, BPD-MA), Chlorophyll based photosensitizer (*e.g.*, chlorins, purpurins, bacteriochlorins), and the dye (*e.g.*, phthalocyanine, naphthalocyanine). Most of the current photosensitizers have porphyrin related structures, including hematoporphyrin derivatives, phthalocyanines, chlorines, and bacteriochlorins [18]. Photosensitizers are further classified based on their chemical characteristics such as charge and solubility into three major groups: hydrophobic, hydrophilic and amphiphilic. Photosensitizers bearing no charged peripheral substituents generally have negligible solubility in water or alcohols and come under the class of hydrophobic photosensitizers. However, the photosensitizer having three or more charged substituents and are freely soluble in water at physiological pH are termed as hydrophilic photosensitizers. Moreover, the amphiphilic photosensitizers have two or more charged substituent and are soluble in alcohol or water at physiological pH [19]. A large number of photosensitizers have been investigated for PDT of cancer both *in vitro* and *in vivo* and it is recognized that the

photosensitizer should have some important characteristics for use in PDT of cancer. The characteristics of ideal photosensitizer are described in detail in following section.

Properties of Ideal Photosensitizer

(i) **Good Absorption coefficient in the longer wavelength region (600-800 nm):** In PDT, light irradiation in the wavelength range from 650 nm to 800 nm is defined as **therapeutic window** (Fig. 1.3) since light in this wavelength region penetrates deeper in tissue. This is due to the fact that tissue contains some endogenous chromophores, mainly hemoglobin and melanin which absorb significantly in the wavelengths region from 400 nm to 600 nm and thus reduce the penetration of light in tissue. At wavelengths >1200 nm, light absorption by water molecules becomes substantial. For wavelengths >850-900 nm, the photons do not have sufficient energy to participate in a photochemical reaction. Therefore, the ideal photosensitizer should exhibit sufficient absorption in the therapeutic window to achieve therapeutic effectiveness at larger tissue depth [11, 18, 19, 21, 22, 25]. Further, with photosensitizer having higher absorption coefficient ($\epsilon > 20,000\text{-M}^{-1}\text{cm}^{-1}$) the therapeutic effect can be obtained at lower drug dose as compared to photosensitizer with low absorption coefficient [25].

(ii) **Triplet and singlet oxygen quantum yields:** The photosensitizer should be able to generate triplet state of appropriate energy ($E_T \geq 22.0 \text{ kcal mol}^{-1} \sim 0.95 \text{ eV}$) which is the minimum energy necessary to excite the triplet ground state of molecular oxygen ($^3\text{O}_2$) to its excited singlet state ($^1\text{O}_2$). A value greater than 0.95 eV (22 kcal/mol) and smaller than

1.63 eV (37.5 kcal/mol) is required to be a good photosensitizer [22]. The photosensitizer is considered as good PDT agent if the quantum yield of the triplet state is high enough ($\phi_T > 0.4$) for generation of sufficient singlet oxygen and/or other reactive oxygen species [22]. In addition, the longer lifetime of the triplet state ($\tau_T > 1 \mu\text{s}$), enables the better interaction of the excited photosensitizer with the surrounding molecules, resulted in the generation of more cytotoxic species.

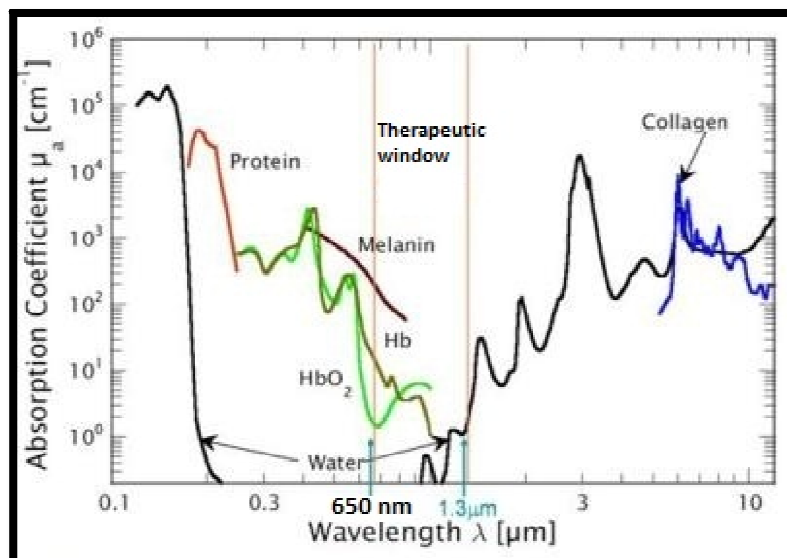


Figure 1.3. Optical absorption spectra of various tissue components in the ultraviolet to infrared wavelength range.

(iii) **Solubility:** The photosensitizer should exhibit good solubility in aqueous medium or if not it should be soluble in biocompatible drug delivery systems such as

liposomes, nanoparticles or polymeric micelles etc. for ease of administration through various routes [24].

(iv) **Photosensitizer should be tumor selective:** This property of photosensitizer is essential to ensure efficient destruction of the cancer tissue and minimize the damage to the healthy tissue. Generally, in the absence of any targeted delivery the preferential accumulation of photosensitizer in tumor is mainly determined by its physicochemical property such as hydrophobicity or hydrophilicity. Several mechanisms have been suggested which govern the preferential accumulation of PS in tumor tissue. An important mechanism is based on interaction of the photosensitizer with low-density lipoprotein (LDL). Cancer cells, due to high rate of cell proliferation require increased supply of cholesterol for membrane biosynthesis. To meet this requirement, cancer cells overexpress LDL receptors [19,24,25,26]. Since hydrophobic photosensitizer binds preferentially with serum lipoproteins, it can internalize via LDL receptor mediated endocytosis into the cancer cells and due to higher expression of these receptors the cancer cells can accumulate more photosensitizer as compared to the normal cells. However, with increase in the hydrophobicity of the photosensitizer its tendency to aggregate in physiological solution also increases which can result in poor accumulation in cancer cells. In contrast, hydrophilic photosensitizer interacts mostly with serum albumin and can accumulate in tumor tissue only through leaky tumor vasculature and poor lymphatic drainage. Thus if the photosensitizer is more hydrophilic it will remain more in tumor vasculature and accumulate less in tumor cells. Further, hydrophilic photosensitizers clear from the body at faster rate as compared to hydrophobic photosensitizers.

The second important mechanism for preferential accumulation of the photosensitizer in tumor is based on pH dependent change in hydrophobicity of the amphiphilic photosensitizer. It is known that interstitial pH in solid tumors can be slightly acidic (6.5-5.00). The amphiphilic sensitizers particularly with one or more ionizable carboxylic group in the molecules tend to accumulate better in tumor tissue because at low pH the hydrophobicity of such photosensitizer increases due to protonation of carboxylic groups in the molecule. Therefore, photosensitizer with amphiphilic nature is considered to be ideal for PDT [19].

(v) **Low/negligible dark toxicity and rapid clearance from body:** To prevent any severe side effect or skin photosensitivity, the PDT drug itself should be non-toxic in the absence of light and its clearance from the skin and body tissue should be rapid [26].

(vi) **Chemically purity:** Photosensitizer should be chemically pure compound, so that its therapeutic effects and side effects can be well characterized [22].

The photosensitizer can be considered suitable for PDT based on properties described above. There are currently only a few PDT photosensitizers that have received official approval around the world. The first FDA approved photosensitizer for PDT is Photofrin[®] (Porfimer sodium; Axcan Pharma, Inc.). Photofrin meets only few of the criteria for ideal photosensitizers and thus suffers from several drawbacks. For example, it is a complex mixture of porphyrins with various monomeric and oligomeric forms, its absorption band in red wavelength region at 630 nm, is well below the wavelength region

of therapeutic interest, it induces cutaneous photosensitivity due to the prolonged retention in skin, (at least for a month or so) after the treatment. Due to these drawbacks a variety of new photosensitizers have been investigated to find more suitable PDT agent and these photosensitizers are generally recognized as class of second generation photosensitizers. Some photosensitizers that belong to second generation are clinically approved for PDT. For example: Foscan[®] (temoporfin, meta-tetrahydroxyphenylchlorin, mTHPC; Biolitec AG), Visudyne[®] (verteporfin, benzoporphyrin derivative monoacid ring A, BPD-MA; Novartis Pharmaceuticals), Levulan[®] (5-aminolevulinic acid, ALA; DUSA Pharmaceuticals, Inc.), and most recently Metvix[®] (methyl aminolevulinate, MLA or M-ALA; PhotoCure ASA.). Several other promising photosensitizers are currently under clinical trials. These include HPPH (2-[1-hexyloxyethyl]-2-devinyl pyropheophorbide-a, Photochlor; Rosewell Park Cancer Institute), motexafin lutetium (MLu, lutetium (III) texaphyrin, Lu-Tex, Antrin; Pharmacyclics Inc.), NPe6 (mono-L-aspartyl chlorin e6, taporfin sodium, talaporfin, LS11; Light Science Corporation), SnET2 (tin ethyl etiopurpurin, Sn etiopurpurin, rostaporfin, Photrex; Miravant Medical Technologies) [18].

1.3.2 Light sources

Light sources suitable for PDT should provide 1) wavelengths of emission matching with the absorption spectrum of the photosensitizer, 2) sufficient power at these wavelengths 3) mode of delivery to the target tissue. The light power required can vary from 1 to 5 W so that light dose of up to several hundred mW cm^{-2} can be delivered in time period of tens of

minutes. It is also required that the light sources are portable, low cost and easy to operate in the clinical set up [27]. High power density is required to reach high photon density at deep tissue layers to achieve maximum activation of the photosensitizer molecules. The depth, at which the power of radiation is reduced to 37%, is known as the effective penetration depth of light. The effective penetration depth of light with λ at 630 nm into soft tissues is typically 1–2 mm, and that of light with λ in the range of 700–850 nm is about twice that. The fluence rate also affects PDT response [11]. Using higher power density the therapeutic effect of PDT can reach to a depth that is 3–5 times the effective penetration depth. For HpD the therapeutic effect of PDT is obtainable at the tissue depth of 5–10 mm. For deeper therapeutic effect, the photosensitizers that absorb light in the wavelength region > 630 nm are considered more suitable [8, 21, 81].

Lasers are preferred light sources for PDT because these sources produce highly intense monochromatic light which depending on type of laser can be matched with absorption band of a particular photosensitizer. The laser light can be tightly focused to allow its efficient delivery to the target site through optical fiber. Argon dye, potassium-titanyl-phosphate (KTP) dye, metal vapor lasers, and most recently diode lasers have been used for clinical PDT around the world [28].

Compared to Lasers, the noncoherent light sources (*e.g.*, conventional arc lamps) are safer, easy to use, and less expensive and the emission can be matched with the absorption band of various photosensitizers in conjunction with optical filters of selective wavelength(s).

The disadvantages of conventional lamps include significant thermal effect, low light intensity, and difficulty in controlling light dose. Nowadays, several noncoherent light sources are available for example, the BLU-U light illuminator (DUSA Pharmaceuticals, Inc.), is an illumination system for PDT of actinic keratosis (AK) using ALA. The LumaCare™ lamp (MBG Technologies) is a compact portable fiber optic delivery system provides interchangeable fiber optic probes containing a series of lenses and optical filters. It can generate light of specific bandwidth between 350-800 nm in a variable power for a broad range of photosensitizers. Light emitting diode (LED) is another emerging PDT light applicator. LED can generate high energy light of desired wavelengths and can be assembled in a range of geometries and sizes [28, 29, 30, 31, 32, 33].

1.4 Mechanism of tumor destruction by PDT

There are three main inter-related mechanisms by which PDT mediates tumor destruction: direct cytotoxic effects on tumor cells, damage to the tumor vasculature, and induction of a robust inflammatory reaction that can lead to the development of systemic immunity [11]. The relative contribution of these mechanisms depends to a large extent on the type and dose of PS used, the time between PS administration and light exposure, total light dose and its fluence rate, tumor oxygen concentration.

1.4.1 Direct killing of tumor cells

It is generally accepted that the intracellular localization of the photosensitizer coincides with the primary site of photodamage. This is because the singlet oxygen generated in

photochemical reaction has a very short life and very limited diffusion in biological systems (half-life: 0.04 μ s, radius of action: 0.02 μ m) [34, 35]. Generally, photosensitizers localizing to the mitochondria or the ER promote apoptosis, while PDT with photosensitizers targeting either the plasma membrane or lysosomes, can either delay or block the apoptotic program predisposing the cells to necrosis [34, 36]. Apoptosis is programmed cell death which can be identified by characteristic morphological changes in cells such as nuclear condensation, cleavage of chromosomal DNA into internucleosomal fragments, cell shrinkage, membrane blebbing, formation of apoptotic bodies without plasma membrane breakdown, exposure of phosphatidylserine in the outer leaflet of the plasma membrane, and phagocytosis by neighboring cells [34,36,38]. In vivo, these apoptotic bodies are scavenged by phagocytes and thus inflammation is prevented, and cells die in an immunologically controlled way. Apoptosis requires transcriptional activation of specific genes, including the activation of endonucleases, consequent DNA degradation into oligonucleosomal fragments, and activation of caspases [38].

Necrosis is generally believed to be an un-programmed accidental cell death [34]. Necrosis is a spontaneous form of cellular damage characterized by cytoplasm swelling, fragmentation of cell organelles and disruption of the plasma membrane, leading to the release of intracellular contents and in vivo inflammation [34, 39-44]. Moreover, evidence indicates that autophagy may also be induced by PDT, when 1 subcellular organelle such as ER and mitochondria are damaged by PDT and survival mechanism are initiated to remove damaged organelle from cells [45-47].

1.4.2 Tumor Vasculature damage

PDT can also induce vascular shutdown, limiting the oxygen and nutrient supply to the tumor. The limitation of oxygen and nutrients supply leads to severe tissue hypoxia and death of tumor cells. There have been a number of reports suggesting that PDT induces microvascular collapse [48-54] and vascular effects were associated with a delay in tumor growth. Photosensitizers, such as a pyropheophorbide derivative [50], benzoporphyrin derivative (BPD) [51], HPD [52] and Photofrin [50] have been shown to induce tumor vasculature damage.

1.4.3 Immune response

It is known since long time that PDT leads to infiltration of immune cells such as lymphocytes, leukocytes and macrophages into the treated tissue, indicating activation of the immune response [55,56]. The inflammatory cytokines interleukin (IL)-6 and IL-1, but not tumor necrosis factor- α (TNF- α), have been shown to be up-regulated in response to PDT [57, 58]. It has also been reported that CD8⁺ T-cell activation and/or tumor infiltration of immune cells is an important factor in PDT efficacy [59-62]. PDT-induced acute local and systemic inflammation is believed to play significant role in the maturation and activation of dendritic cells (DCs) which in turn is required for the activation of tumor-specific CD8⁺ T cells and the induction of antitumor immunity [62-66]. It has also been suggested that since activation of DCs by dead and dying tumor cells is associated with

enhancement of antitumor immunity, the *in vitro* PDT-treated tumor cells may act as effective antitumor vaccines [67, 68, 69, 70].

1.5 Brief history of Photodynamic Therapy

Light has been used as therapy for more than three thousand years. Ancient Egyptian, Indian and Chinese civilization used light to treat various diseases including psoriasis, rickets, and vitiligo and skin cancer [71]. In one of India's sacred books *Atharva-veda* (1400 BC) the use of seeds of the plant *Psoralea corylifolia* for the treatment of vitiligo is described. Psoralens are the photoactive components of these seeds. However, around 100 years ago, O. Raab showed the cytotoxic effects of the combination of acridine and light on infusoria (*Paramecium caudatum*) [72]. But, actually N. Finsen during 1900s used the term 'Phototherapy' or the use of light to treat disease like small pox and tuberculosis. He was awarded with Nobel Prize in 1903 for his work in phototherapy [73, 74]. Moreover, the term 'photodynamic action' was coined by A. Jesionek and H.v.Tappeiner (Professor of O.Raab). They had treated the skin tumors with eosin and white light in 1903 [75].

The class of compounds most often used today i.e. porphyrins was investigated by F. Meyer-Betz in 1913. He studied the PDT effects of hematoporphyrin (HP) and its derivatives in rat tumors following systemic administration of the photosensitizers [76]. Modern photodynamic therapy (PDT) was initiated by R.L. Lipson and E.J. Blades, who

showed that an impurity in HP was the tumor-localizing agent, and not the parent compound. This led to the “synthesis” of hematoporphyrin derivative (HPD), a mixture of porphyrins produced by the acid treatment of HP [77]. The exact chemical composition and structure of this mixture remains unclear. T. J. Dougherty and colleagues developed HPD further for laboratory and clinical investigations in 1970s and 1980s [78]. The history of photodynamic therapy can be depicted as shown in Fig. 1.4.

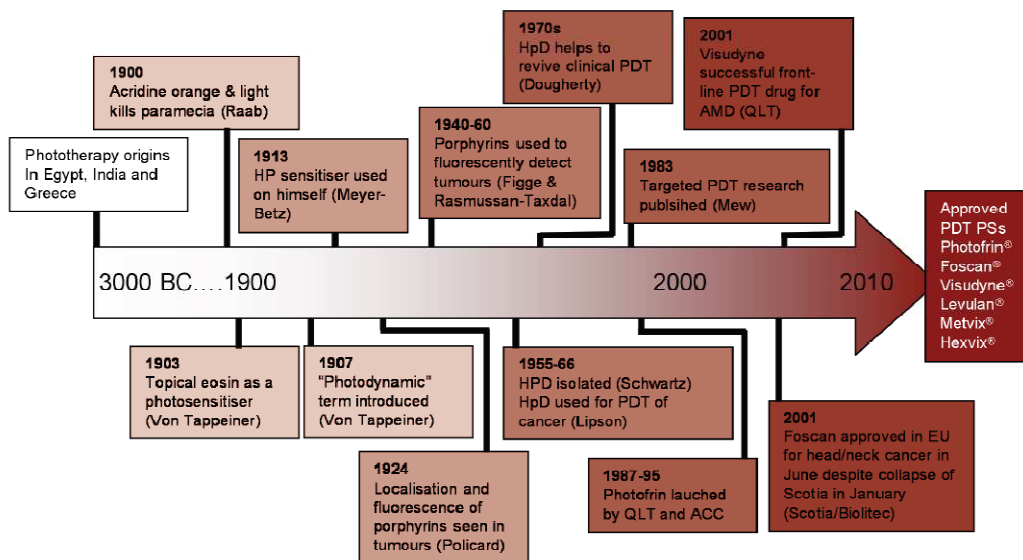


Figure 1.4. Historical development of PDT [Adopted from Celli et al, 2010]

1.6 Status of Photosensitizer in the development of PDT

Most of the currently approved clinical photosensitizers belong to the porphyrin family. Conventionally, the photosensitizers that developed between the 1970s and early 1980s are called **first generation photosensitizers** (*e.g.*, Photofrin[®]). While the Porphyrin derivatives or other synthetic photosensitizer made since the late 1980s are called **second generation photosensitizers** (*e.g.*, ALA). The **third generation photosensitizers** generally refer to the modifications such as conjugates of photosensitizer with biological molecules for *e.g.*, antibody conjugate, liposome conjugate for which cancer cells shows higher affinity [18,78].

1.6.1 First Generation Photosensitizers

Hematoporphyrin and its derivatives comprise the first generation of photosensitizers. The first generation photosensitizers starts in the 1960s, when R. Lipson *et al* initiated the modern era of PDT at the Mayo Clinic [80]. HPD has been partially purified to remove the less-active porphyrin monomers, to form Photofrin[®] (also called porphyrmer sodium) [19], a widely used photosensitizer in clinical PDT. Photofrin[®] was first approved for prophylaxis of bladder cancer in Canada on April 16, 1993 [78]. Since then, it has been approved in several countries for the treatment of not only bladder but also oesophageal, gastric, cervical, and lung cancers [78,81]. Photofrin fits some of the criteria for ideal photosensitizers but suffers from several drawbacks. First, it is a complex mixture of

porphyrins with various monomeric and oligomeric forms, so poorly characterized chemically. Secondly, its long wavelength falls at 630 nm, which lies well below the wavelength necessary for maximum tissue penetration. Finally, it induces prolonged cutaneous photosensitivity, and patients are advised to keep away from direct sunlight (at least for a month or so) after treatment [82, 83].

1.6.2 Second Generation Photosensitizers

To overcome the drawbacks recognized with Photofrin, a variety of other photosensitizers that exhibit a stronger absorption band in the red wavelength region have been investigated. These, photosensitizers are pure synthetic compounds, composed of an aromatic macrocycle such as porphyrins benzoporphyrins, chlorins, bacteriochlorins and phthalocyanins. Some of the important second generation photosensitizers that are clinically approved or are under clinical investigations are listed in Table 1.1.

Tetra (m-hydroxyphenyl) chlorin (mTHPC or Foscan[®]) marketed by Scotia Pharmaceuticals, Kentville, Nova Scotia, Canada is clinically approved for recurrent head and neck cancers in Europe and undergoing clinical testing in US [11]. The only other photosensitizer that has been clinically approved is Benzoporphyrin derivative monoacid ring A (BPD-MA or Verteporfin[®]) marketed by QLT Phototherapeutics Inc. Although, BPD-MA is mainly used for PDT of age-related macular generation, it appears to be useful for the treatment of pancreatic and skin cancer also [83]. BPD-PDT also has been tested for treatment of atherosclerotic plaques [84] and psoriasis [86, 87]. Tin ethyl etiopurpurin (SnET2 or Purlytin[®]) marketed by Miravant, Santa Barbara, CA, USA is under phase II/III clinical trials for advanced breast cancer, Kaposi's sarcoma in patients with AIDS, and

prostate cancer [88]. The silicon phthalocyanine (Pc 4) is developed at Case Western Reserve University and University Hospitals of Cleveland [89]. Pc 4 has high extinction coefficient ($\epsilon > 2 \times 10^5$) at 672 nm and has been found effective in preclinical studies in human tumor cells *in vitro* and in animal tumor models [90, 91]. Currently it is under clinical trials in US for the treatment of cutaneous T cell lymphoma. Lutetium texaphyrin/Lutex (LutrinTM) marketed by Pharmacyclics, Sunnyvale, CA, USA is a long wavelength absorbing (λ_{abs} is 732 nm) water-soluble photosensitizer that is undergoing clinical trials in US for the PDT of breast cancer [11].

Table 1.1: Current status of Clinically Applied Photosensitizers. Adopted from [Patrizia Agostinis *et al*, Photodynamic Therapy of Cancer: An Update, CA Cancer J Clin. 2011; 61:250–281]

Photosensitizer	Structure	Wavelength (nm)	Approved	Trials	Cancer types
ALA esters	Porphyrin-precursor	635	Europe		Skin, bladder
Temoporfin (Foscan) (mTHPC)	Chlorine	652	Europe	United States	Head and neck, lung, brain, skin, bile duct
Verteporfin	Chlorine	690	Worldwide-(AMD)	United-Kingdom	Ophthalmic, pancreatic, skin
SnEt2 (Purlytin)	Chlorin	665		United States	Skin, breast
Silicon phthalocyanine (Pc4)	Phthalocyanine	675		United States	Cutaneous T-cell lymphoma
Motexafin lutetium (Lutex)	Texaphyrin	732		United-States	Breast

1.6.2.1 Chlorophyll derivatives as potential photodynamic agents:

However, most of the second generation photosensitizers are prepared by total synthesis where the yield remains often low, resulting in a lot of chemical waste and a high price for the final product. These drawbacks can be minimized if the photosensitizer is a natural compound or can be prepared from a natural precursor by simplistic synthetic procedures [81]. Among second generation photosensitizers the derivatives prepared from plant pigment 'chlorophyll-a' have received considerable attention because they possess significantly higher absorption in the longer wavelength region (660-800 nm) which is a desirable feature for achieving adequate yield of singlet oxygen using lower concentrations and higher depth of treatment due to use of longer wavelengths (> 650 nm) [81,92]. The chlorophyll-a (Chl-a), itself is a hydrophobic photosensitizer due to the presence of lipophilic phytyl group and tends to aggregate in aqueous solvents and in nonpolar organic solvents, which hinders significantly its ability to generate $^1\text{O}_2$. Also, it is very unstable, undergoing oxidative degradation in the presence of light, acid, bases and alcohols. Although its photophysical properties are suitable for PDT, Chl a has only rarely been used as a photosensitizer in biological systems because of its high aggregation tendency and low solubility in physiological liquids [81,93, 93, 95]. However, Chl-a is not suitable for pharmaceutical application but may provide a suitable source for the synthesis of new stable derivatives. Also, various Chl-derivatives have been synthesized and evaluated for their PDT efficacy. On the basis of chemical nature Chl-a derivative can be categorized in two classes: the hydrophobic such as pheophorbide and its derivatives and the hydrophilic one such as chlorin e6 and chlorine p_6 and their derivatives.

1.6.2.2 Pheophorbide and its derivatives:

Pheophorbide-a (Pheid a) is a metal-free chlorophyll (Chl) derivatives prepared from the directly Chl mixture, by partitioning the mixture between 30% (w/w) aqueous hydrochloric acid and diethyl ether [81]. However, Pheid a ($\epsilon \sim 43980$ at 660 nm) contains a hydrophilic propionic acid residue, which makes it an amphiphilic photosensitizer, but in aqueous solutions, Pheid a forms aggregates. The singlet oxygen quantum yield (Φ_{Δ}) of Pheid a in organic solvents such as in ethanol and carbon tetrachloride is 0.51 and 0.80 respectively [81, 96]. Pheid-a and its derivatives have been widely investigated for PDT of uterine, colon, hepatic and pancreatic cancers. Recent studies using Zn-pheophorbide a has been shown that it exerts strong photodynamic effect, leading to 100% cell mortality at very low concentrations ($\sim 1 \times 10^{-6}$ M) and at low light doses (5 J/cm^2) [97]. Another pheophorbide-a derivative HPPH (2-[1-hexyloxyethyl]-2-devinyl pyropheophorbide-a) with trade name Photochlor[®] is under clinical trials for lung, skin, head and neck, and esophageal cancers [98]. The clinical results with HPPH-PDT in patients were reported to be quite promising without any significant skin phototoxicity after 4-5 days post-treatment [98, 99]. Recently, the conjugates of the pheophorbide-a with anticancer drugs doxorubicin (DOX, 2) and paclitaxel (PTX, 3) indicated that the conjugate is found to more effective in various cell lines including MCF7 (breast adenocarcinoma), KB (mouth carcinoma), HeLa (cervical cancer), U-87MG (glioblastoma), A549 (lung adenocarcinoma), AT-84 (oral cancer), and YD-10B (oral cancer) cells [99-102].

1.6.2.3 Chlorin e6 and its derivatives:

Chlorin- e_6 (Ce_6) because of three carboxylic acid groups in the molecule is a hydrophilic photosensitizer, which is synthesized by alkaline hydrolysis of Pheid-*a*. Although, Ce_6 has good photodynamic properties ($\epsilon \sim 25000$ at 654 nm) with good singlet oxygen yield [81, 103] to utilize it for PDT it has been converted into various derivatives, including mono-L-aspartyl chlorine e_6 (MACE), diaspartyl Ce_6 , monoseryl Ce_6 and other amino acid derivatives which had improved efficacy and decreased side effects compared to the first generation photosensitizers. MACE, also termed as talaporfin sodium is currently undergoing clinical trials in various countries under various trade names such as Laserphyrin, Litx, LS-11, ME-2906, NP_{e_6} , by the Nippon Petrochemicals (Japan), Meiji Seika Kaisha Ltd. (Japan), Light Sciences Oncology (USA) [104]. MACE is synthesized by joining L-aspartic acid with an amide bond to the propionic acid residue of Ce_6 . MACE is more hydrophilic than Ce_6 because of presence of extra ionizable carboxyl group of aspartic acid. It exhibit very strong absorption peak ($\epsilon \sim 38000 \text{ M}^{-1} \text{ cm}^{-1}$ at 664 nm) and high singlet oxygen yield of 0.77 in phosphate-buffered D_2O solution. It has been reported that the skin photosensitivity caused by MACE disappeared faster than the existing photosensitizer, which leads to limited duration of skin sensitivity [81]. Clinically, in the patients with early lung cancer the complete response was obtained in 85.7% of the lesions (36/42 lesions) by the administration of 40 mg/m^2 followed by laser irradiation at 100 J/cm^2 4-6 hours later [104, 105]. The clinical trials using MACE has been first started in Japan under the supervision of Nippon Petrochemical (Osaka, Japan) for superficial malignancies of the skin and nasopharynx. Good response rates were seen for light

fluences of 50–200 J/cm², applied at 4–8 h after drug, and skin photosensitivity was limited to the first 2–4 days [105]. In USA, MACE-PDT is currently undergoing phase II trials for glioma and phase III trials for metastatic colorectal cancer and hepatoma.

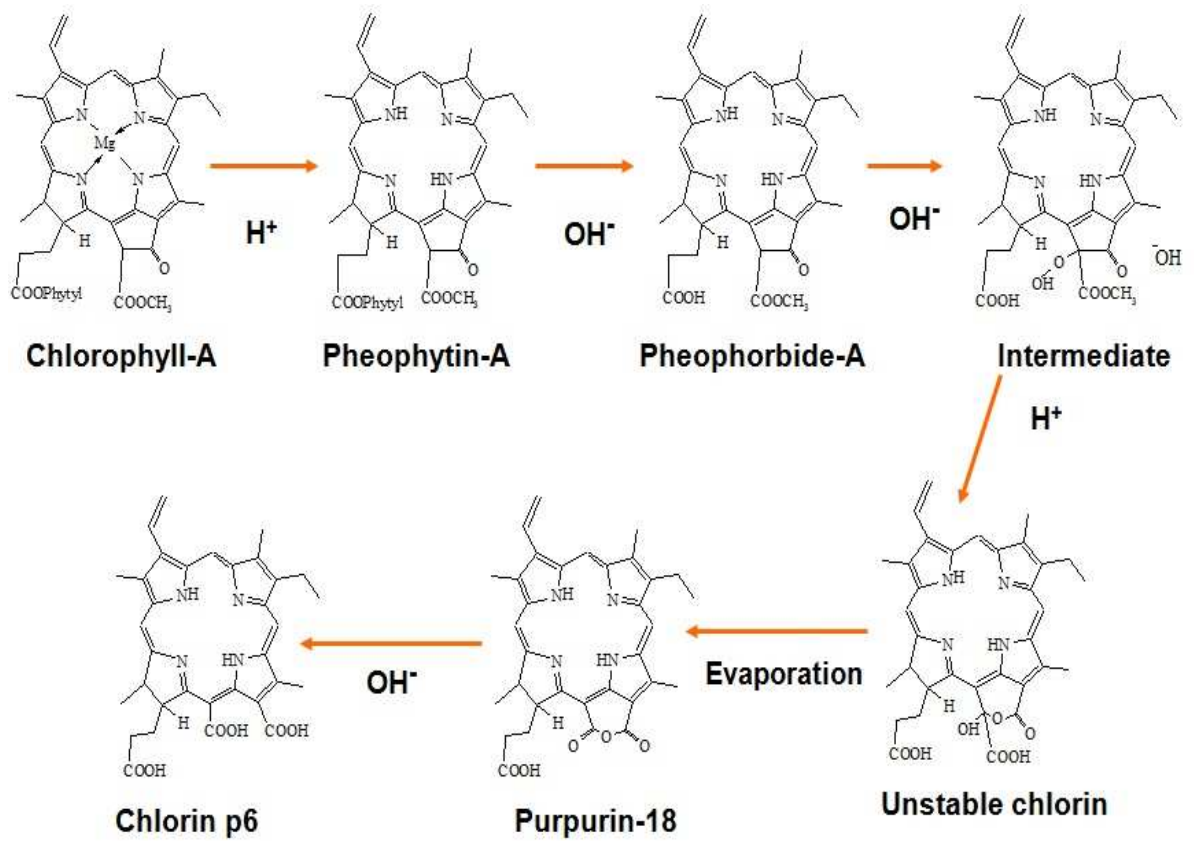
Some other *Ce₆* derivatives such as Radachlorin (RADA-PHARMA Ltd., Russia) and Photodithazine (Veta Grand Co., Russia) are in clinical trials or approved for some diseases in Russia [105, 107, 108]. *Ce₆* is the common component in Photolon, Radachlorin and Photodithazine. Radachlorin contains sodium *Ce₆* (90-95%), sodium chlorin *p₆* (5-7%) and an unidentified chlorin (1-5%) [108]. Photodithazine is a mixture of *Ce₆* (60%), chlorin *p₆*, and purpurins 7 and 18 [108]. PVP is additionally used in Photolon to increase its stability by preventing *Ce₆* aggregation and to improve solubility of more hydrophobic mono- and diethyl ethers of *Ce₆* in aqueous media [110]. Photolon, Radachlorin and Photodithazine have absorption maxima at around 400-410nm and 650-670 nm [111, 112]. Clinical trials with Photolon, Radachlorin and Photodithazine have demonstrated very low dark toxicity, high selectivity (within 0.5-5 h), high phototoxicity and rapid clearance (around 2 days) [112-115]. However, these *Ce₆* derivatives are mixtures of many compounds and due to this unstable for the longer time periods, had low therapeutic efficiency, required high doses and had low selectivity. Additionally, *Ce₆* in Photolon contain process and degradation related impurities chlorin e4, 151-hydroxyphyllochlorin, rhodochlorin, etc. [105,107,108]. Moreover, due to these drawbacks additional clinical studies are needed to evaluate their clinical potential for eventual use in other countries [103] [100].

1.6.2.4 Chlorin p_6 and its derivative:

Chlorin p_6 is another chlorophyll-a derivatives can be prepared from pheophorbide-a. Pheophorbide-a first converted in to Purpurin-18 (Pp-18), which upon alkaline hydrolysis converted in to chlorin p_6 . The schematic diagram for synthesis of chlorin p_6 from chlorophyll-a is shown in Fig. 1.1. While, Pp-18 is a hydrophobic photosensitizer having good photophysical and photochemical properties such as high absorption coefficient ($\sim 41,800 \text{ M}^{-1} \text{ cm}^{-1}$) at 700 nm and good singlet oxygen yield (~ 0.7 in diethyl ether), but gets aggregated more often in aqueous medium [116]. Thus, a suitable delivery vehicle is required for its administration in to the body. Moreover, the anhydride ring of P18 is very sensitive to the presence of nucleophiles. Therefore, P18 may not be very stable in the body, because of the presence of biomolecules, such as proteins, which can act as nucleophiles and causes opening of the anhydride ring [117]. However, this can ultimately lead to the formation of a photoactive compound chlorin p_6 , which is a amphiphilic photosensitizer having three ionizable carboxyl groups in the lower periphery of the molecule and a absorption band at 656 nm with absorption coefficient $\sim 24,300 \text{ M}^{-1} \text{ cm}^{-1}$ and good singlet oxygen generation capacity ($\Phi_{\Delta} \sim 0.60$ in ethanol) [81]. Chlorin p_6 (Cp_6) is structurally similar to Chlorin e_6 except the absence of a methyl group at meso positioned carboxylic group. The synthesis and phototoxic property of chlorin p_6 was first reported in 1986 by Hooper et al [117]. Studies have been reported on the use of some derivatives of chlorin p_6 for PDT of both *in-vivo* as well as *in-vitro* studies such as lysyl chlorin p_6 for glioma tumors in rats, lysyl chlorin p_6 diester and triester analog for murine leukemia

L1210 cells, 13, 15-N-(3'-hydroxypropylcycloimide) chlorin p_6 and its methyl ester for A549 human adenocarcinoma cells [118-121].

Detailed studies carried out at RRCAT on photophysical, photochemical and photo biological characterization of Cp_6 revealed that it is a promising photosensitizer for PDT of cancer. Cp_6 is a water soluble photosensitizer due to presence of three ionizable carboxylic groups; it is therefore easier to prepare its injectable physiological solution for systemic delivery [122]. Studies have been carried out on the photophysical properties of chlorin p_6 , its uptake in cell lines and photodynamic treatments of tumors in hamster cheek pouch model. These studies have shown that chlorin p_6 which exists predominantly as anionic species at physiological pH, undergoes change in the state of ionization upon decrease in the pH to form an anionic species with smaller charge and higher hydrophobicity [123].



Scheme 1.1. Synthesis of Chlorin p_6 from Chlorophyll-A.

The increase in hydrophobicity at lower pH is believed to be the main reason for higher uptake of hydrophilic chlorin-type molecules in tumor where intercellular pH is known to be slightly acidic than physiological pH. Studies with model membrane system (liposomes) showed that change in pH from physiological to slightly acidic lead to deeper penetration of Cp_6 in lipid regions [123]. Measurements on fluorescence emission lifetimes as well as quenching of fluorescence with KI suggest that at pH 5.0 the drug localizes in the central region of lipid bilayer and for pH 6.0 and higher the drug binds closer to the liposome interface [123]. These results suggested that increase in hydrophobicity at low pH would have significant influence on the cellular uptake of Cp_6 . Indeed, results of our studies on colon cancer cell line show that the uptake as well as the phototoxicity of Cp_6 increases with decrease in pH of extracellular medium from 7.4 to 6.0 [124]. This effect was however cell line dependent since no significant change in uptake and photosensitivity was observed at different extracellular pH in breast carcinoma cell lines [124]. Measurements on intracellular site of photodamage showed that in Colon cancer cells photosensitivity to lysosomes increases with decrease in pH whereas in MCF-7 cells damage to mitochondria predominates at all pH suggesting that the mechanism for uptake is different for the two cell lines. While the drug accumulation in Colo-205 cells appeared to occur mainly through endocytosis, its uptake in MCF-7 is primarily through diffusion rather than endocytosis [124].

In-vivo studies carried out in hamster cheek pouch model on efficacy of Cp_6 for photodynamic treatment of tumors led to promising result. Cp_6 showed preferential accumulation in small size tumors (dia < 5 mm), rapid clearance from skin and complete

tumor regression after PDT [125]. However, for relatively large tumors its uptake was poor which compromised the PDT efficacy. Although, increasing drug dose (4 mg/kg body weight) led to complete tumor regression for larger tumor of size $\sim 130 \text{ mm}^3$, tumors beyond this size regressed only partially [126]. Though Cp_6 was found effective it required higher dose for larger tumors increasing the risk of systemic toxicity therefore further studies are necessary to improve its tumor selectivity and PDT efficacy, which is the main motive of the present research work, and will be discussed in detail in the later part of this chapter.

In fact, various innovative attempts have been employed by researchers to enhance the selectivity of photosensitizers and improve its therapeutic efficacy by utilizing several drug delivery strategies, which was developed by exploiting unique characteristics of tumor biology [127]. This concept has led to the origin of third generation photosensitizers, which was devised for targeted photodynamic therapy.

1.6.3 Third Generation Photosensitizers or Targeted Photodynamic therapy

Most of second generation photosensitizers accumulate in tumor tissue through passive targeting mechanism, which is regulated mainly by physicochemical properties of the photosensitizer. Moreover, due to this PS may distribute in normal tissue and thus can lead to systemic phototoxicity. The selectivity of PDT can best be increased employing a photosensitizer that is enriched more in the target tissue. The targeted delivery of photosensitizer to defined cancer cells is one of the main challenges and a very active field

of research in the development of treatment strategies to minimize side-effects of PS. Therefore one goal in the field of targeted therapies is to develop chemically derivatized drugs or drug vectors able to target cancer cells via specific recognition mechanisms [128]. The more precise targeting would enhance photosensitizer efficiency and reduce harmful side effects of the treatment. There are several strategies, which devised to enhance PS selectivity based on either use of suitable delivery vehicles or exploitation of level of difference in expression of specific cellular antigens and cellular surface receptor by cancer cells compared to normal cells [127]. Photosensitisers have been shown to target tumors when incorporated into delivery vehicles such as liposome preparations [129,130] and nanoparticles [135].

The most promising approach is to targeted delivery of photosensitizer via receptors present on cancer cells. This approach utilizes the fact that tumor cells typically have increased expression of cell surface receptors for various growth factors or regulatory bio-molecules. For this purpose, photosensitizer conjugated to monoclonal antibodies or small antibody fragments have been investigated [132,133,134]. Monoclonal antibodies (mAb) have been used in a variety of ways in the management of cancer, including diagnosis, monitoring, and treatment of disease because of their inherent abilities to recognize and bind to tumour-associated antigens that are either exclusively expressed on tumour cells - a rarity - or over-expressed as compared to normal tissue [133,134,135]. The first time in 1983 Mew et al was conjugated the photosensitizer hematoporphyrin derivative (HpD) with a monoclonal antibody anti DBA/2J myosarcoma M-1, [136, 137] since then several conjugates of various photosensitizers with MAbs have been prepared

and investigated for their tumor selectivity and PDT efficacy. For example anti-EGFR MAb-BPD PIC directed against squamous cell carcinoma [138,139,140], Chlorin e6-dextran-anti-Leu-1 or anti BSA MAbs [141,142,143,144], pyropheophorbide *a* (Ppa) with anti-HER2 mAbs for ovarian and breast cancer cells [145,146], also Ppa coupled to various MAbs C6.5 anti-HER2, MFE-23 anti-CEA, HuBC-1 anti EDB fibronectin used against for ovarian, colorectal and fibroblast cancer cells [146], 5-(4-isothiocyanatophenyl)-10,15,20-tris-(4-N-methylpyridiniumyl)porphyrin trichloride (PS2)- 35A7MAb conjugates for colon carcinomas [147,148], AlPc(SO₂Cl)₄ to an antibody (E7) for human bladder carcinoma [149], photosensitizer (tin(IV) chlorin e6) couples to phage-derived antibody fragment (anti-fibrogen antibody L19) directed against endothelial cells [150,151], *meso*-5,10,15,20-tetrakis(*N*-methyl-4-pyridyl)porphine (TMPyP4) conjugated with monoclonal antibody 425, recognizing epidermal growth factor receptors towards vulvar cells [152,153]. However, the feasibility of this drug delivery strategy is highly dependent on PS-to-mAb ratio, which makes the syntheses complicated, especially since the mAb and photoactive drug need to retain their biochemical and photophysical functions, respectively, after conjugation [154, 155, 156]. Indeed, the majorities of reports in the literature describing the synthesis of such constructs highlight the significant problems with systemic delivery and reduced singlet oxygen yields, both of which will substantially decrease the efficacy of PDT for these strategies. Moreover, this class of selective PS targeting strategy has been widely investigated but the concept still needs the clinical successes due to some of the reasons, such as nonspecific uptake by the liver, kidney, and spleen [157]; shared antigen cross-reactivity [158,159]; significant losses in biological activity of the antibody, probably due to interference in the antigen-binding region by PS

molecules [154]; and poor penetration into solid tumours [160,161]. Thus, research has focused on the targeting of receptors rather than antigens that are preferentially expressed in tumor tissues.

Photosensitizers conjugated directly to ligand or molecules specific to receptors on cancer cells is another way for improving the tumor selectivity and PDT efficacy of photosensitizers [162]. This approach has been investigated in various studies by conjugating PSs with the ligands or molecules such as low-density lipoprotein (LDL), epidermal growth factor (EGF), carbohydrate, folic acid, insulin and transferrin etc [162,163]. These studies are described below.

1.6.3.1 LDL Receptor targeting:

The expression of LDL receptors is higher in most of neoplastic cells and proliferating endothelia because of the more demand for exogenous cholesterol for membrane synthesis [164,165]. Consequently, lipophilic PSs provide enhanced tumour localization by virtue of binding to LDL and exhibit greater retention than hydrophilic drugs [166,167,168]. Therefore, the role of LDL receptors as carrier molecules to improve phototoxicity has been investigated using various photosensitizers, including hematoporphyrin derivative, zinc phthalocyanine, and chlorin e6 (Ce6). Polo et al have shown that both an amphiphilic hematoporphyrin IX (Hp) and a hydrophobic Zn (II)-phthalocyanine (ZnPc) photosensitizers bind to human LDL with molar ratios of 5-6:1 and 10-12:1 by human

HT1080 fibroblasts cells respectively. While, the hematoporphyrin-LDL complex is accumulated mainly through the high affinity LDL receptors, the changes in the apoB LDL structure induced by phthalocyanine association led to non specific endocytosis mediated internalization of Zn-phthalocyanine-LDL complex. Moreover the uptake of LDL-delivered hematoporphyrin, but not Zn-phthalocyanine, is about 4-fold higher in HT1080. However, human LDL-bound hematoporphyrin and Zn-phthalocyanine are up taken by 4R rat fibroblasts with similar efficiency [169]. Similarly, it has been reported that chlorin e6 (Ce6), covalently conjugated to LDL had significantly higher uptake of Ce6 (4-5 times) and phototoxicity (8 folds) in fibroblast and retinoblastoma cell line (Y79) [170] [170]. However, the use of LDL as carriers for photosensitizer delivery to target tumor tissues imposes certain limitations, connected with redistribution in the blood, depending on dynamics of interactions between photosensitizers and blood components, which are not yet fully understood [162,171].

1.6.3.2 EGF receptor targeting:

The most established cell proliferation targets used for actively targeting photosensitizers include human epidermal growth factor receptor (EGFR), which is widely expressed in many human tumors, particularly in glioblastoma multiform and in many epithelial tumors, such as head and neck, breast, renal cell or esophageal cancers [172,173]. This makes EGFR an important target for treatment of the type of cancers given above and epidermal growth factor (EGF) – a potent mitogenic and angiogenesis-stimulating factor – a potential

drug carrier. To date, this strategy has not been thoroughly investigated; only few research groups have used photosensitizer-EGF model [174,175,176,177]. Lutsenko and colleagues showed that conjugate of disulfochloride aluminium phthalocyanine with mouse EGF were seven times more phototoxic against human breast carcinoma cell line MCF-7 than free disulfochloride aluminium phthalocyanine [174]. As human EGF, in contrast to that of mice, may lose its biological activity due to presence of two amino groups in the lysyl residue after direct conjugation to photosensitizer, therefore Gijssens *et al.* conjugated tin (IV) chlorin e6 monoethylene diamine (SnCe6(ED)) with EGF through human serum albumin (HSA) as a linker. This conjugate showed a potent phototoxicity (IC₅₀ = 63 nM) towards MDA-MB-468 human breast adenocarcinoma cells dependent on EGF, because free SnCe6(ED) and SnCe6(ED) conjugated only to HSA revealed no phototoxic effect against these cells [175]. Animal studies (C57B1/6 mice) on the murine melanoma cell line B16 using the CoPC-EGF model exhibited promising results the mean life spans and survival times of the tumour bearing mice were increased [176]. Similarly, in-vivo studies carried out by Slastnikova et al in A431 human epidermoid carcinoma-bearing mice have shown that chlorin e(6)-modular nanotransporters{EGF} conjugate led to 94% tumor growth inhibition with 75% of animals surviving for 3 months as compared with free chlorin e(6), which resulted only 20 % growth inhibition [177]. Further work needs to be undertaken on EGF conjugates to fully evaluate their potential as PDT targeting agents [178].

1.6.3.3 Carbohydrate receptor based targeting:

Coupling of sugars to photosensitisers has also shown promise in the selective targeting of tumour cells [179,180,181,182]. Tumour cells have high energy requirements and their proliferation is often dependent on glucose uptake – elevated glycolysis rates are observed in cancer cells in comparison to healthy cells. Glucose traverses the cell membrane *via* receptor mediated endocytosis [180,181,182]. Porphyrin-saccharide bioconjugates have demonstrated greater binding affinities for cancer cells, which overexpress glucose transporter receptors [182]. Similarly, many conjugates have been synthesized to specifically target the lectin family of receptors which are overexpressed in certain malignant cells since they are involved in cell growth [183], cell adhesion [184], immune response and angiogenesis [185]. These receptors possess a carbohydrate recognition domain and exhibit a high affinity for b-galactoside glycoprotein [186, 188].

1.6.3.4 Folic acid receptor targeting:

Furthermore, the conjugates of PSs with folic acid, which target the folate receptor (FR) seems to hold better promise in targeted PDT [189, 190,191]. This approach of using folic acid as a potential tumour-targeting ligand has several unique advantages including: lack of immunogenicity; small size; chemical and functional stability; and simple and defined conjugation chemistry [190]. Folic acid has a high affinity for folate receptors which are up-regulated in numerous cancer cell types, such as ovary, kidney, lung, breast and brain carcinomas, and at the same time are absent in most normal tissues. Moreover, folic acid

can be easily conjugated with PDT sensitizers [191]. Schneider *et al.* synthesized conjugates of monocarboxylic acid tetraphenylporphyrin with folic acid, which were taken up by KB nasopharyngeal cells 7-fold as much as free photosensitizer. These conjugates showed also significant photodynamic effects against KB cells while free tetraphenylporphyrin showed no photodynamic action at the same conditions [192]. Stevens *et al.* synthesized folate receptor-targeted SLN (a mean diameter <200 nm) as a carrier for lipophilic derivative of hematoporphyrin in folate receptor overexpressing tumor cells. The results of *in vitro* study showed that introduction of folic acid into hematoporphyrin-stearylamine SLN greatly increases phototoxicity and cellular uptake in FR-positive KB cells when compared with non-functionalized nanoparticles [193]. Furthermore, Stefflova *et al.* observed an enhanced accumulation of Pyropheophorbide a-peptide-Folate conjugate in KB cancer cells (FR+) compared to HT 1080 cancer cells (FR-), resulting in a more effective post-PDT killing of KB cells over HT 1080 or normal CHO cells. *In vivo* studies showed that the conjugate also accumulate preferentially in KB tumors (KB vs. HT 1080 tumors 2.5:1) [194]. Recently, Syu *et al.* have shown that a single dose of folate-conjugated m-THPC-loaded micelles led to 92% tumor growth inhibition and reduction of vessel density [195]. García-Díaz *et al.* reported that incorporation of a model photosensitizer (ZnTPP) into a folate-targeted liposomal formulation led to 2-fold higher uptake and also improved photocytotoxicity by HeLa cells (folate receptor positive cells) than the non-targeted formulation [196]. However, additional pharmacokinetic and photodynamic effect studies are necessary to further validate this.

1.6.3.5 Insulin and other receptor based targeting:

Studies have also been carried out to target insulin receptors in human hepatoma cell line. For this purpose a conjugate of BSA insulin-chlorin e6 has been prepared and it was demonstrated that the conjugate was internalized by receptor-mediated endocytosis and required much lower concentration as compared to free chlorin e6 and also lower light doses was needed to activate the conjugate compared to free Ce6 [197]. However, no further studies have been carried out to explore this conjugate. In addition to the tumor surface receptors, nuclear receptors are targeted, as well and also limited number of studies have been performed to actively target tumor endothelial markers (ED-B domain of fibronectin, VEGF receptor-2, and neuropilin-1) [163].

1.6.3.6 Transferrin receptor based targeting:

Several types of cancer cells exhibit increased expression of transferrin receptors and therefore conjugate of transferrin and various photosensitizers have also been studied extensively [162]. Transferrin is a blood plasma glycoprotein for delivery of ionic iron. Bioconjugates composed of transferrin and hematoporphyrin were found to induce phototoxicity in erythroleukemic cells and the surviving cells did not reveal resistance to subsequent treatment with these conjugates [162]. The aluminium phthalocyanine tetrasulfonate encapsulated in distearoyl phosphatidylethanolamine-PEG liposomes

conjugated to transferrin exhibits 10-fold higher photodynamic effect than free photosensitizer, while the same photosensitizer in nontargeted liposomes revealed no photodynamic activity [198]. Derycke et al (2004) have reported that photodynamic therapy of HeLa cells incubated with 1 μ M Tf-Lip-ALPcS4 or ALPcS4 resulted in cell viabilities of 0.19% (95% CI = 0.02% to 0.36%) and 1.32% (95% CI = 0.46% to 2.19%), respectively. Higher concentrations of either ALPcS4 or Tf-Lip-ALPcS4 resulted in cell kills of more than 3 logs [198]. Also, same group had reported that transferrin-conjugated liposomes (Tf-Lip-ALPcS4) had much higher intracellular accumulation in AY-27 cells (384.1 versus 3.7 microM; difference = 380.4 microM, 95% CI = 219.4 to 541.3; P = .0095) compared to unconjugated liposomes (Lip-ALPcS4) [199]. Also, rats bearing AY-27 cell-derived bladder tumors exhibit higher tumor to normal tissue accumulation of Tf-Lip-ALPcS4, whereas free ALPcS4 resulted in nonselective accumulation throughout the whole bladder wall, and Lip-ALPcS4 led to no tissue accumulation [199]. In contrast with these studies Derycke et al have shown that targeting of hypericin by transferrin-conjugated PEG-liposomes did not significantly favour the photocytotoxicity and the intracellular accumulation of hypericin, in comparison with non-targeted PEG-liposomes or free hypericin [200]. Recently, Paszko et al [201] have synthesized polyethylene glycol (PEG)-grafted, transferrin (Tf)-conjugated liposome formulations of 5,10,15,20-tetra(m-hydroxyphenyl)chlorin (Foscan) in order to increase the efficiency of PDT in oesophageal cancer therapy. They had confirmed the expression of transferrin receptors (CD71) in the oesophageal cancer cell line, OE21 by immunoblot and confocal laser scanning microscopy. But, surprisingly delivering Foscan by transferrin-conjugated PEG-liposomes to oesophageal cancer cells did not improve the photocytotoxicity or the intracellular

accumulation of Foscan when compared to unmodified liposomes or indeed free photosensitizer. Although, Tf-targeted drugs and drug delivery systems have shown improved the therapy of many cancers, however, did not corroborate with these findings. This may be due to the tumour type, the choice of in vitro model or the delivery systems. Moreover, since the type and level of receptor expression can differ in different types of malignancies [201]. Therefore, there is a need to explore new targets and targeting molecules. Currently, there is considerable interest in identifying biomolecules and cell surface receptors that play significant role in tumor growth and development so that they can be used for selective targeting of tumor cells [162,163].

1.6.3.7 Histamine receptors can be exploited as potential therapeutic target:

Histamine is one of such bio-molecule that has received lot of attention due to increasing evidence on its involvement in tumor growth and development. Histamine is a biogenic amine which apart from its classical role in gastric acid secretion, inflammation, immunomodulation and in nervous regulation [202], has also been suggested to play an important role in tumor growth and development [203,204]. There are four types of histamine receptors H1, H2, H3, and H4 classified on the basis of their pharmacological properties, play different important role in various physiological process of body (Table 1.2). These receptors belong to the G protein coupled receptor family and are expressed in endothelial, mesodermal and epithelial cells. H1 and H2 receptors were the first two histamine receptor subtypes described and thus, the most frequently investigated in tumor cells and tissues. Typically, H1 receptors have been described as functionally coupled to

PLC activation and mediate many of its effects via the products of inositol phospholipid hydrolysis. However, many other signaling pathways have been shown to be activated after the stimulation of H1 receptors such as cGMP, arachidonic acid metabolites and cAMP [205, 206]. The H1 subtype, cellular responses mediated by the H2 receptor are probably due to the activation of various signaling pathways [205, 207]. The most common coupling described for the H2 receptor is the stimulation of cAMP production through a direct activation of adenylyl cyclase via a GTP mechanism, [205,208] which is present in a number of systems including brain slices, stomach mucosal cells and glands, canine fat cells, heart myocytes, vascular smooth muscle, basophiles and neutrophils [208,209]. Selective activation of the H1 or H2 receptor has been shown to produce inhibition or stimulation of tumor growth respectively, in a dose-dependent manner [205, 210, 211]. Although the four histamine receptors share a degree of sequence similarity, a considerable variation exists in their binding affinities with respect to histamine as well as towards other ligands. Relative abundance and differences in the affinity of the histamine receptor subtypes may explain these diverse effects of histamine. For example, in *N*-nitroso- *N*-methylurea (NMU)-induced mammary adenocarcinoma, the activation of the receptor with histamine concentrations up to 50 nM increases tumor cell proliferation whereas higher histamine levels inhibit cell growth via receptor activation [212]. Similarly, in the human pancreatic carcinoma PANC-1 cells, histamine at low concentration (0.01 μ M) increases tumor cell proliferation whereas at high concentration (10 μ M) decreases cell proliferation via receptor activation thereby inducing a G0/G1 cell cycle arrest associated with partial stimulation of cell differentiation [213]. The results reported by Medina et al. well illustrate this bivalent behaviour of histamine in regulating tumor cell growth [214]. They

investigated, for the first time, the expression of the H3 and H4 receptors in human benign and malignant mammary lesions. Although previous work demonstrated that the H3 receptor is expressed primarily in the central nervous system, Medina and colleagues have demonstrated the upregulation of H3 in breast carcinomas and its significant association with proliferating cell nuclear antigen expression and elevated HDC expression and histamine levels in the same samples. Moreover, they found that histamine at low concentration (0.01 nM) can increase breast cancer cell proliferation and this effect is mediated by receptor activation. On the other hand, histamine at 10 μ M decreases cell growth through activation of the H1, H2 and H4 receptors. H4 receptor activation can also induce apoptosis and decrease migration of the MDA-MB-231 cells. Taken together, these results clearly demonstrate that histamine can behave as a pro- or an anti-proliferative factor within the same tumor type cells, depending on its concentration and the receptor subtype to which it binds [214].

Table 1.2: Different types of histamine receptors, their location and functions [Adopted from ref.]

Type	Location	Function
H1 histamine receptor	Found on smooth muscle, endothelium, and central nervous system tissue	Causes vasodilation, bronchoconstriction, bronchial smooth muscle contraction, separation of endothelial cells (responsible for hives), and pain and itching due to insect stings; the primary receptors involved in allergic rhinitis symptoms and motion sickness
H2 histamine receptor	Located on parietal cells	Primarily stimulate gastric acid secretion
H3 histamine receptor	Found on central nervous system and to a lesser extent peripheral nervous system tissue	Decreased neurotransmitter release: histamine, acetylcholine, norepinephrine, serotonin
H4 histamine receptor	Found primarily in the basophils and in the bone marrow. It is also found on thymus, small intestine, spleen, and colon.	Plays a role in chemotaxis

Table 1.3: Expression of histamine receptor, intracellular histamine content and effect of histamine on cell proliferation in various types of carcinoma [Rivera ES, Cricco GP, Engel NI, Fitzsimons CP, Martin GA, Bergoc RM. Histamine as an autocrine growth factor: an unusual role for a widespread mediator. *Semin Cancer Biol* 2000; 10:15-23.]

Cell line references	Histamine receptors	HDC and histamine content	Effects on cell proliferation
Pancreatic carcinoma: Panc-1	H1 and H2	Hi release 3–4 nM Hi content 4–9 pmol/10 ⁶ cells	Inhibition by Hi or H2 agonists
Melanoma :A375-P, A875, WM35, WM983, HT168, M1/15	H1 and H2	Hi content 3–6 pmol/10 ⁶ cells, Hi release 3–4 nM	Different effects dependent on histamine concentration and cell line
Epidermoid carcinoma :A431 Uterine carcinoma ,HeLa.	H1		Increase in DNA synthesis and cell division
Gliomas:U-87MG, UT-98G, A-172,U-251MG, KALS-1, KINGS-1	H1	Hi release 50–120 nM	Hi increases 3H-timidine uptake in the six cell lines
Other glioma cell lines Colon carcinoma:59 C-170	H2		Inhibition by cimetidine Cimetidine inhibits, Hi-stimulated cell proliferation
Breast cancer :MCF-7,SKBR3, MDA-453	H1 and H2		
Ovarian carcinoma: SKOV-3			Hi stimulates cell growth
Mielocytic leukemia :HL-60	H1 and H2		Differentiation induced byHi via H2 receptors
Histiocytic linfoma:U937	H1 and H2		
Gastric carcinoma:MKN-45, MKN-45G,HGT-1	H2	Hi content < 1pmol/10 ⁶ cells	Inhibition by cimetidine
Basophilic leukemia KU-812-F		Hi content 9 pmol/mg prot.	

Although the hypothesis that histamine might be involved in carcinogenesis was proposed in the 1960s [215], it still remains under discussion today. Clarification of the molecular structure of histidine decarboxylase (HDC), i.e., the only enzyme responsible for the generation of histamine from L-histidine, has clarified up to certain extent the connections between histamine and cancer. The endogenous activity of HDC in tumor cells and tumor-infiltrating mast cells is likely to establish an autocrine loop in which histamine acts as a growth factor. Paradoxically, the exogenous administration of histamine at higher concentration seems to exert anti-tumoral properties through both direct and indirect effects on tumor cells. However, accumulated evidence points to a direct relationship between upregulation of HDC activity and growth of several types of human tumors. Overexpression of HDC at both the mRNA and protein levels and increased levels of histamine compared to the content of normal surrounding tissues have been shown in melanoma [216], small cell lung carcinoma [217], breast carcinoma [218], endometrial cancer [219] and colorectal carcinoma [220]. Nevertheless, evidences for the direct involvement of histamine in cancer progression remains to be elucidated. [221]

Histamine receptors are expressed in multiple malignant cell types (Table 1.3), and they can activate multiple signaling pathways [212]. It has been demonstrated in experimental mammary carcinomas, histamine becomes an autocrine growth factor capable of regulating cell proliferation via H1 and H2 receptors, as one of the first steps responsible for the onset of malignant transformation and remarkably, the treatment of animals with H2 antagonists produces the complete remission of 70% of tumors. Furthermore, the histamine antagonist led to tumor regression and also enhances patient survival after postoperative treatment.

For instance diverse clinical reports suggest that H2 antagonists have potential beneficial effects in the treatment of advanced malignant disease such as colorectal cancer, gastric cancer, liver metastasis, multiple myeloma, chronic lymphocytic leukemia and melanoma [222,223,224,225]. For instance, cimetidine (CIM), a H2 antagonists which is known to inhibit the growth of several types of tumors, including gastrointestinal cancers, both *in vitro* and *in vivo* in animal models [226,227]. Studies of the anti-tumor effects of CIM indicate multiple potential mechanisms of action, characterized by three overall characteristics: a) a direct inhibitory effect on tumor growth by blocking the cell growth-promoting activity of histamine [227,228] (Fig. 1.5) and an indirect effect by inhibiting tumor associated angiogenesis [229]; b) a cell-mediated immunomodulation by enhancing the host's immune response to tumor cells (Fig. 1.6) [230,231,232]; c) an inhibition of cancer cell migration [233] and adhesion to endothelial cells [234].

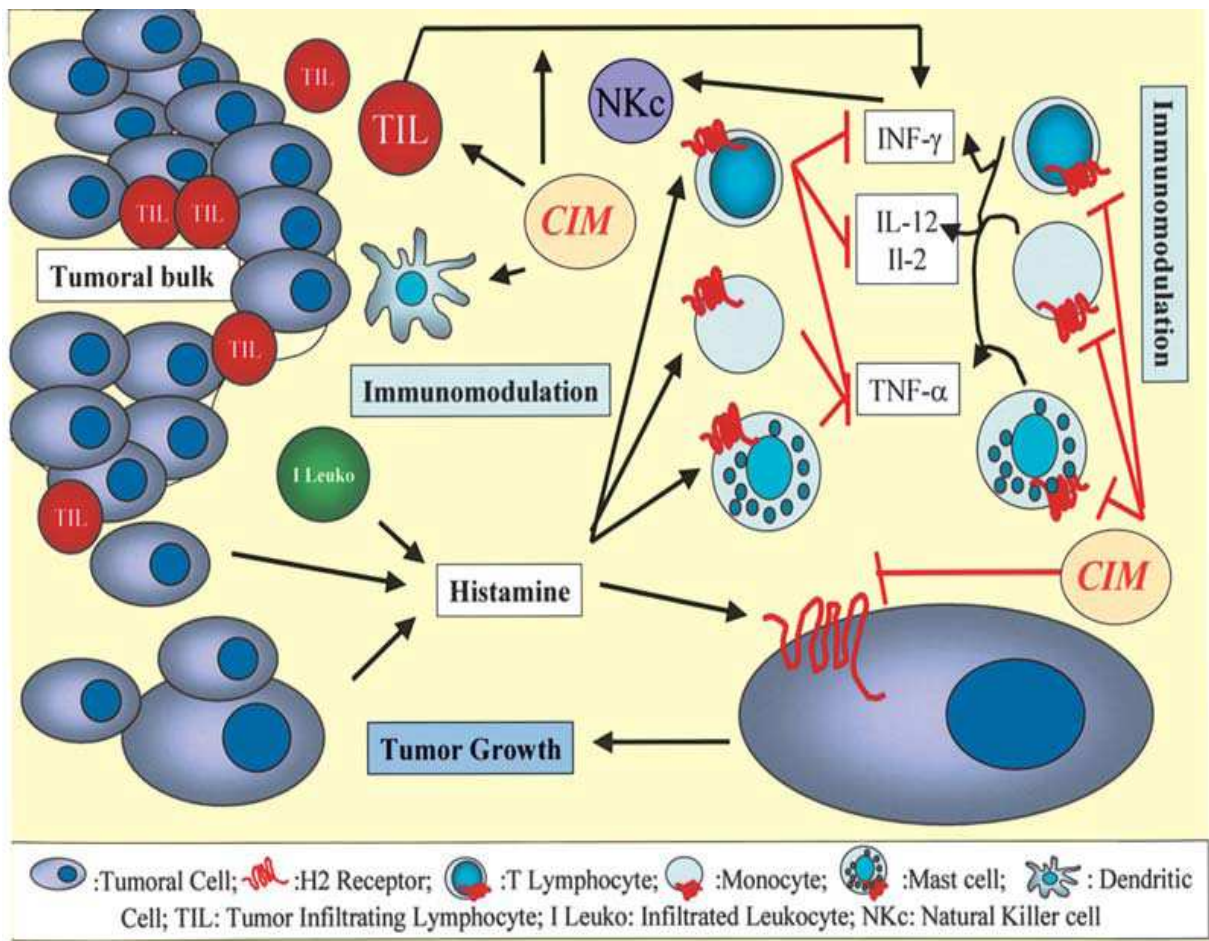
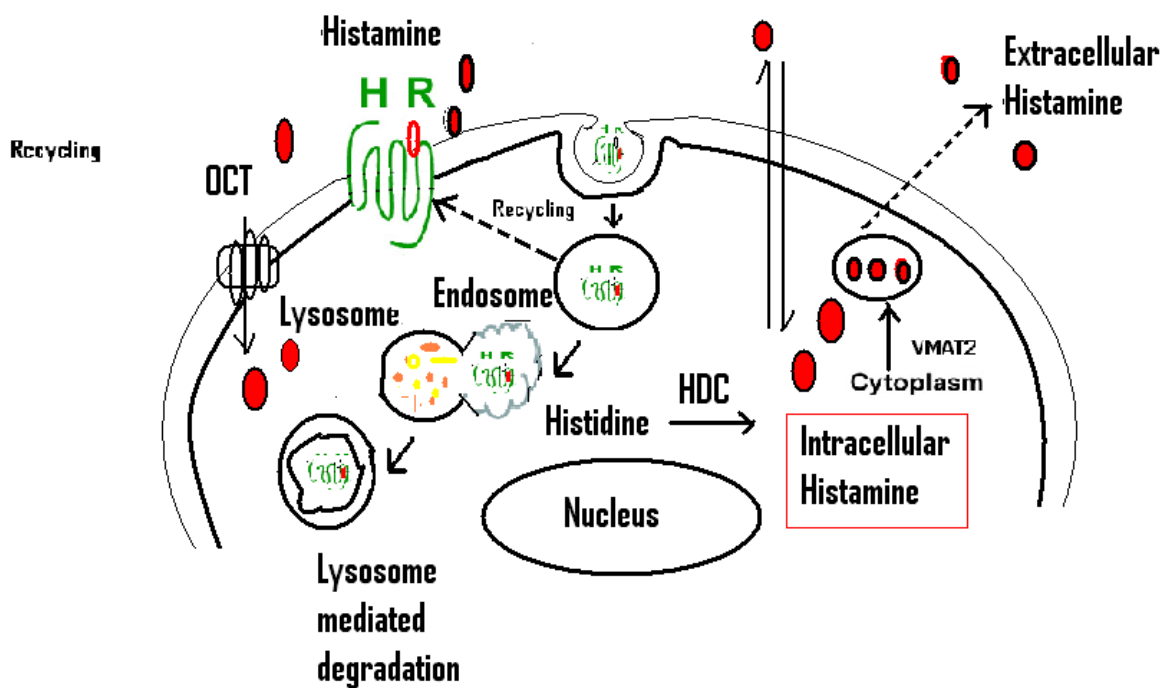


Figure 1.5. CIM inhibitory effect on tumor growth. CIM blocks the cell growth-promoting activity of histamine. The mechanisms proposed for the cell-mediated immunomodulation of CIM include the inhibition of suppressor T lymphocyte activity, the stimulation of natural killer cell (NKc) activity, an increase in interleukin-2 (IL-2) and interleukin-12 (IL-12) production in helper T lymphocytes, an increase in tumor inhibitory cytokines and the enhancement of the host's anti-tumor cell-mediated immunity [Adopted from reference no.233].

However, Studies in melanoma cells have shown a positive correlation between histamine production and histamine receptor expression suggesting up-regulation of histamine receptors and existence of autocrine control of melanoma progression by histamine [235].The schematic in Fig. 1.7 shows that how histamine established an autocrine loop for tumor growth and development.



Scheme1.2. The schematic shows autocrine loop of Histamine. It binds on histamine receptor or with other site such as OCT (organic cation transporter) and gets internalized. In addition to this it can also be generated in intracellular compartment by oxidative decarboxylation of histidine by HDC (histidine decarboxylas) [Adopted and remodified from reference no. 259].

Elevated levels of histamine receptors in malignant tissue almost 2-5 times higher than normal tissue has been reported in several types of malignancies e.g. breast carcinoma [236], melanoma [236] and adrenocortical cancer [237]. The expression of histamine receptor H1 and H2 has been found in several human cancer cell lines (Table 1.3) [212].

It has been suggested by various studies that the histamine receptors can be exploited as novel approach to treat cancer [238,239]. The use of Histamine for targeting photosensitizer in PDT of cancer has not been explored so far.

1.7 Aims of the present study:

In the present work, we have examined the possibility to exploit histamine receptors for improving delivery and photodynamic efficacy of Cp_6 in oral cancer cell lines and hamster cheek pouch model of oral squamous cell carcinoma. The use of Histamine for targeting photosensitizer in PDT of cancer has not been explored so far. The main objectives of this study are as follows:

1. To study cellular uptake and phototoxicity of Cp_6 -histamine conjugate in oral cancer cells
2. To explore the intracellular site of Cp_6 -histamine conjugate localization and PDT-induced cell organelle damage

3. To evaluate efficacy of Cp_6 -histamine conjugate for Photodynamic treatment of tumor in Hamster cheek pouch model
4. To study interaction of Cp_6 -histamine conjugate and Cp_6 with BSA and liver microsomes

CHAPTER 2

MATERIAL AND METHODS

2.1. Materials

DMEM (Dulbecco's modified essential media), N-2-hydroxyethylpiperazine-N'-2-ethanesulphonic acid (HEPES) phosphate buffered saline (PBS), trypsin, nystatin, 3-(4,5-dimethylthiazol-2-yl)-2,5-diphenyltetrazolium bromide (MTT), and fetal bovine serum (FBS) were obtained from Himedia, Mumbai, India., N-2-hydroxyethylpiperzaine-N-2-ethanesulfonic acid (HEPES), streptomycin and penicillin were obtained from Sigma, St. Louis, MO, USA. Cell culture wares i.e. culture flask, petri plates, multiwell plates etc., were obtained from Tarsons, India. Bovine serum albumin (BSA) fraction V and 2-thiobarbituric acid (TBA) were purchased from Sigma. 2, 4-Dinitrophenyl hydrazine (DNPH) was from Hi-Media, India and N, N-dimethyl-4-nitrosoaniline (RNO) was from Fluka. Other chemicals were of the highest grade available and procured locally.

Human oral squamous cell carcinoma (OSCC) cell lines NT8e, derived from tumor specimen of the upper aerodigestive tract (pyriform Fossa) and cell line 4451, derived from a recurrent tumor in the lower jaw were obtained from Cancer research Institute, Tata Memorial Hospital, Mumbai, India and Institute of Nuclear Medicine and Allied Sciences, Delhi, India, respectively. Human breast carcinoma (MCF-7) cells were purchased from the National Centre for Cell Sciences (NCCS), Pune, India.

2.2 Procedures and methods

2.2.1 Cell culture

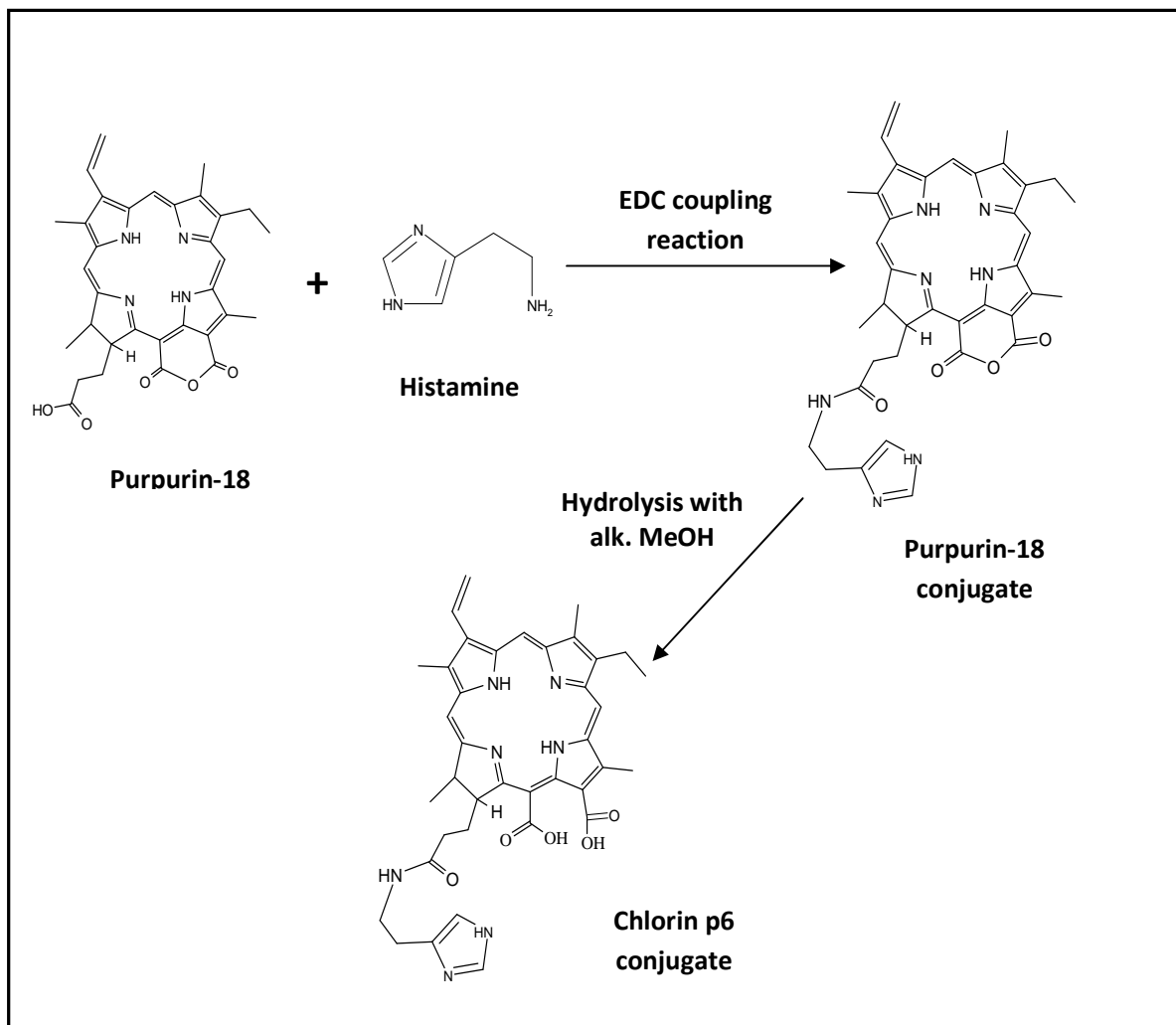
Human oral squamous cell carcinoma (OSCC) cell line NT8e and 4451 were maintained in DMEM containing essential amino acids, 25 mM N-2-hydroxyethylpiperazine-N'-2-ethanesulphonic acid (HEPES), 10% fetal bovine serum and antibiotics. The cells were grown in monolayer at 37 °C in humidified incubator (Nuair, USA) under 5% CO₂ – 95% air atmosphere. The cells were harvested by trypsinization, re-suspended in culture media and plated either in plastic Petri dishes or in 96 microwell plate. After ~ 18 h of growth, the cells in log phase were used for all further experiments. Human breast carcinoma (MCF-7) cells were maintained in MEM supplemented with 10% fetal bovine serum and antibiotics.

2.2.2 Animal model

Male Syrian Golden hamsters (*Mesocricetus auratus*, retired breeders 150–200 g, 20 animals) were used for the experiments. The animals were housed in plastic cages under controlled environmental conditions with a 12 h light/dark cycle, and had free access to both water and standard food. A 0.5% solution of 7, 12-dimethyl-benz(a)anthracene (DMBA, Sigma) in mineral oil was applied topically in left cheek pouch mucosa three times a week for 14 weeks to induce tumors. All procedures involving animals were approved by Institutional ethical committee in accordance with institutional guidelines on animal care.

2. 2.3 Preparation of Cp_6 and Cp_6 -histamine (Cp_6 -his) conjugate

Chlorophyll-a was extracted from dry spinach leaves and converted into Purpurin-18 (Pp-18) following the procedure described by Hooper *et al.* [240]. The Pp-18 was conjugated to histamine by standard carbodiimide coupling reaction. In brief, Pp-18 (2 mg, 1.5 mM) was dissolved in dry DCM (2.5 mL) and mixed with 3 mM 1-Ethyl-3-(3-dimethylaminopropyl)-carbodiimide (EDC) under continuous stirring. After 10 min, a solution of Histamine hydrochloride (0.9 mM) in methanol (5 ml) was added drop wise and the solution was stirred at room temperature for 24 h. The crude reaction mixture was loaded directly onto a silica gel column and eluted using a mixture of DCM/MeOH 95:5 with 1% of triethylamine (TEA). The dark red solution eluted from the column was washed with water to remove the triethylammonium salt impurity. The organic phase containing Pp18-histamine conjugate was evaporated to dryness and converted into Cp_6 -his by hydrolytic cleavage of the anhydride ring of Pp-18 using alkaline methanol. The schematic of chemical reaction is shown in the scheme 2.1. The resultant green solution was loaded onto silica gel column and eluted with MeOH/DCM (90:10). The faster eluting fraction containing Cp_6 -his was collected and dried under vacuum. The purity of the conjugate was checked by thin layer chromatography (TLC) on preparative silica gel plate using 90% aqueous methanol as mobile phase. Mass spectrum was obtained from IIT, Mumbai India.



Scheme2.1. The schematic of chemical reaction showing synthesis of Cp_6 -his from purpurin 18.

2. 2.4 Absorption and fluorescence spectra

Cp_6 and Cp_6 -his were dissolved in Ethanol: PEG(400):HEPES buffer (20:30:50) to obtain the absorption and fluorescence emission spectra. The absorption spectra were recorded from 250-750 nm using 1 nm band-pass on a Cintra-20 spectrophotometer (GBC, Australia). Fluorescence measurements were done using a Fluorolog-2 spectrofluorometer (Spex, USA). The samples were illuminated with 400 nm light and fluorescence emission was scanned from 600-750 nm keeping both excitation and emission slits at 1 mm corresponding to a band-pass of 3.6 nm and 1.8 nm, respectively.

2. 2.5 Photosensitizer treatment

Cp_6 -his is hydrophilic and can be dissolved in aqueous solutions, but storage at physiological pH (7.4) results in its partial aggregation. Solubilization in alkaline buffer (pH 9.0,) containing PEG-400 maintains it in the monomeric state because the molecule remains in anionic form at this pH. Therefore, Cp_6 -his was first dissolved in ethanol and then reconstituted in HEPES buffer (10 mM, pH 9.0) containing 30% PEG-400. For comparison, stock solution of Cp_6 was also made in the same system.

The cells grown in microplate wells or culture Petri dishes were treated with Cp_6 -his or Cp_6 by adding their specified concentrations in growth medium (DMEM with 10 %

serum) followed by incubation at 37 °C in a 5% CO₂, 95% air atmosphere for different time periods varying from 1/2 h to 7 h. The cellular uptake of Cp₆ or Cp₆-his was also measured in the presence of histamine (1mM and 5mM), Ranitidine (100 μM) and Pheniramine (100 μM) and the incubation time used in this case was 3 h. For studies on cellular uptake of photosensitizer at lower temperature, the microplates were placed on a refrigerant gel pack pre-cooled to ~12 °C in a thermocol box and the box was transferred to 5% CO₂, 95% air atmosphere inside the CO₂ incubator. The temperature and the pH of the culture media measured before and after 3 h incubation remained nearly constant.

2. 2.6 Extraction and estimation of photosensitizer content in cells

At the end of each incubation time point, the culture supernatant was aspirated and the cell monolayer was washed twice with cold PBS. To extract the photosensitizer from the cells, 250 μl detergent solution (0.1 M NaOH containing 0.1% SDS) was added in each well and the cell monolayer was scrapped with plastic pipette tip. The detergent solution was pipetted several times to make a homogenous cell suspension. After 60 min incubation at room temperature to allow complete solubilization, the solution was mixed with 750 μl PBS and centrifuged at 6,900 g for 10 min. The supernatant from each sample was collected and used for fluorescence measurements. Fluorescence spectra were recorded from 610 nm to 750 nm keeping excitation wavelength at 400 nm. The relative fluorescence intensity at 674 nm was measured and used to estimate the concentration of the photosensitizer from a standard curve. The concentration of the photosensitizer was

normalized with respect to the total protein content estimated by the Lowery's method [241]. The cell number was kept approximately equal in each experiment for comparison purpose.

2. 2.7 Photodynamic treatment

The cells were incubated with Cp_6 -his or free Cp_6 as described above. After incubation for 3 h, the cell monolayer was washed twice with DMEM medium (no serum), followed by addition of fresh growth medium. The cells were irradiated with red light (660 ± 25 nm) using light source LC-122A (Ci tek, USA) coupled to optical fiber probe (Dia. 1.2 cm, length 1 m) with an in-built narrow band-pass filter. The distal end of fiber optic probe was placed at a height of ~ 14 cm to expand the beam area for illumination of the entire microplate or three culture dishes simultaneously. The light intensity measured by a power meter model AN/ 2 (Ophir) at the sample position was ~ 79 W/m². The light dose was varied by changing the irradiation time from 0-8 min corresponding to irradiation dose of 0-38 KJ/m².

2. 2.8 Measurements on phototoxicity

For determination of phototoxicity, cell viability was measured by MTT assay [242]. Nearly 18 h after irradiation, the growth medium was removed and 100 μ l DMEM medium

(w/o serum) containing MTT (5.0 mg /ml) was added to each well. After 4 h incubation, the medium was removed and the formazan crystals formed within cells were solubilized by addition of 0.4 N hydrochloric acid in isopropanol. The optical density of the blue solution was measured at 570 nm and 690 nm using a microplate reader (Power Wave 340, Bio-tek Instruments Inc., USA). Phototoxicity was calculated as the percent decrease in MTT reduction with respect to a control sample, which received no photosensitizer and no light.

2. 2.9 Western Blot for detection of histamine H2 receptor

The cells were solubilised by incubation in a sample buffer (50 mM Tris-HCl, 2% SDS, 100 mM 2-mercaptoethanol, 10% glycerol, and 0.05% bromphenol blue, pH 6.8) at 100 °C for 5 min. The aliquots of cell extract were electrophoresed in 12% SDS-PAGE gel and transferred to nitrocellulose membranes using a semidry electroblotting apparatus (Hoefer). The residual binding sites were blocked with 5% nonfat powdered milk in PBST (phosphate-buffered saline containing 0.05% Tween 20), and membranes were incubated with (Dilution, 1:400) polyclonal rabbit anti-H2 receptor antibody (Santa Cruz Biotechnology, Santa Cruz, CA) in PBST. All subsequent washes were performed with the same buffer. Reactivity was developed using an (Dilution, 1:5000) Goat Anti-Rabbit IgG linked to horseradish peroxidase (Millipore) via enhanced chemiluminescence reagents (Amersham Biosciences).

2. 2.10 Intracellular localization of photosensitizer

The cells were grown on gelatin coated glass coverslips and incubated with the photosensitizers for 3h. After washing with DMEM medium the coverslips were mounted on to the stage of an inverted microscope (Olympus, Japan) and the cells were observed at 1000X magnification using an epifluorescence illumination set up (excitation 530–560 nm, barrier filter 580 nm). The images were recorded using a CCD Camera Model 'ProgRes CFscan' and a ProgRes Capture Pro software (Jenoptik, Germany).

2. 2.11 Monitoring cellular and nuclear morphology

The cells were grown in plastic culture dishes, treated with the photosensitizers for 3 h and then exposed to red light at $\sim 38 \text{ kJ/m}^2$. After ~ 18 h, each of the culture dishes from control and treatment groups were mounted on to the stage of an inverted microscope (Olympus, Japan) and the cells were observed at 400X magnification under phase contrast illumination. The morphology of the cells was recorded using a CCD camera and analyzed. To visualize the nuclear morphology, the cells were stained with DNA specific fluorescence probe Bis-benzimidazole Hoechst 33342 (HS) (Sigma, USA) by adding a 10 μl of its stock solution ($1 \mu\text{g ml}^{-1}$) directly into the culture dishes. After 5 min, the cells were observed under epi-fluorescent microscope (Olympus, Japan) using a fluorescent filter cube (excitation 340–380 nm, barrier filter 430 nm) and images were recorded.

2. 2.12 DNA fragmentation by gel electrophoresis

The cells were grown in plastic culture dishes and subjected to photodynamic treatment. After ~ 18 h, the cells attached to the culture dish were released by trypsinization and mixed with the culture supernatant that contain detached cells if any. After centrifuged at 600 g, the cell pellet was washed once with PBS followed by addition of 200 µl lysis buffer (0.1% Triton X-100, 20 mM EDTA in 5 mM Tris-HCl, pH 8.0). The cells in lysis buffer were kept in an ice bath for 10 min to allow cell lysis. The bulk DNA present in the cell lysate was precipitated by addition of 1 M NaCl solution containing 2.5% PEG-1800 and after centrifugation at 16000 g for 10 min at room temperature the supernatant was used for electrophoresis on 1.5 % agarose gel. The DNA in gel was stained with Syber Green Gold dye (Invitrogen, USA) and its fluorescence was visualized and recorded using a Gel-doc system (Syngene, USA).

2. 2.13 Assessment of apoptosis and necrosis

Percentage of cells undergoing apoptosis and necrosis following photodynamic treatment was determined by fluorescence microscopy. In brief, ~18 h after PDT the cells were incubated with Hoechst (final concentration 10 µg/ml) and propidium iodide (final concentration 20 µg/ml) in the medium. After 5 min, the cells were observed under epi-fluorescent microscope (Olympus, Japan) using a fluorescent filter cube (excitation 340–

380 nm, barrier filter 430 nm). Cell stained with Hoechst showing characteristic chromatin condensation and fragmentation were identified as apoptotic cells. Cells showing red fluorescence of PI indicated loss of plasma membrane integrity and therefore identified as necrotic cells (A representative picture is shown here in Fig. 2.1). A minimum of 500 cells were counted in both control as well as each treatment group. Percentage of apoptotic and necrotic cells was calculated from the total number of cells counted.

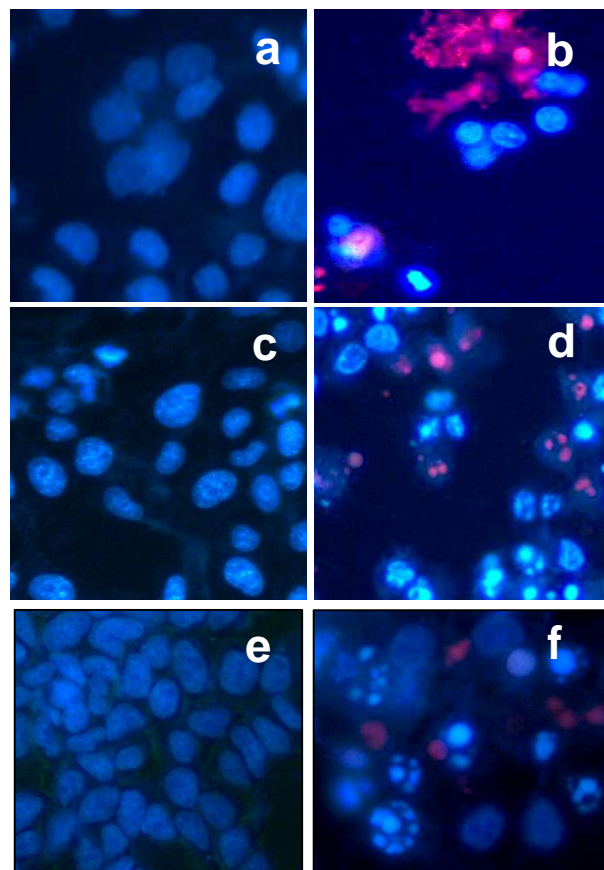


Figure 2.1: Representative microphotographs of 4451 (a-b), Nt8e (c-d) and MCF-7 (e-f) cells showing nuclear morphology.

2.2.14 Mitochondrial membrane potential in cells

To visualize the changes in mitochondrial membrane potential, the cells grown on glass coverslips were incubated in serum free culture medium containing 2 μ M JC-1 (5,5',6,6'-tetrachloro-1,1',3,3'-tetraethylbenzimidazolylcarbocyanine iodide) for 15 min at 37°C in dark. Then the coverslips were washed twice with PBS and mounted on a larger coverslip in PBS. The cells were visualized under an Inverted microscope IX70 (Olympus) at 100 X magnification using brightfield and fluorescence (excitation 450–480 nm, long-pass filter 515 nm) imaging modes to observe changes in cell morphology and mitochondrial membrane potential, respectively. The images were recorded using CCD Camera Model 'ProgRes CFscan' and a ProgRes Capture Pro software (Jenoptik, Germany).

2.2.15 Confocal fluorescence imaging of Cp₆-his localization in cells

For the determination of the subcellular localization of Cp₆-his, Nt8e cells were grown on coverslips fixed at the bottom of 35 mm petri dish and incubated with Cp₆-his (10 μ M) for 3 hr. The organelle probes were added at a concentration of 2 μ M at 30 min before the completion of incubation with Cp₆-his. Organelle probes used were Mito Tracker for mitochondria, LysoTracker for lysosomes, ER Tracker for endoplasmic reticulum, and Bodipy TR-C for Golgi apparatus (Molecular Probes, Invitrogen). After incubation, the cells were washed twice with PBS, immersed in same and the petri dish was mounted onto the stage of an inverted microscope. Fluorescence images of cells were recorded with a

Zeiss LS510 laser scanning confocal microscope using a 63x NA 1.4 oil-immersion objective (Gottingen, Germany). The fluorescence of organelle probes was activated by 488 nm Ar/Vis laser line and visualized using 512-554 nm band pass filter. For *Cp₆-his*, excitation with 543 nm He/Ne laser line and 650 nm long pass filter were used.

2.2.16 3D fluorescence imaging of cells

For assessing the PDT induced damage to subcellular organelle, the cells grown on coverslips were pre-labeled with specific organelle probes followed by the 3 hr incubation with *Cp₆-his* and irradiated with red light as described in previous section. After the treatment, the control and treated cells were fixed in 4% paraformaldehyde, washed with PBS and mounted on a glass slide in PBS solution. Fluorescence imaging of the labeled cells was done using a Nearfield Optical Microscope System using 60x oil emersion objective. Fluorescence of organelle probes was activated by 488 nm argon ion laser line and the emitted fluorescence was collected through a 100 micron optical fiber. Image acquisition in XY direction was done through the sample depth of 10 μ M with Z stack of size 15-20. Images were acquired at 150x150 pixel image resolution. Images were processes using ImageJ software to reduce background, improve contrast and convolve enhance the images. For 3D reconstruction software “Image surfer” (Developed by UNC Centre for Computer-Integrated System, USA and available freely at web site (www.imagesurfer.org) was used.

2. 2.17 Photosensitizer administration in hamsters

Cp_6 and Cp_6 -his conjugate were dissolved in ethanol: PEG (400): HEPES buffer (2:3:5) pH 8.0 and administered in animals through intra-peritoneal injection at dose of 3.0 mg/kg body weight. The animals were kept in diffuse light during the experiments to avoid any unwanted phototoxicity.

2. 2.18 In vivo fluorescence measurements

Photosensitizer accumulation in tumor, surrounding tissue, normal cheek pouch and abdominal skin of abdomen was monitored using a Spectrofluorometer (fluorolog-2, Spex, USA) equipped with a fiber optic probe. The animals were anesthetized by injecting ketaminium hydrochloride intramuscularly both during fluorescence measurements and photodynamic treatment. The fluorescence emission was recorded from 610 to 750 nm (excitation 400 nm). The measurements on photosensitizer accumulation in tumor and normal mucosa were done in 8 animals, which were randomly divided in two groups each for Cp_6 -his and Cp_6 . To determine the level of Cp_6 -his and Cp_6 , in tumor the auto fluorescence of endogenous Pp was mathematically removed by subtracting each spectrum with a reference spectrum that was obtained from the tumor before photosensitizer injection. From the resultant spectra, the intensity of fluorescence band (Cp_6 -his and Cp_6) was obtained by subtracting the baseline value at 650 nm from the peak fluorescence

intensity (674 nm) value. In case of spectra from normal mucosa, the value of fluorescence intensity obtained in similar manner (F674-F650nm) is used for comparison.

For monitoring clearance of Cp_6 -his and Cp_6 , fluorescence spectra from the abdominal skin were recorded at 4, 24, 48 and 72 h after photosensitizer administration and the percent change in fluorescence intensity at each time point with respect to intensity at 4 h was calculated.

2. 2.19 Photodynamic treatment of tumors

At 4–5 h after photosensitizer administration, the buccal cheek pouch of the animal under anesthesia was everted with the help of index finger. Each tumor was exposed to red light (660 ± 25 nm) through a fiber optic probe (diameter 1.2 cm) using Lumacare LC122-A light source (Ci-Tec, USA). The power density measured with a power meter (Ophir) at the fiber optic tip was ~ 0.2 W/cm² and the total light dose delivered was ~ 100 J/cm².

2.2.20 Tumor volume measurements

Tumor volume was measured before and one week after PDT. For this, Tumor length (L), height (H), and width (W) was measured using a Digimatic vernier calipers (Mitutoyo, Japan) with measurement accuracy of 0.025 mm and tumor volume (D) was calculated in

cubic millimeters (L x H x W) [16]. Tumor regression values (Tr) was obtained from the formula, $Tr (\%) = 100 - (DT \times 100 / DC)$, where DC and DT are tumor volume before, and 1 weeks after PDT treatment, respectively.

2.2.21 Tissue Histology

The animals were sacrificed by excessive ether inhalation; tissues were excised and placed in 10% buffered formalin for routine histological preparation. The tissues sections were stained with hematoxylin and eosin (HE) and examined under inverted microscope (Olympus, Japan). The images were recorded using a CCD Camera Model 'ProgRes CFscan' and ProgRes Capture Pro software (Jenoptik, Germany).

2.2.22 Immunohistochemistry

The presence of histamine H₂ receptors in tissue specimens was determined by immunohistochemistry. The animal tissue were fixed in 10% buffered-formalin solution, dehydrated, and then embedded in paraffin. The sections of thickness ~4 μm were cut, allowed to adhere on a glass slide, deparaffinized and than treated for 10 min with citrate buffer (10 mM citric acid; pH 6.0) on boiling water bath. Endogenous peroxidase activity was quenched by incubation in 3% hydrogen peroxide in 90 % methanol for 7 min. The non-specific binding sites were blocked with 10% Goat serum for 1hr and the tissue

sections were incubated with polyclonal rabbit anti-H2 receptor antibody (Santa Cruz Biotechnology, Santa Cruz, CA) overnight at 4°C. The tissue sections were washed with PBS, incubated with goat anti-rabbit IgG-horseradish peroxidase conjugate (Millipore) for 1 hr at room temperature, rinse with PBS and then incubated with substrate diaminobenzidine for 20-30 min. The tissue sections were counterstained with hematoxylin, covered with glass coverslips in a mounting medium and viewed under an inverted microscope (Olympus) using 40X brightfield objective. The specificity of immunoreactivity was confirmed by negative controls in which non immune 10 % goat serum was used instead of the primary antibodies.

2.2.23 Western Blot for detection of histamine H2 receptor in tissues

The presence of histamine H2 receptor protein in tumor, surrounding mucosa and normal mucosa of the hamster was also detected by western blot. For this, the tissue samples were homogenized in phosphate buffer saline containing protease inhibitor cocktail (Sigma) and centrifuged at 10000 rpm for 10 min. The supernatant was mixed with equal volume of sample buffer (50 mM Tris-HCl, 2% SDS, 100 mM 2-mercaptoethanol, 10% glycerol and 0.05% bromophenol blue, pH 6.8) and kept at 100°C for 5 min. The samples were loaded on 12% SDS-PAGE gel for electrophoresis and then the gel was processed for western blot and detection of H2 receptor as described in section 2.2.9.

2. 2.24 Isolation of microsomes

Mice livers were homogenized (1: 2 w/v) in ice-cold 50 mM-potassium phosphate buffer, pH 7.4, containing 0.9% NaCl. After centrifugation at 12000 g (20 min, 4 °C), the supernatant was centrifuged at 100000 g for 60 min (4 °C). The microsomal pellet was resuspended and again centrifuged at 100000 g for 60 min (4 °C). The pellet was resuspended in 100 mM-potassium phosphate, pH 7.4, containing 0.1 mM-EDTA and 20 % (w/v) glycerol. Microsomes (25 mg/ml) were stored at -80 °C. Protein was determined according to Lowry et al. using BSA as a standard.

2. 2.25 Measurement of binding parameters

Interactions of chlorin p_6 and chlorin p_6 - histamine (Cp_6 -his) conjugate with BSA and microsomes were studied spectrofluorometrically using Flurolog 2, (SPEX, USA) at room temperature (25 °C). Three milliliters solution of BSA (1 μ M ~ 67 μ g) or microsomes (100 μ g), in 25 mM phosphate buffer pH 7.4, was titrated spectrofluorometrically by adding Cp_6 and Cp_6 -his conjugate from a concentrated stock. Protein intrinsic fluorescence was monitored at 338 nm with excitation wavelength at 295 nm.

2.2.26 Spectroscopic measurements

Cp_6 and Cp_6 -his were dissolved in 25mM phosphate buffer pH- 7.4 and a concentrated stock (~ 1 mM) was prepared. The absorption and fluorescence spectra of Cp_6 and Cp_6 -his were recorded either alone or in presence of microsomes (100 μ g) or BSA (1 μ M ~ 67 μ g). The absorption spectra were recorded from 350 to 750 nm using 1nm band-pass on a Cintra-20 spectrophotometer (GBC, Australia). Fluorescence measurements were done using a Fluorolog-2 spectrofluorometer (Spex, USA). The samples were excited with 400 nm light, and fluorescence emission was scanned from 600 to 750 nm keeping both excitation and emission slits at 1 mm corresponding to a band-pass of 3.6 and 1.8 nm, respectively.

2.2.27 Irradiation procedure

Suitable aliquots of samples (either BSA, microsome, buffer alone or with Cp_6 / Cp_6 -his) was taken in cuvet of path length 1 cm. The cuvet containing the liquid covered with lid under constant stirring was then directly irradiated at the front face with 660 nm light using a LED source. The beam dia was 1 cm and the light intensity measured by a power meter model AN/ 2 (Ophir) at the sample position was ~ 50 W/m². The light dose was varied from 0-30 kJ/m² by changing the irradiation time from 0-10 min.

2.2.28 Assay of singlet oxygen yield

The singlet oxygen generation on photoactivation of Cp_6 and Cp_6 -his conjugate was measured by the method described by Kraljic and El-Mohsni [243]. Briefly, a solution containing RNO ($A_{440} \sim 0.8$), 10 mM imidazole and 10 μ M of either Cp_6 or Cp_6 -his in 25 mM Na_2HPO_4 buffer of pH 7.4 was irradiated with red light (660 ± 25 nm) for different time period and at the end of each irradiation absorbance of irradiated and un-irradiated samples was measured at 440 nm.

2.2.29 Octanol/ water partition coefficient

Partition coefficients of Cp_6 and Cp_6 -his were evaluated in a system of 1-octanol–sodium phosphate buffer of pH 7.4. The 50 μ M of each photosensitizer was dissolved in buffer and then this was mixed with equal volume of 1-octanol and the mixture was shaken vigorously and kept for 1 hr with constant shaking every after 10 min and then centrifuged at 1500g for 10 min to separate buffer and 1-octanol phases. The concentration of Cp_6 and Cp_6 his present in both the phases was determined by spectrophotometer. The partition coefficients ($P_{oct/buffer}$) were calculated according to

$$\mathbf{Log} P_{oct/buffer} = \mathbf{Log} [C_{oct} / C_{buffer}]$$

Where, C_{oct} and C_{buffer} are absolute concentrations of the drug in the 1-octanol and buffer phase, respectively. All the measurements were carried out at room temperature.

2.2.30 Protein carbonyl estimation

Protein carbonyls were measured as reported by Levien et al. [244]. Briefly, 1 ml sample was mixed with 400 μ l of ice-cold 40% trichloroacetic acid (TCA) and centrifuged at 4 $^{\circ}$ C for 10 min at 12,000g. The Protein pellet was dissolved in 200 μ l of 100 mM PBS pH 7.4. To this solution 200 μ l water and 400 μ l 20 mM DNPH in 4 N HCl was added and the tubes were incubated at room temperature (RT) for 90 min at 37 $^{\circ}$ C with vortexing every 10-15 min, followed by addition of 350 μ l of 40% TCA. The tubes were centrifuged at 12,000 rpm for 10 min. The pellets obtained were washed thrice with a mixture of ethanol and ethyl acetate (1:1 v/v) to wash off the excess DNPH. Finally, protein pellet was dissolved in 6 M guanidine hydrochloride and absorbance was measured at 360 nm using microplate reader (Power Wave 340, Bio-tek Instruments Inc., USA). The actual amount of protein carbonyl was calculated with the help of extinction coefficient of dinitrophenylhydrazine at 370 nm 22,000 $M^{-1} cm^{-1}$.

2.2.31 Assay for Lipid peroxidation

Lipid peroxidation was assayed by measuring malondialdehyde (MDA) and lipid hydroperoxide. Malondialdehyde was measured by the thiobarbituric acid reaction following the method of Placer et al. [245] with suitable modification. Usually 1.0 ml microsomal suspension (~0.5 mg protein/ml) was mixed with 1.0 ml TBA reagent

containing 20% TCA, 0.5% TBA, 2.5 N HCl and 6 mM EDTA and heated for 20 min. in boiling water bath. After cooling, the solution was centrifuged at 2,000 rpm for 10 min and the precipitate obtained was removed. The absorbance of the supernatant was determined at 532 nm against a blank that contained all the reagents except the biological sample. For correction of endogenous TBARS, fresh samples were boiled without light exposure, and values were subtracted. Absorbance reading at 532 nm were converted to TBARS values (n mol/mg protein), using an extinction coefficient of $1.57 \times 10^5 \text{ M}^{-1} \text{ cm}^{-1}$.

2. 2.32 Fluorescence quenching by iodide ions

The fluorescence of Cp_6 or Cp_6 .his (10 μM) in 50 mM-sodium phosphate buffer, pH 7.4, was determined in the presence and absence of liver microsomes (10 μg of protein/ml) (excitation 400 nm; emission 667 nm). KI was used as a fluorescence quencher (0-0.24 M). The ionic strength of the system was kept constant by addition of suitable amounts of KCl. The fluorescence quenching data were analyzed by the Stern-Volmer equation:

$$F_0/F = 1 + K_Q[X]$$

Where F_0 and F represent the fluorescence intensities in the absence and presence of the quencher respectively, $[X]$ is the molar concentration of the quencher and K_Q is the quenching constant.

2. 2.33 Effect of Cp₆ and Cp₆-his on activity of microsomal enzymes

For the measurement of P-450 reductase activity, liver microsomes (0.125 mg of protein/ml) were incubated with cytochrome c (75 μM) and NADPH (0.25 mM) at 37 °C. Similarly, to measure the activity of NADH cytochrome b5 reductase, liver microsomes (0.016 mg of protein/ml) were incubated with cytochrome c (75 μM) and NADH (0.2 mM) at room temperature. The reduction of cytochrome c was monitored spectrophotometrically at 550 nm (molar absorption coefficient: 21000 M⁻¹ cm⁻¹) [246]. For the assessment of effect of photosensitizers on the activity of these microsomal enzymes, the liver microsomes are either pre-incubated with PS for different time period or the PS was directly added in to reaction mixture.

2.2.34 Statistics

All the experiments were repeated at least three times and data are presented as average ± standard deviation (n=3). Student's *t*- test was applied to test the significance of the difference between control and the treatment. A level of *P* < 0.01 and *P* < 0.05 was considered to be statistically significant.

The measurements on photosensitizer accumulation in tumor and normal mucosa were done in 8 animals, which were randomly divided in two groups each for Cp_6 -his and Cp_6 . The values of peak fluorescence intensity (674 nm) obtained from the fluorescence measurements from tumors and normal mucosa of all the animals were used to calculate mean \pm standard deviation. To find significance of the differences between values for Cp_6 -his and Cp_6 student's *t*-test was applied. For skin clearance, the values of percent fluorescence intensity obtained from measurements done in four animals are presented as mean \pm standard deviation.

Photodynamic treatment was performed in 8 animals, out of which the tumors from three of the treated animals were excised for histology and in remaining five animals measurements on tumor volume were done to assess tumor damage and percent tumors regression, respectively. Four untreated animals were used as control and tissues excised from two of these were used for histology as well as immuno-histochemistry and other two for Western blot. The results of immuno-histochemistry, western blot and histology shown in Fig. 3, 4, and 5 were qualitatively reproducible.

CHAPTER 3

UPTAKE AND PHOTOTOXICITY OF

*Cp*₆-HISTAMINE CONJUGATE IN

CANCER CELLS

Oral squamous cell carcinoma (OSCC) is the most common type of cancer in India and other south East Asian countries [247]. Currently, PDT using Foscan (meta-tetra(hydroxyphenyl)chlorin or m-THPC) has been clinically approved for the treatment of head and neck squamous cell carcinoma (HNSCC) in European countries [11]. Several clinical studies on OSCC have demonstrated that PDT can help retain normal tissue function such as speech, swallowing and voice with no scarring [248]. So far, there exist no report on use of conjugated PS for PDT of oral cancer except studies by Soukos et al where Chlorin e6 (Ce_6), conjugated to epidermal growth factor receptor monoclonal antibody (EGFR-MAB) has been investigated for PDT of oral pre-cancer in hamster [249]. In this chapter, the cellular uptake and phototoxicity of Cp_6 -his and free Cp_6 has been studied in two human oral cancer cell lines 4451 and Nt8e. Among the two cell lines, 4451 which is derived from a recurrent tumor in the lower jaw is a p-53 mutant cell line for which resistant to radiotherapy has been reported previously [250]. The other cell line NT8e is derived from tumor specimen of the upper aerodigestive tract (pyriform Fossa) and has wild type p-53 [251]. Since the status of H2 receptor is not known in oral cancer, we have first confirmed the presence of histamine receptors in the both cell lines by western blot. Similar studies on the cellular uptake and phototoxicity of Cp_6 -his and free Cp_6 has also been investigated in human breast carcinoma cell line MCF-7, in which the expression of histamine receptors is well documented [236, 238]. Also, the receptor mediated uptake of the conjugate in these cell lines was explored by studying the effects of low temperature, agonist and antagonist on cellular uptake of Cp_6 -his or Cp_6 . In addition to this, mode of cell death induced by Cp_6 -his or Cp_6 was assessed by estimation of

percentage of necrotic and apoptotic cells after PDT using Hoechst 33342-propidium iodide staining.

3.1 Results

3.1.1 Characterization of the conjugate:

The purity of Cp_6 -his was checked by thin layer chromatography (TLC) on preparative silica gel plate using 95% methanol as mobile phase. The results of TLC show that Cp_6 -his separated as a single spot on silica gel plates with retardation factor (Rf) of ~0.9 and in comparison the Rf for Cp_6 was ~0.1 (Fig.3.1a). The mass spectrum of the conjugate gave anticipated molecular ion peak at 719.8 (calculated mass 719.76 for disodium salt $C_{38}H_{39}N_7Na_2O_5$) (Fig. 3.1b). The chemical structures of Cp_6 and its conjugate are shown in Fig. 3.1c.

Fig. 3.2 shows the absorption spectra of free Cp_6 and Cp_6 -his dissolved in Ethanol: PEG(400):buffer system. Attachment of histamine to Cp_6 did not cause any major change in its absorption peak positions in visible region except that the q band position was slightly red shifted to 666 nm from 663 nm. The molar absorption coefficient of Cp_6 -his was estimated to be $42,314 \text{ M}^{-1} \text{ cm}^{-1}$ and $12,750 \text{ M}^{-1} \text{ cm}^{-1}$ at soret and q band position which is ~1/2 of the molar absorption coefficient of Cp_6 at the same wavelengths. The 400 nm excited fluorescence of Cp_6 and Cp_6 -his are shown in inset.

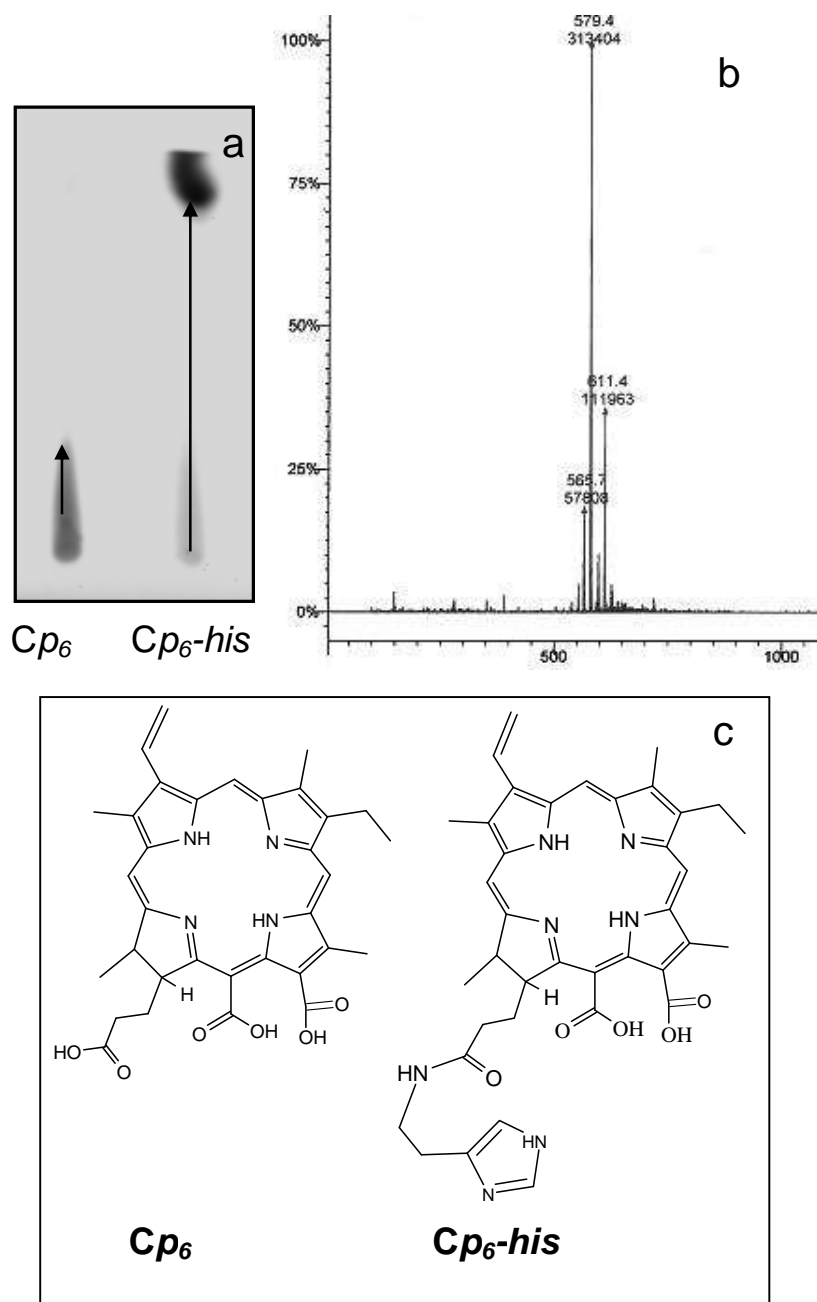


Figure 3.1. Photograph of TLC plate showing mobility of Cp_6 and Cp_6 -his after chromatography using 90% methanol as mobile phase (a), Mass spectrum of Cp_6 -his showing heaviest molecular ion peak at 719.8 (b), Chemical structure of Cp_6 and Cp_6 -his (c).

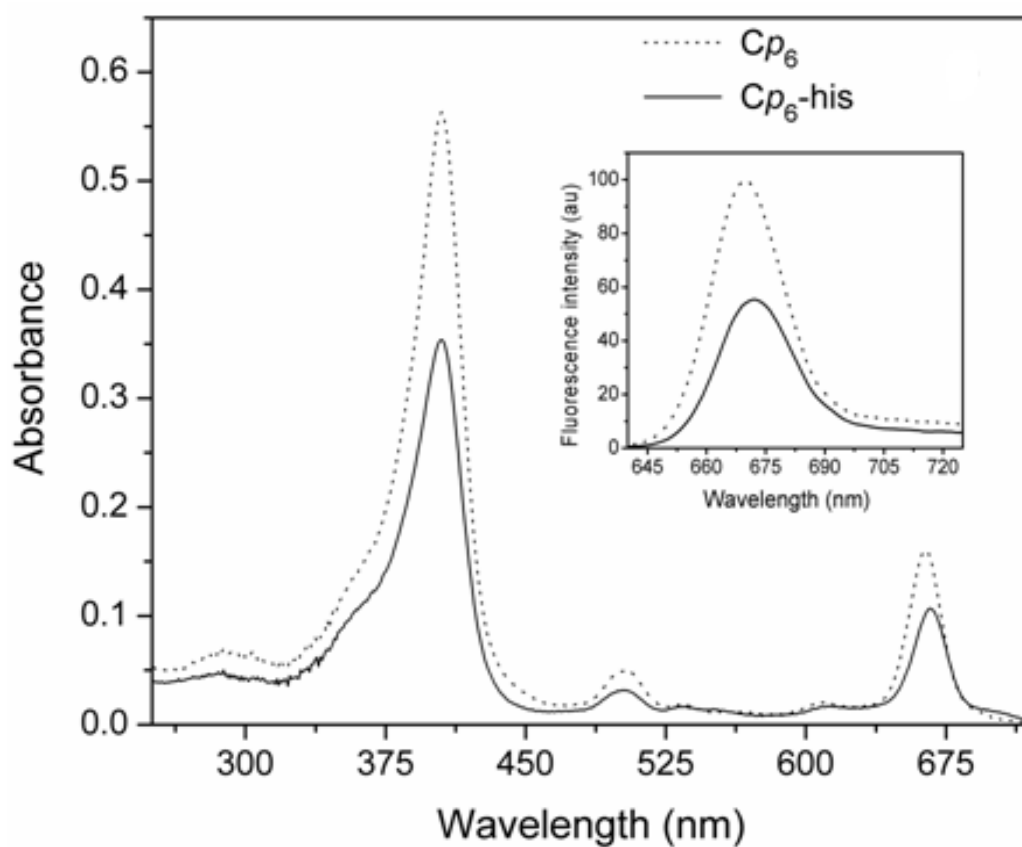


Figure 3.2 Absorption spectra of Cp_6 and Cp_6 -his in Ethanol: PEG: Water system. Respective fluorescence emission spectra are shown as Inset.

3.1.2 Intracellular uptake of Cp_6 and Cp_6 -his:

The kinetics of intracellular uptake of Cp_6 (5 μ M) and Cp_6 -his (5 μ M) in 4451 and Nt8e cells is shown in Fig. 3.3(a). In both the cell lines the uptake of Cp_6 was seen to increase up to 1 hr and saturated thereafter. In case of Cp_6 -his cellular uptake showed an initial rise till 1 hr followed by a slower phase of increase up to 5 h. The intracellular concentration of Cp_6 -his was noticeably higher as compared to Cp_6 by a factor of 5 and 10 at 1 h and 3 h incubation, respectively. The cellular uptake of Cp_6 -his in MCF-7 cells also followed similar trend with the increase in intracellular content of Cp_6 -his by a factor of 2 and 3 at 1 h and 3 h incubation, respectively when compared to free Cp_6 (Fig. 3.3b).

The effects of histamine (1 mM and 5 mM), ranitidine (100 μ M) and pheniramine (100 μ M) on the cellular uptake of Cp_6 -his and Cp_6 are shown in Fig. 3.4 and table 1. Cells were incubated with each photosensitizer (5 μ M) alone and in combination with above test compounds for 3 h. While, in the presence of histamine in case of both oral cancer cell lines, a significant increase ($p < 0.01$) in cellular uptake of Cp_6 -his was observed (Fig. 3.4a). In contrast with this slight but not significant ($p < 0.01$) decrease in cellular uptake of Cp_6 -his was found in MCF-7 cells (Table 1). However, addition of histamine H2 receptor antagonist ranitidine led to ~30% reduction (p value < 0.01) in the cellular uptake of Cp_6 -his whereas pheniramine, a histamine H1 receptor antagonist showed less inhibition (15-20%, p value < 0.05) (Fig. 3.4b and table 1) in all three cell lines. For Cp_6 , no

significant change in the cellular uptake was observed in the presence of any of these compounds (Fig. 3.4a-b and table 1).

Figure 3.5 shows the effect of lower temperature on the cellular uptake of Cp_6 -his and Cp_6 in the presence or absence of 10% serum in the culture medium. The cellular uptake of both Cp_6 -his and Cp_6 was found to decrease due to incubation of cells at lower temperature and in the presence of serum in the medium (fig. 3.5a). The percent inhibition was slightly higher for Cp_6 -his (50-60%) as compared to Cp_6 (30-40%). When serum is omitted from the culture medium, the inhibition in cellular uptake due to lower temperature was found to almost diminish in case of Cp_6 (7-10%) whereas for Cp_6 -his, it remained nearly same (40%) (Fig.3.5b). Similar results were found in case of MCF-7 cells (Table 1).

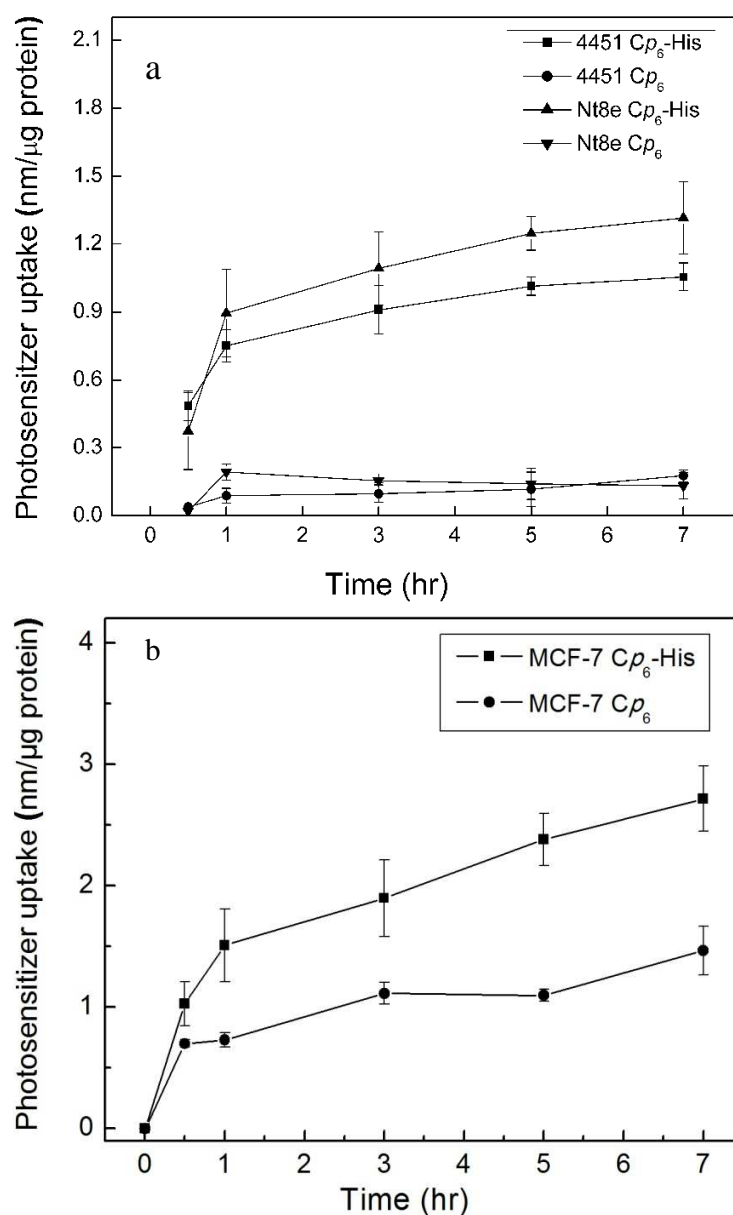


Figure 3.3. Time dependent cellular uptake of Cp_6 and Cp_6 -his Conjugate in (a) 4451 and Nt8e cells and (b) MCF-7 cells. Cells were incubated with 5 μ M of Cp_6 and Cp_6 -his each for different time periods (0.5-7 h). Each data point represents the average \pm SD of values obtained from three independent experiments.

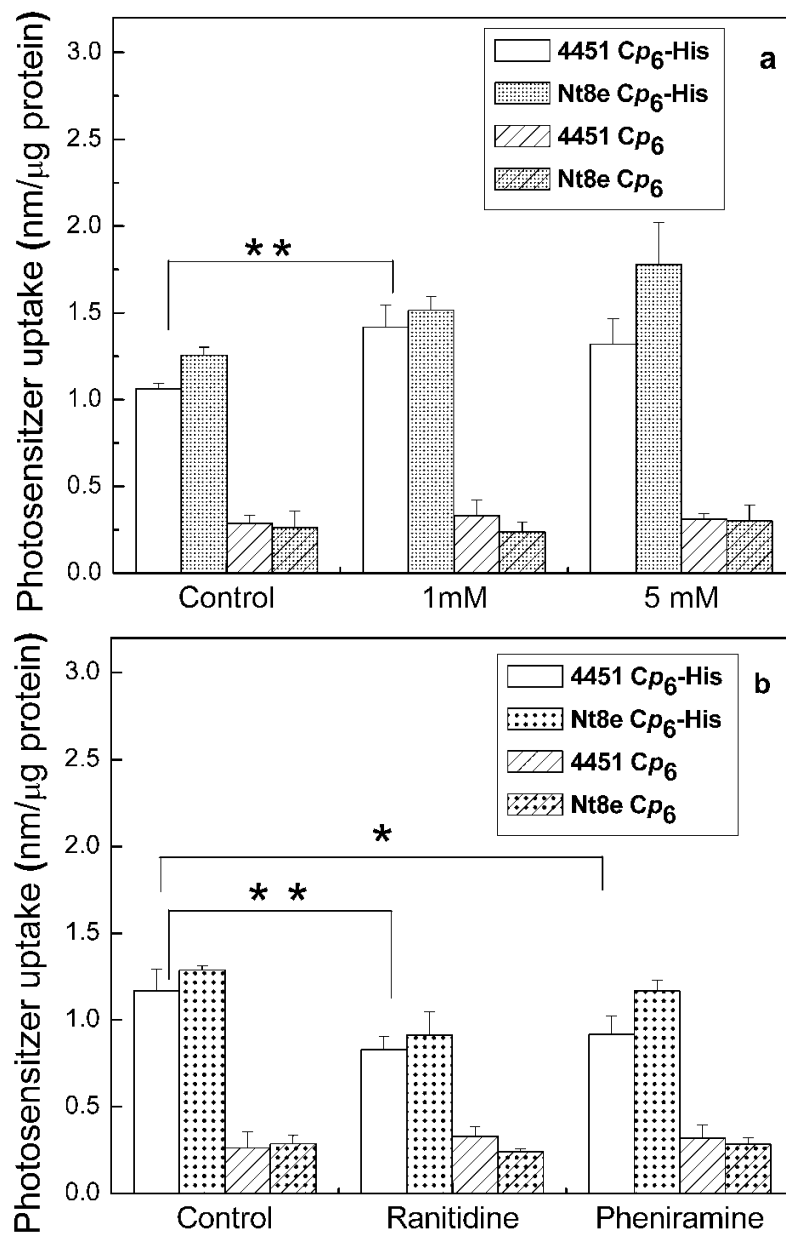


Figure 3.4. The effect of histamine (a) and histamine receptor antagonist (b) on the cellular uptake of Cp_6 and Cp_6 -his conjugate. Cells were incubated with 5 μ M Cp_6 and Cp_6 -his alone or with histamine (1 mM and 5 mM), ranitidine (100 μ M) and pheniramine (100 μ M) for 3 hr. Each data point represents the average \pm SD values obtained from three independent experiments. [** p value < 0.01, *p value < 0.05]

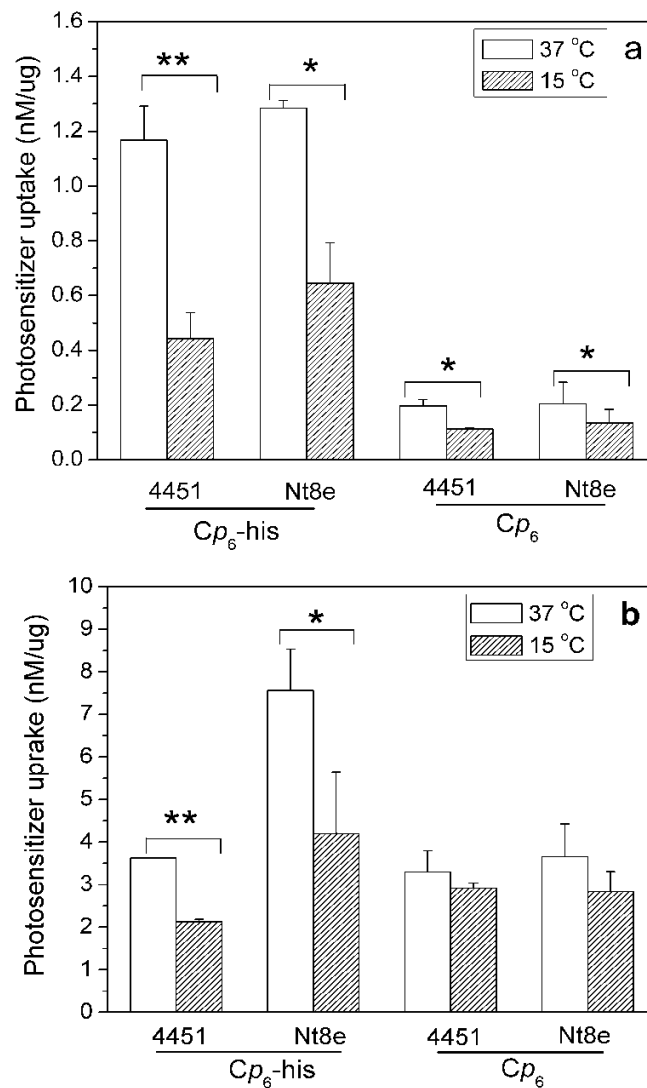


Figure.3.5. The effect of temperature on the cellular uptake of Cp_6 and Cp_6 -his conjugate. Cells were incubated with 5 μ M Cp_6 and Cp_6 -his at 37 °C or 15 °C in culture medium containing 10% serum (a) or without serum (b) Each data point represents the average \pm SD values obtained from three independent experiments. [*p value < 0.05, ** p value < 0.01].

Table 3.1. The effect of histamine receptor antagonist ranitidine, pheniramine, low temperature and histamine on the cellular uptake of Cp_6 and Cp_6 -his conjugate. MCF-7 Cells were incubated with 5 μ M Cp_6 and Cp_6 -his alone or with ranitidine (100 μ M), pheniramine (100 μ M), histamine (1 mM), and low temperature (15 °C) for 3 hr. Each data point represents the average \pm SD values obtained from three independent experiments. [** p value < 0.01]

Effect of agonist, antagonist and low temperature on cellular uptake of PS	Photosensitizer uptake (nm/ μ g protein)			
	Control		Treatment	
	Cp_6 -his	Cp_6	Cp_6 -his	Cp_6
Ranitidine (100 μ M)	1.18 \pm 0.17	0.59 \pm 0.19	0.87 \pm 0.11 p value < 0.01	0.52 \pm 0.19
Pheniramine (100 μ M)	1.18 \pm 0.17	0.59 \pm 0.19	1.31 \pm 0.12	0.59 \pm 0.21
Low temperature (15 ^o C)(without serum)	4.68 \pm 0.29	5.94 \pm 0.331	3.27 \pm 0.58 p value < 0.01	4.38 \pm 0.057
Histamine (1 mM)	4.68 \pm 0.29	5.94 \pm 0.33	3.48 \pm 0.26 p value < 0.05	5.43 \pm 0.53

3.1.3 Detection of histamine receptor in cells:

In order to find out the presence of histamine receptor in two oral and in a breast cancer cell lines western blot was performed. Immunoblotting with H2 receptor antibody revealed four bands with molecular masses of approximately 30 kDa, 60 kDa, 80 kDa and 100 kDa (Fig. 3.6). The presence of four bands for H2 receptor is in agreement with the previous studies and suggests presence of oligomeric form of H2 receptors with actual molecular masses of 31.5 kDa, [252].

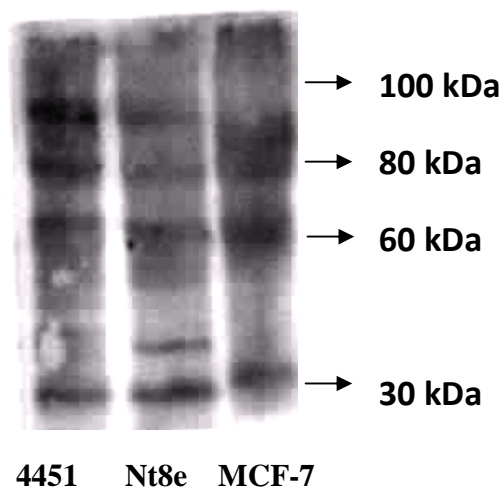


Figure 3.6. Image of nitrocellulose membrane showing presence of H2 receptor in 4451, Nt8e and MCF-7 cells after Western blot of the cellular protein using polyclonal rabbit anti-H2 receptor antibody and HRP conjugated Goat Anti-Rabbit IgG and detection by use of enhanced chemiluminescence reagents.

3.1.4 Intracellular Localization:

In Fig. 3.7 the bright field (left panel) and fluorescence images (right panel) of 4451, Nt8e and MCF-7 cells showing cell morphology and intracellular localization of Cp_6 and Cp_6 -his are displayed. In all three cell lines the fluorescence of Cp_6 was observed in punctuated granular structures indicating its localization at multiple sites inside the cells Fig. 3.7b, f & j. The intracellular localization of Cp_6 -his was noticeably different from Cp_6 (Fig. 3.7 d, h & l). The fluorescence of Cp_6 -his in 4451 and MCF-7 cells is observed in discrete vesicle type structures around the perinuclear region of the cytoplasm (Fig. 3.7 d & l). While Nt8e cells displayed the fluorescence of Cp_6 -his within granular structures as diffused patch near the nucleus (Fig. 3.7 h). In all the cell lines, the fluorescence labeling of the cell membrane by Cp_6 -his is also clearly visible (Fig. 3.7 d, h & l). Moreover, the fluorescence of Cp_6 -conjugate was much more intense as compared to the fluorescence of Cp_6 due to higher uptake. The brightness and contrast of the images shown in Fig. 3.7 were adjusted for proper visualization of the intracellular localization of Cp_6 and Cp_6 -his.

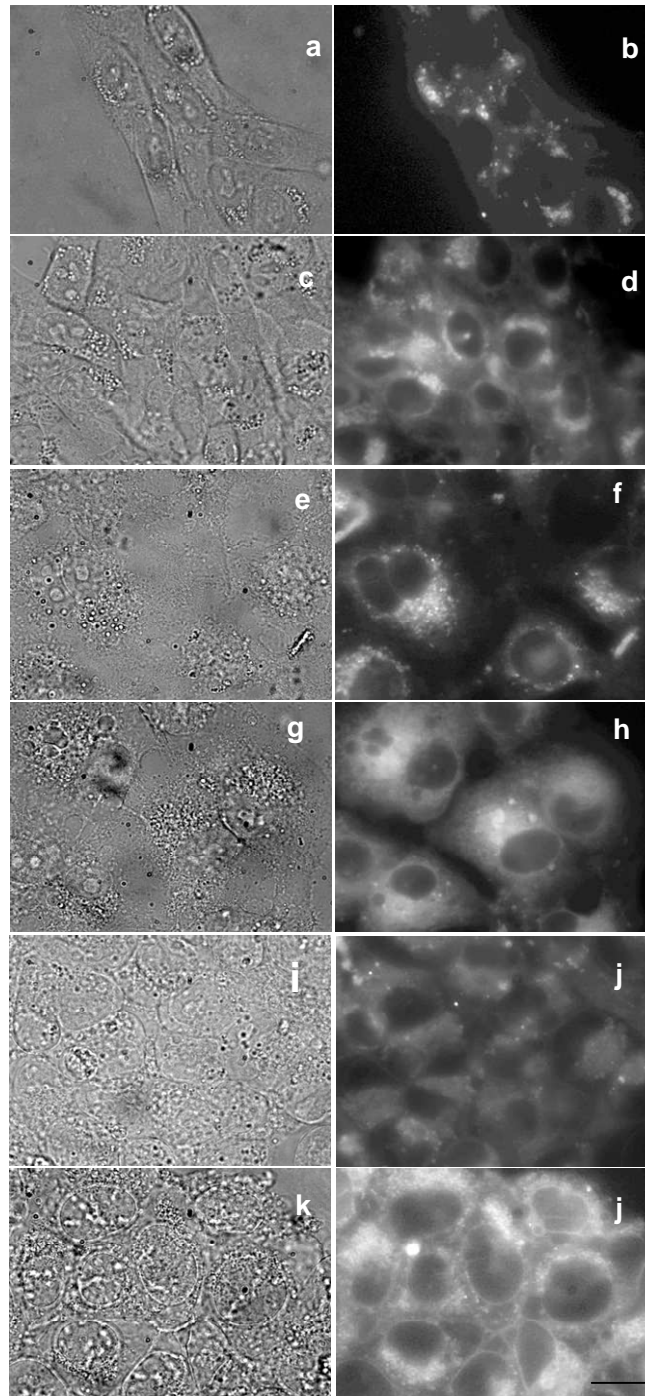


Figure.3.7. Microphotographs of 4451 (a-d), Nt8e (e-h), MCF-7 (i-l) cells incubated with 5.0 μM Cp_6 or Cp_6 -his in growth medium. Left panel – Bright filed images of the cells, Right panel – corresponding fluorescence images showing localization of Cp_6 (b & f) and Cp_6 -his (d, h). Magnification 100X, Bar -20 μM .

3.1.5 Phototoxicity

The phototoxicity of Cp_6 -his was determined by subjecting the cells to photodynamic treatment using different concentrations of the conjugate and a fixed red light irradiation dose at 28 kJ/m^2 . Percent phototoxicity was measured with respect to a control sample that received no drug and no light exposure and these results are presented in Fig. 3.8. The percent phototoxicity can be seen to increase in a concentration dependent manner in 4451, Nt8e and MCF-7 cell lines. The concentration of Cp_6 -his required to obtain 95% phototoxicity at the light dose of 28 kJ/m^2 was found to be $5 \text{ }\mu\text{M}$ (Fig. 3.8a & c). To compare the effectiveness of Cp_6 -his with Cp_6 , all three cell lines were subjected to photodynamic treatment using same concentration ($5 \text{ }\mu\text{M}$) and variable light dose (0 - 38 kJ/m^2). The results presented in Fig. 3.8b & d show that for a given light dose the phototoxicity was much higher with Cp_6 -his than Cp_6 . The light dose required to achieve 50-60% cell killing was $\sim 12 \text{ kJ/m}^2$ and 32 kJ/m^2 for Cp_6 -his and Cp_6 respectively. At 28 kJ/m^2 light dose, the phototoxicity induced by Cp_6 -his was $\sim 95\%$ and in comparison, Cp_6 led to $\sim 50\%$ phototoxicity. These data clearly show that Cp_6 conjugate is more effective than Cp_6 . No dark toxicity was noticed for either Cp_6 -his or Cp_6 at the concentration used.

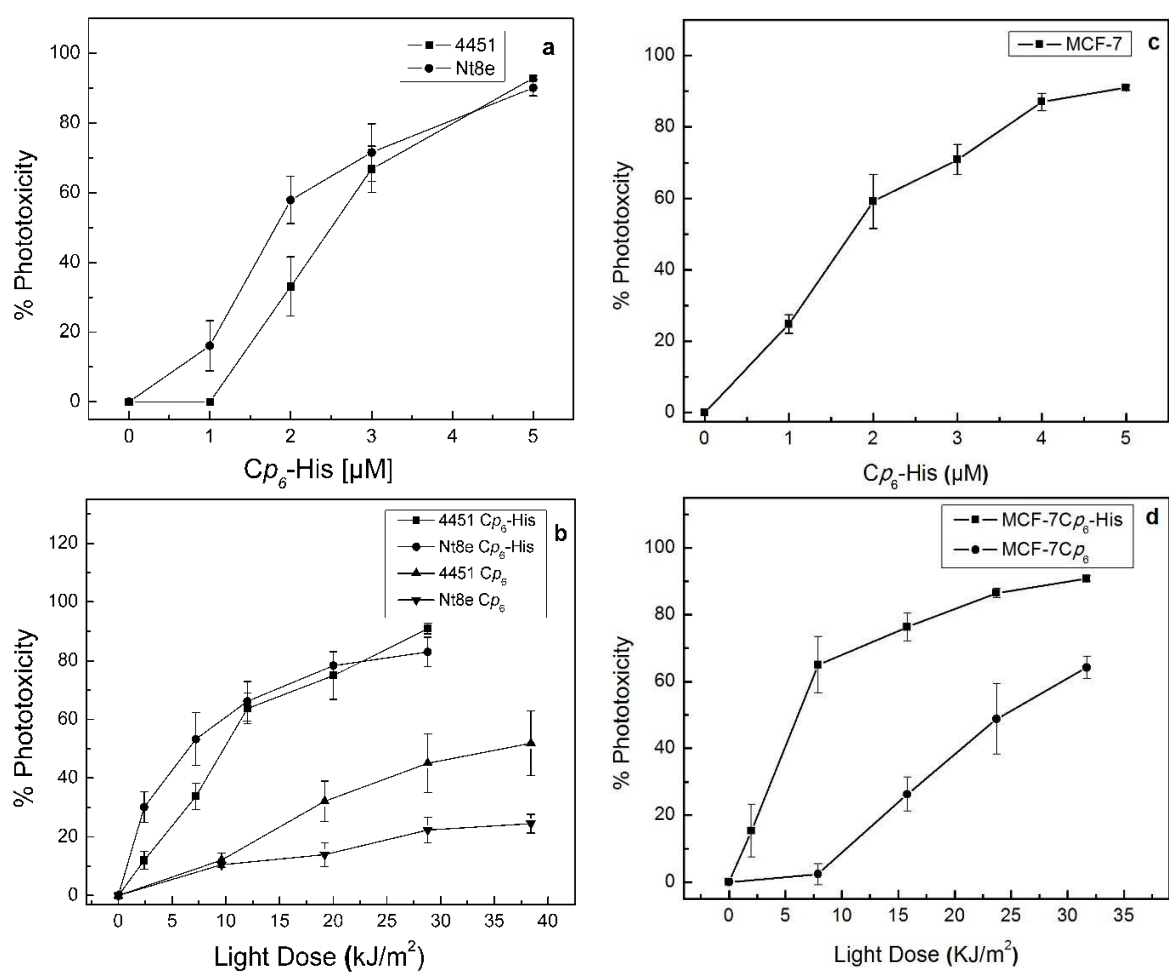


Figure. 3.8. Percent phototoxicity induced by Cp_6 -his at varying concentration from 1-5 μ M and fixed light dose at $28 \text{ kJ}/\text{m}^2$ (a-c) and both Cp_6 and Cp_6 -his conjugate at fixed concentration 5 μ M with varying light dose from 0- 38 kJ/m^2 (b-d) in 4451, Nt8e and MCF-7 cells. Cells were incubated for 3 h with photosensitizer in growth medium and irradiated with respective light dose. Phototoxicity was calculated as percent decrease in MTT reduction with respect to a control sample, which received no photosensitizer and no light. The zero dose point shows phototoxicity in cell sample incubated with photosensitizer but not exposed to light. Each data point represents the average \pm SD values obtained from three independent experiments.

3.1.6 Mode of cell death induced by Cp₆-his

To identify the mode of cell death in the cells subjected to photodynamic treatment with Cp₆-conjugate, parameters such as cellular and nuclear morphology, and DNA fragmentation were studied. The cellular morphology of the untreated cell and cells subjected to photodynamic treatment is shown in Fig. 3.9. Photodynamic treatment of 4451 cells led to rupture of cell membrane and release of cytoplasm indicating necrotic cell death (Fig. 3.9b). In contrast, the cell morphology of Nt8e and MCF-7 cells (Fig. 3.9 c & e) after photodynamic treatment (Fig. 3.9d & f) shows formation of plasma membrane blebs and cellular shrinkage, hallmark of apoptosis in nearly 50% cells. In 20-30% cells formation of membrane bubbles and release of content of the cytoplasm typical of necrotic death was observed in case of Nt8e and MCF-7 cells.

To further confirm the apoptotic DNA fragmentation, DNA isolated from cells was subjected to gel electrophoresis and the results are shown in Fig.10. It can be seen that the DNA of 4451 cells after PDT show smeared patterned DNA fragmentation whereas, in Nt8e and MCF-7 cells ladder DNA fragmentation typical of apoptosis is clearly visible (Fig. 3.10). Together, these results suggest that in 4451 cells PDT with Cp₆-histamine conjugate led to cell death via necrosis while apoptosis was predominant in Nt8e and MCF-7 cells.

A comparison of the relative magnitude of necrosis or apoptotic cell death in both oral cell lines treated with Cp_6 or Cp_6 -his is shown in fig.3.11. There was no major difference between the PDT treatment by Cp_6 and Cp_6 -his with respect to the percentage of apoptotic or necrotic cells in both the cell lines. Also in both the cases, the cell line 4451 showed higher percentage of necrotic cells as compared to Nt8e cells for which the percentage of apoptotic cells in turn was more. Similarly, in case of MCF-7 cells both apoptosis and necrosis contributes equally following PDT with Cp_6 -his (table 2).

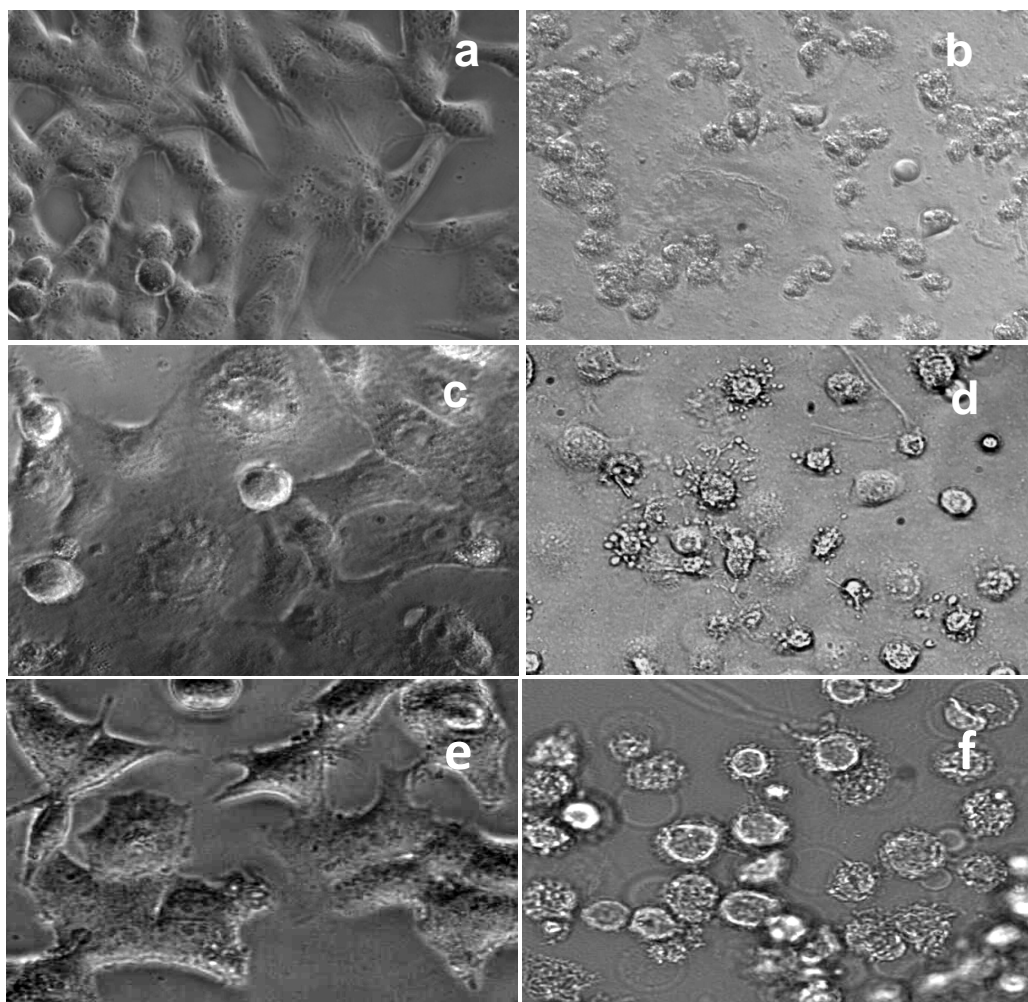


Figure3.9: Microphotographs of 4451 (a, b), Nt8e (c, d) and MCF-7 cells (e, f) showing changes in the cellular morphology after PDT with Cp_6 -his. Untreated cells (a, c, e) cells 18 hr after PDT (b, d, f). Cells were incubated with $5.0 \mu\text{M}$ Cp_6 -his for 3 h in growth medium and then irradiated with red light at $\sim 28 \text{ kJ/m}^2$. Magnification 40X, Bar $-50 \mu\text{M}$.

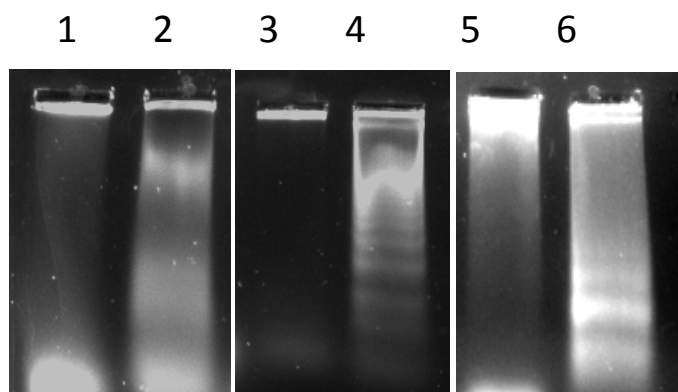


Figure3.10: DNA gel electrophoresis. Lane 1- untreated 4451 cells, 2- 4451 cells subjected to PDT, 3- untreated Nt8e cells, 4- Nt8e cells subjected to PDT, 5- untreated MCF-7 cells, 6- MCF-7 cells subjected to PDT. Cells were incubated with 5.0 μM Cp_6 -his for 3 h in growth medium and then irradiated with red light at $\sim 22 \text{ kJ/m}^2$. DNA was isolated 18 h after PDT.

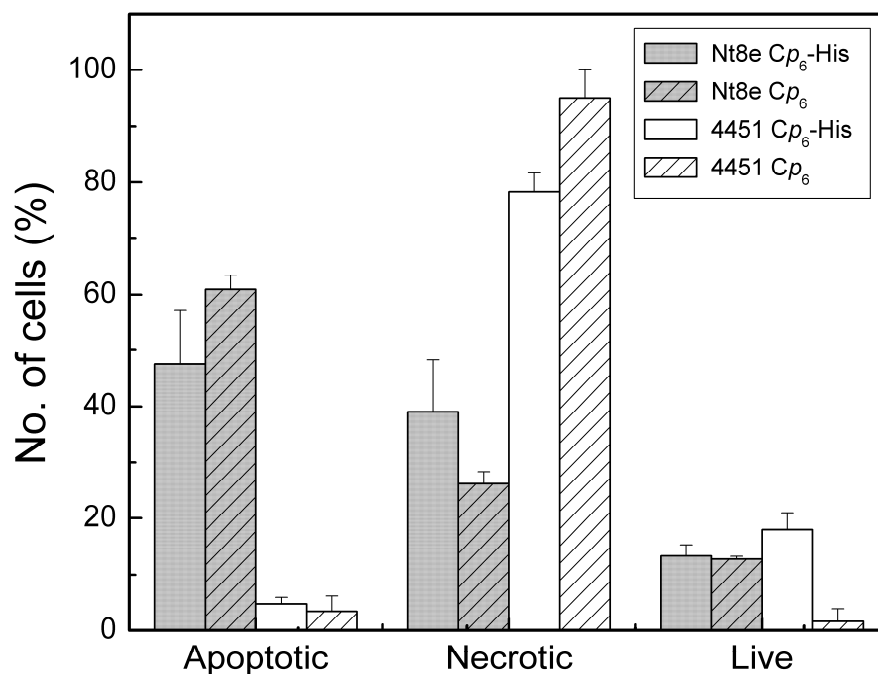


Figure3. 11. Percentage of apoptotic and necrotic cells in 4451 and Nt8e cells after 18 hr of photodynamic treatment with Cp_6 or Cp_6 -his. Cp_6 was used at 10.0 μM with light dose 38 kJ/m^2 and for Cp_6 -his, 5.0 μM concentration and $\sim 28 \text{ kJ}/\text{m}^2$ was used to obtain $\sim 95\%$ phototoxicity in both the cases. Fluorescence microscopy after staining the cells with Hoechst and propidium iodide was used to recognize the apoptotic, necrotic and live cells. Each data point represents the average \pm SD values obtained from three independent experiments.

Table 3.2. Percentage of apoptotic and necrotic cells in MCF-7 cells after 18 hr of photodynamic treatment with *Cp6*-his. *Cp6*-his was used at 10.0 μM with light dose 38 kJ/m^2 and for *Cp6*-his, 5.0 μM concentration and $\sim 28 \text{ kJ}/\text{m}^2$ was used to obtain $\sim 95\%$ phototoxicity in both the cases. Each data point represents the average \pm SD values obtained from three independent experiments.

Mode of cell death	Number of cells (%) average \pm SD
Apoptosis	40.2 \pm 6.3
Necrosis	55.3 \pm 8.8
Live	4.2 \pm 5.6

3.2 Discussion

The motivation for the present study was to investigate the use of histamine, a biogenic amine to enhance the uptake and tumor selectivity of Cp_6 by exploiting histamine receptors for delivery of photosensitizer in cancer cells. The results of cellular uptake studies presented in fig. 3.3a-b show that the Cp_6 -his is taken up more efficiently by the cells than free Cp_6 . To check if the uptake occurred via histamine receptors we also measured the cellular uptake of Cp_6 -his in the presence of histamine. Instead of the expected inhibition, histamine led to slight increase in the uptake of Cp_6 -his in case of both oral cancer cell lines(fig 3.4 a). The reason for this effect is presently not clear. Based on the fact that the receptor affinity of some agonist/antagonist is higher than histamine [253] one can assume Cp_6 -his to have stronger receptor affinity which prevented histamine to compete efficiently for the binding site. Moreover since exogenous histamine has been shown to up-regulate expression of histamine receptors [212,236,254], this would also be considered as possible reason for observed increase in uptake of Cp_6 -his. However, in MCF-7 an expected decrease in uptake of Cp_6 -his was observed. Furthermore to confirm the involvement of histamine receptors, cellular uptake of the conjugate was measured in presence of pheneramine and ranitidine which are known antagonist for H1 and H2 histamine receptors, respectively. In Nt8e, 4451 and MCF-7 cell lines these antagonists at 100 μ M led to significant inhibition in the cellular uptake of Cp_6 -his and the inhibition was more pronounced in the presence of ranitidine, a potent H2 receptor antagonists suggesting that at least a part of cellular uptake or binding of the conjugate occurred via H2 receptors. Using western blot we found that H2R receptor is expressed in all three cell lines.

However, since higher concentration of the antagonist did not lead to further inhibition in the uptake of the Cp_6 -his, the possibility that receptor independent mechanism also contribute to its intracellular uptake cannot be ruled out. Indeed some histamine agonist, antagonist and BODIPY FL histamine, a fluorophore used to label histamine receptors, have also been shown to be internalized and sequestered in cells by a receptor-independent mechanism [255]. Therefore to further confirm that the uptake is receptor-mediated, the effect of low temperature on cellular uptake of both Cp_6 -his and Cp_6 was studied. Interestingly, incubation at 15 °C led to inhibition of cellular uptake of both the photosensitizers (figure 3.5a). Although the magnitude of inhibition for Cp_6 was slightly lower than Cp_6 -his, it was not unexpected due to the fact that hydrophilic Cp_6 via interaction with serum LDLs can also be taken up by receptor mediated endocytosis [256]. To check this possibility, we omitted serum from the culture media during the incubation period. Results show that the inhibition of cellular uptake due to lower temperature is persistent for Cp_6 -his but in case of Cp_6 it is almost diminished (figure 3.5b and table 1). These results confirmed that the uptake of Cp_6 -his is indeed receptor mediated. Apart from histamine receptors, there also exists membrane associated organic cation transporters (OCTs) which function to remove excess amount of histamine from the extra-cellular space by its re-uptake and transport into the cytoplasm to a yet unidentified site where it is metabolized into inactive metabolite N^t -methylhistamine [254]. However, studies in murine hematopoietic progenitor cells and basophiles have shown that the uptake of histamine by OCT is not affected by the presence of H1 or H2 receptor antagonist [258,259]. Since we found significant inhibition in uptake of Cp_6 -his by histamine antagonist the possibility of role of OCTs in its cellular uptake is less likely. Since

attachment of Cp_6 to histamine can lead to alterations in its physico-chemical properties such as relative hydrophobicity, molecular charge and amphiphilicity, one would expect this also to contribute to the improved cellular uptake of Cp_6 -his in a manner similar to reported for N-aspartyl ce6 (MACE, LS11) a conjugate of chlorin e6 with aspartic acid [260].

Our results on intracellular localization show that in all three cell lines Cp_6 -his localizes on the cell membrane and also inside the cells in the form of vesicles near the perinuclear region. This is similar to the intracellular localization of histamine reported earlier in rat immune cells [261]. In contrast, the intracellular localization of Cp_6 was distinctly different and occurred in the form of punctuated granular structures inside cytoplasm indicating its localization at multiple sites such as endoplasmic reticulum, Golgi apparatus and lysosomes. This is consistent with our previous studies [262]. The uptake of Cp_6 -his via histamine H2 receptor would lead to its accumulation in endosome/lysosome pool. This is due to the fact that histamine H2 receptor is G protein-coupled receptor (GPCRs) which when binds to agonist or antagonist undergoes internalization through the process of endocytosis resulting in its accumulation in the perinuclear endosomal pool and subsequent trafficking to the lysosomes [263]. The receptor is either recycled back to the plasma membrane or undergoes proteolytic degradation for down regulation [264]. For GPCRs which utilize endocytosis machinery for receptor regulation, it is generally believed that the receptor and ligand are internalized together [242]. It is therefore likely that the vesicles in the perinuclear region where Cp_6 -his is localized represents the endosome/lysosome compartments. Intracellular binding site of histamine to microsomal

cytochrome P450 and nucleus have also been identified through which histamine is believed to regulate cell growth and homeostasis [266]. These binding sites designated as H_{IC} are not specific because it can interact with several other compounds also such as imidazoles (including HA, 1-histidine, histidinol), polyamines (putrescine, spermidine, spermine) and hormones (androgens, estrogens, progestins and, to a lesser extent, adrenal steroids) etc [266]. However, we did not find localization of Cp_6 -his in the cell nucleus. The identification of the exact site of Cp_6 -his localization needs further investigations.

The results presented in fig. 3.8 show that the phototoxicity induced by Cp_6 -his was ~4 times higher as compared to Cp_6 whereas, the magnitude of increase in the uptake of the conjugate was ~ 10 times higher than free Cp_6 . One important factor that can contribute to this observation is that the absorption coefficient of the conjugate was ~1/2 than Cp_6 at 660 nm. Since the mode of PDT-induced cell death is determined by the intracellular localization of the photosensitizer [267] and significant differences were observed in the intercellular localization of Cp_6 and Cp_6 -his, we also investigated the cell death response induced by the two photosensitizers. The results on cell morphology(fig 3.9) and DNA electrophoresis (fig 3.10) suggest that while cell death in 4451 is mostly by necrosis, for NT8e and MCF-7 cells both apoptotic and necrotic cell death is induced by photodynamic treatment with Cp_6 -his. Measurements on the percentage of apoptotic and necrotic cells after PDT with Cp_6 and Cp_6 -his (fig 3.11) showed no difference except that in case of Cp_6 -his slight increase in necrotic cells was observed which can be attributed to the observed localization of Cp_6 -his on the cell membrane. The reasons for the differences in the PDT-induced cell death response observed between the two cell lines may be because of their

p53 status. While the 4451 cells are reported to be a p53 mutant [250], the cell line Nt8e contains wild type p53 [254]. The tumor suppressor gene p53 is known for its ability to induce apoptosis by activating downstream cell death effectors including bax, Puma, and Noxa [268,269]. In a study on PDT with haematoporphyrin derivative (HpD) similar results have been reported in 4451 cells and in cell line BMG-1 having wild type p53 [248]. Moreover, in case of MCF-7 cells, percentage of apoptotic and necrotic cells was found to be same, showing that both the mechanism contributes equally to the cell death following PDT with Cp_6 -his (table 2).

3.3 Conclusion

To conclude, the results of our study show that conjugating Cp_6 to histamine improves its cellular uptake and hence the PDT efficacy in both oral and breast cancer cell lines. The observations that the cellular uptake of Cp_6 -his is significantly inhibited by ranitidine and lower temperature, suggest that part of its uptake occurred via histamine receptors. Similarly, in human breast carcinoma cell line MCF-7 in which the expression of histamine receptors is well documented, higher uptake of Cp_6 -his and the expected enhancement in phototoxicity was observed. It is concluded that conjugating Cp_6 with histamine can help to improve the effectiveness of PDT in oral and breast cancer cells by enhancing its intracellular delivery.

CHAPTER 4

INTRACELLULAR SITE OF Cp_6 -HIS

LOCALIZATION AND PDT-INDUCED

CELL ORGANELLE DAMAGE

Photosensitizer depending on its physicochemical properties and cellular uptake mechanism can localize in different cell organelles such as mitochondria, endoplasmic reticulum, Golgi or lysosomes and since the diffusion of singlet oxygen in cellular environments is limited (half-life: $<0.04 \mu\text{s}$, radius of action: $<0.02 \mu\text{m}$), the primary sites of intracellular damage is determined by the distribution of a photosensitizer in various organelles [34]. Studies have shown that damage to various subcellular structures could determine the cell death mechanism and PDT efficacy [34, 273]. Generally, the localization of photosensitizer in the cell membrane or lysosomes contributes to cell death via necrosis e.g. as reported for photofrin and cationic cycloimide derivatives of chlorin p_6 , respectively [274,275,276]. In contrast, cell death via apoptosis is determined by the PDT-induced alterations in mitochondrial structure and function either if photosensitizer localizes directly in mitochondria [277], or also in case of photosensitizer localizing in other organelles such as endoplasmic reticulum, Golgi apparatus and lysosomes involving cross-talk between damaged organelle and mitochondria [278,279,280,281,282].

Our studies in chapter 3 in oral cancer cells have shown that the cellular uptake of chlorin p_6 -histamine conjugate was higher than for free Cp_6 which led to significant enhancement in phototoxicity and the mode of cell death induced by Cp_6 -his was found to be mediated by both apoptosis and necrosis [283]. In this chapter, we report studies on the subcellular localization and identification of intracellular target sites of Cp_6 -his in human oral cancer cells. So far, the structural alterations in the cell organelles following PDT have been investigated only in some studies where these have been generally characterized as generalized damage or swelling of cell organelles [284,285,286,287]. However, since the cell organelle are organized in the three dimensional cellular space and in close association

with one another, the structural damage to one organelle can result in disturbance in organization of other organelle which can also contribute to PDT-induced cell death. Here we have identified site of localization of Cp_6 -his by colocalization studies using organelle specific fluorescent probes and have analyzed the PDT-induced alterations in the structure of cell organelles in more details using confocal fluorescence microscopy combined with three-dimensional image reconstruction technique. This technique provides valuable information regarding the detailed structure of cell organelles as well as their interaction or association with one another. For example, this technique has allowed visualization of distribution of microtubules in tumor cells in relation to cell shape and position of other cellular organelles [288], organization of cell nuclei in rat hippocampal neurons [289], fragmentation of the mitochondrial network following Ischemia and reperfusion injury in cardiac myocytes [290] and internalization and interaction of chrysotile fibers with the chromatin during mitosis [291].

4.1 Results

4.1.1 Intracellular localization of Cp_6 -his

In figure 4.1, confocal images of Nt8e cells showing intracellular fluorescence of Cp_6 -his in red color (a-d), fluorescence of organelle specific probes in green color (e-h), overlay image of Cp_6 -his fluorescence and organelle probes (i-l) and the respective 2D histogram of the red Vs. green pixel intensities (m-p) with the value of correlation coefficient (inset)

are shown. Images a-d shows that Cp_6 -his accumulated in the regions of cytoplasm which corresponds to site of ER (e) and lysosomal compartments (h) as indicated by overlap of red-green fluorescence (i & l). The value of correlation coefficient obtained from 2D histogram for ER and lysosomes (m & p) was 0.787 and 0.793 respectively. In case of Golgi (f) and mitochondria (g), the fluorescence of Cp_6 -his (b & c) showed very little overlap (j & k) as also indicated by low correlation coefficient of 0.335 and 0.262, respectively. With Cp_6 the value of correlation coefficient obtained from 2D histogram for ER (m) and mitochondria (g) was 0.805 and 0.610 respectively. The fluorescence of Cp_6 (b & d) showed very little overlap with Golgi (f) and lysosomes (p) (j & i) as indicated by low correlation coefficient of 0.435 and 0.423, respectively (fig 4.2).

4.1.2 Phototoxicity

In fig 4.3, we show changes in the cellular morphology and mitochondrial membrane potential (MMP) of Nt8e cells at 1 h after PDT. Cells were treated with Cp_6 -his for 3 h followed by irradiation with red light at 38 kJ/m^2 . Compared to intact cell morphology and the presence of active polarized mitochondria (red fluorescence) in control cell (fig 4.3a-b), the cells after PDT show extensive cell damage in cytoplasmic region and loss of MMP (green fluorescence) in most of the cells (fig 4.3c-d). MTT Assay performed after 24 hr shows that the phototoxicity was ~80% as compared to the dark control.

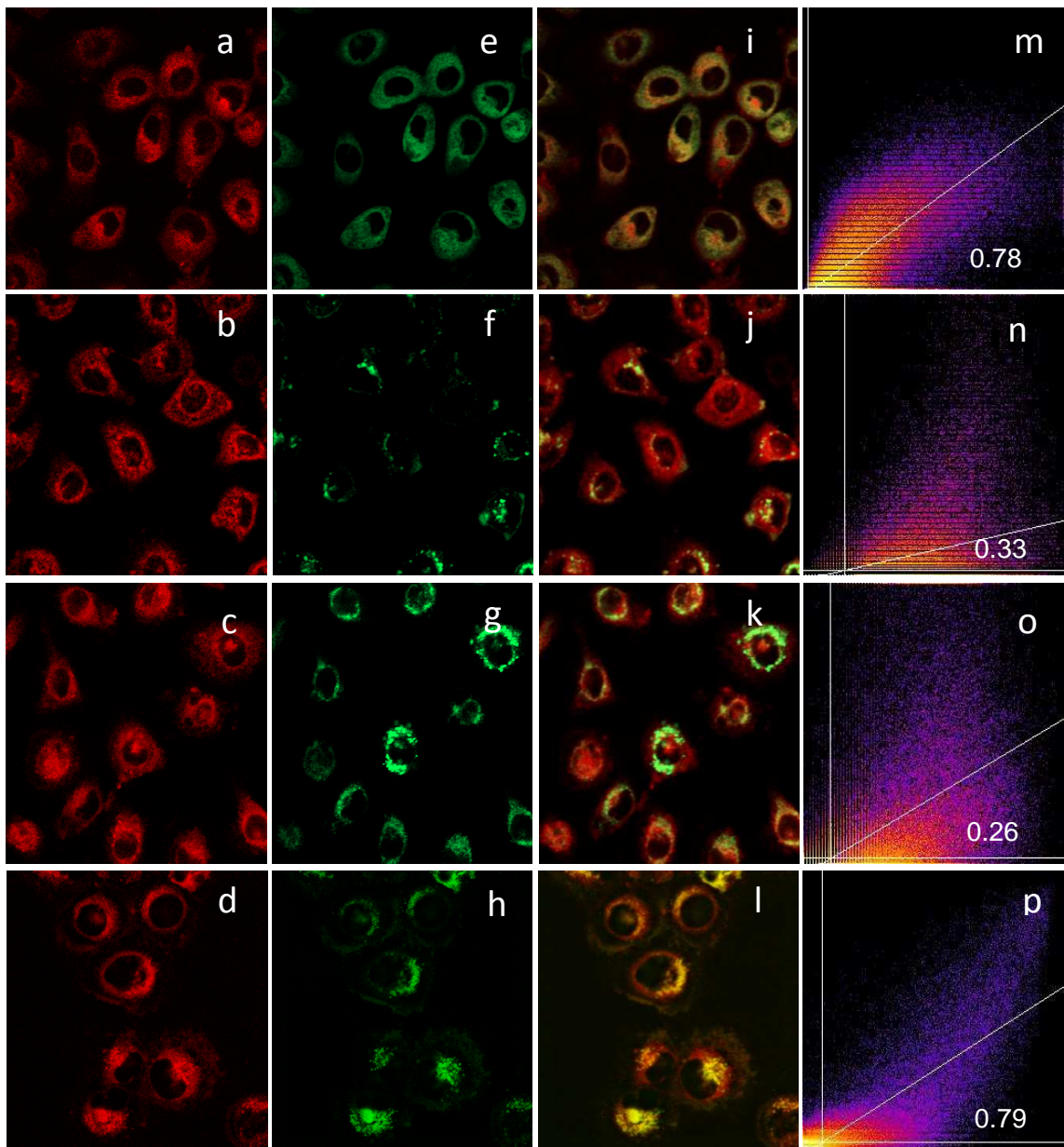


Figure 4.1. Microphotographs of Nt8e cells showing subcellular localization of Cp_6 -his. The cells were treated with $10 \mu\text{M}$ Cp_6 -his (first panel from left) and specific fluorescence probes for endoplasmic reticulum, Golgi, mitochondria and lysosomes (second panel). The overlay of Cp_6 -his fluorescence with respective organelle probe (third panel) and histogram with value of correlation coefficient (right panel) is also shown.

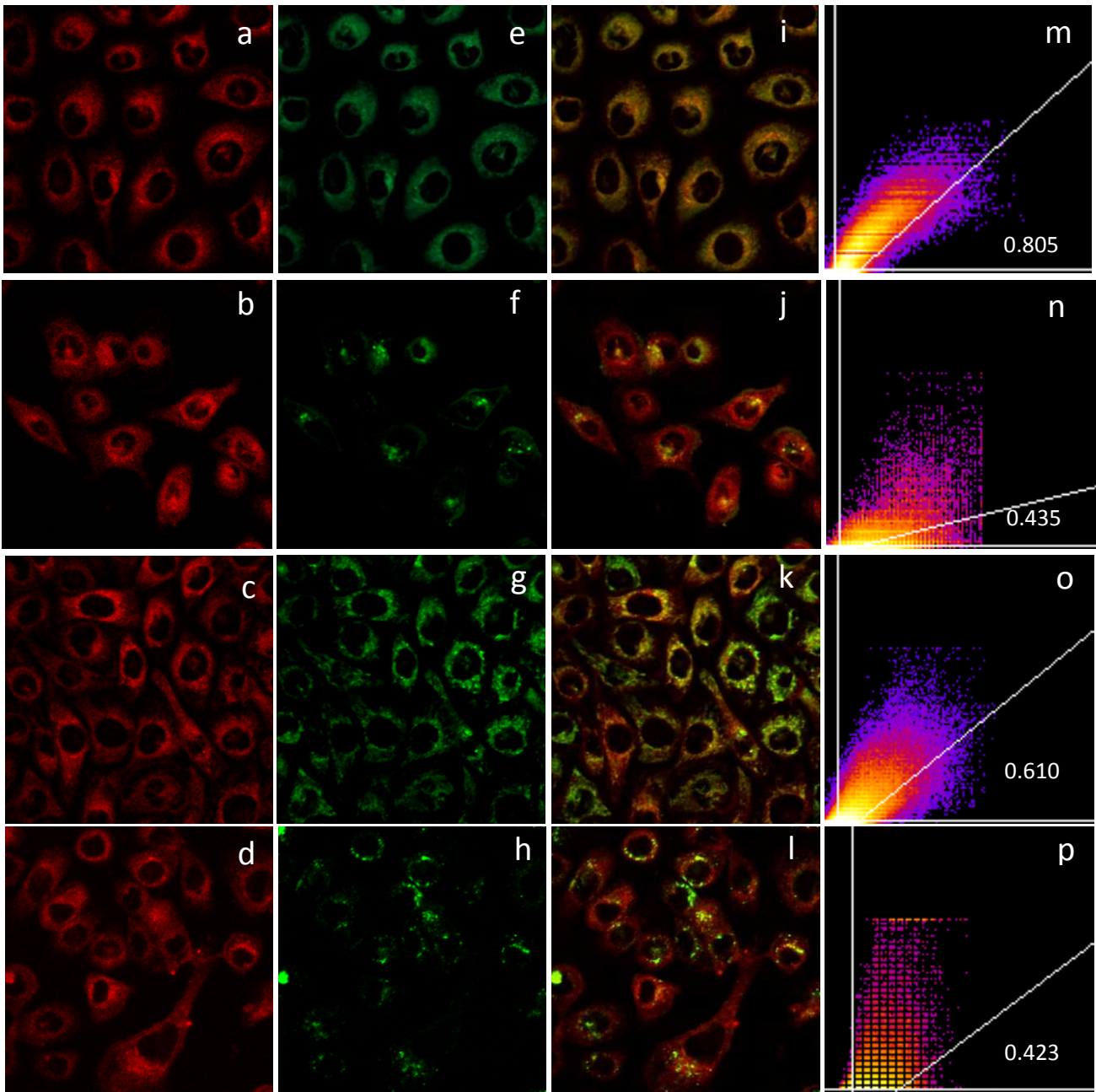


Figure 4.2. Microphotographs of Nt8e cells showing subcellular localization of Cp_6 . The cells were treated with $10 \mu\text{M}$ Cp_6 (first panel from left) and specific fluorescence probes for endoplasmic reticulum (e), Golgi (f), mitochondria (g) and lysosomes (h) (second panel). The overlay of Cp_6 fluorescence with respective organelle probe (third panel) and histogram with value of correlation coefficient (right panel) is also shown.

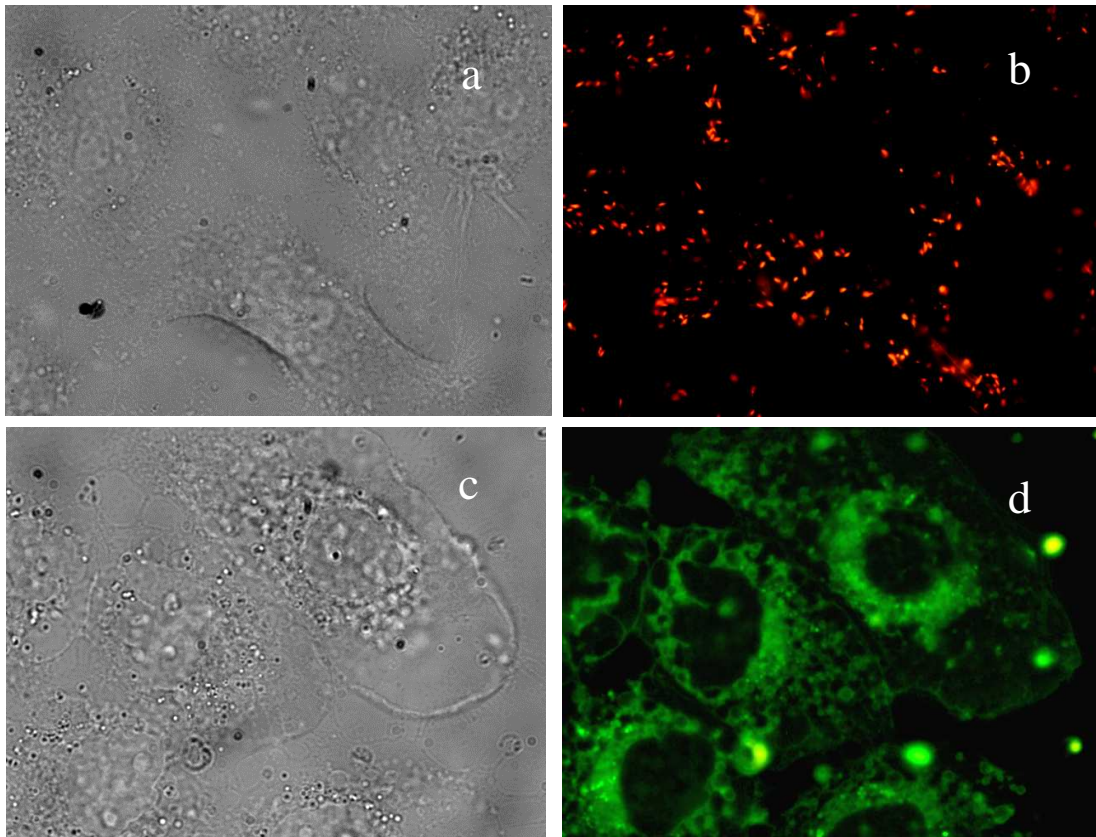


Figure 4.3. Brightfield and fluorescence images of Nt8e cells 1 h after PDT with 10 μ M Cp_6 -his showing changes in morphology (right panel) and mitochondrial membrane potential (left panel), respectively. Control (a, b), PDT (c, d). Magnification - 100 X.

4.1.3 Alterations in ER morphology due to PDT

For a control cell stained with ER tracker dye, the volume rendered image constructed from the Z stack fluorescence images is shown in Fig 4.4a. In this image, the typical morphology of ER can be seen as forming a dense network around the nucleus and a less dense peripheral network evenly distributed in the entire cytoplasm. We constructed 3D model of ER by isosurface rendering of the Z stack images (Fig 4.4b) and the resultant model is zoomed to show the detailed architecture of ER (Fig 4.4c). Since the fluorescence signal of ER tracker dye was more intense in the region around the nucleus than the peripheral region, the 3 D model constructed by isosurface rendering using fixed threshold revealed only the dense perinuclear region of the ER (Fig 4.4b). A zoomed portion of this region presented in Fig 3c clearly shows structural details of ER comprising sheets or cisternae (thin arrow) and small tubular connections between these (thick arrow). These structures appeared intact and evenly distributed around the nuclear region. The middle panel in Fig 4.4 shows images representing a cell that underwent necrosis due to PDT-induced damage. In the volume rendered image (fig 4.4d), the formation of membrane bubbles (arrow) typical of necrotic death is clearly visible and one can also note that ER is highly fragmented. The 3D reconstruction by isosurface rendering provided better visualization of the fragmentation of ER (fig 4.4e). Here, the ER network in perinuclear region is discontinuous and surrounded by several large and small ER fragments. A closer view of this region shown revealed that the ER fragments comprised of cisternae but no tubular connection between these (fig. 4.4f). The images in the left panel of fig. 4.4 show ER structural alterations in a damaged cell having no obvious morphology typical of

necrosis. In the volume rendered image (fig 4.4g), the ER network appears highly condensed surrounded by several large fragments. The isosurface rendered image clearly displays the presence of ER fragments as large clumps in the perinuclear region (Fig 4.4 h). A portion of 3D model zoomed in this region revealed that the clumps are swelled ER cisternae with some portion of connecting tubule attached to it (fig4.4i).

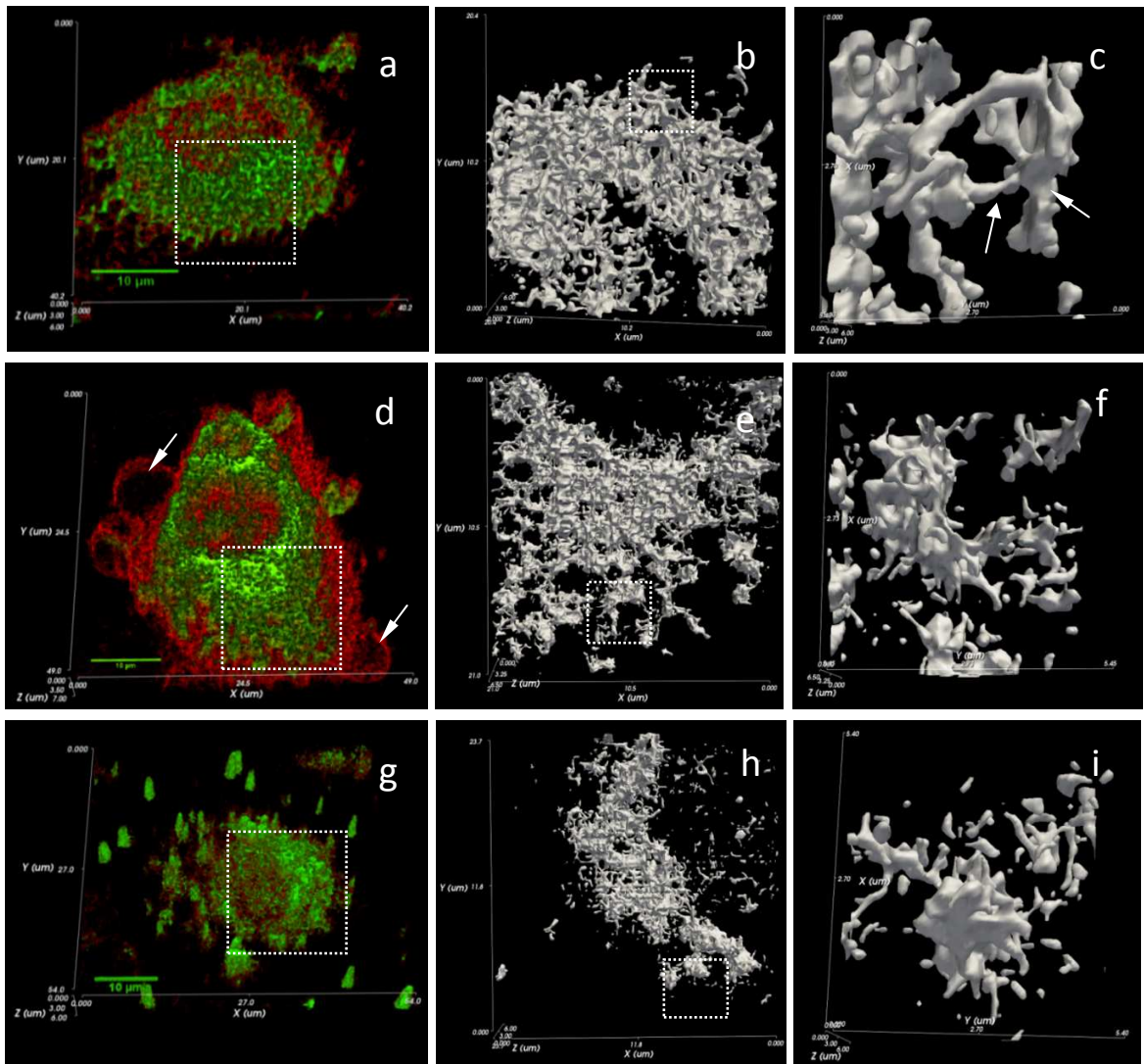


Figure 4.4. 3D reconstructions of z-stacked images of Nt8e cells stained with ER-tracker green. Volume rendered images (left panel) in top on tilted view showing regions of pronounced staining (green) and weak staining (red) corresponding to ER and other cellular regions, respectively. The top view of smaller regions of images (dashed rectangle) is shown as Isosurface rendered images (middle and left panel). A cell representing control show intact cell morphology and ER network (a) comprising a dense perinuclear region of ER (b) having cisternae (c, thin arrow) connected by tubules (c, thick arrow) (c). A damaged cell with typical morphology of necrotic death (d) having formation of membrane bubbles (arrows) and fragmentation of ER (e), the fragments appear to be part of ER cisternae with no tubular connections (f). A damaged cell with

shrinkage in morphology and condensation of ER network (g), ER clumps in perinuclear region (h) and a close view of ER clump (i).

4.1.4 Alterations in the morphology of Golgi due to PDT

In Fig 4.5 we show images of cells stained with bodipy ceramide that particularly label the trans Golgi network. In the 3D volume rendered image of a control cell, the intact Golgi can be seen as floret like bodies around the nuclear region (fig 4.5a). A close view of smaller region shown from the top in isosurface rendered image provided better clarity showing interconnected trans-Golgi cisternae (fig 4.5b) which in the side view of 3D model appear to form a tower like structure and one can also note several small vesicles budding out from the trans Golgi cisternae (fig 4.5c). At 1h after PDT, the architecture of Golgi showed two types of alterations. For a cell representing necrotic morphology, the 3D volume rendered image is shown in fig 4.5d. The Golgi structure in the center (dashed square) appeared broken and a large fragment of Golgi (thick arrow) in the cytoplasm can be observed (fig 4.5d). The smaller fragments of Golgi which are located at cell periphery are associated with membrane bubbles (thin arrow, fig 4.5d). In a close view shown as isosurface rendered image (fig 4.5e), the main Golgi region in the center portion clearly shows leftover portion of Golgi surrounded by some remains which seem to demarcate the location of a large Golgi fragment (shown in fig 4.5d by thick arrow). In the side view of the 3D model, the Golgi fragments appear detached from its base and swelling of Golgi is also clearly discernible (fig 4.5f).

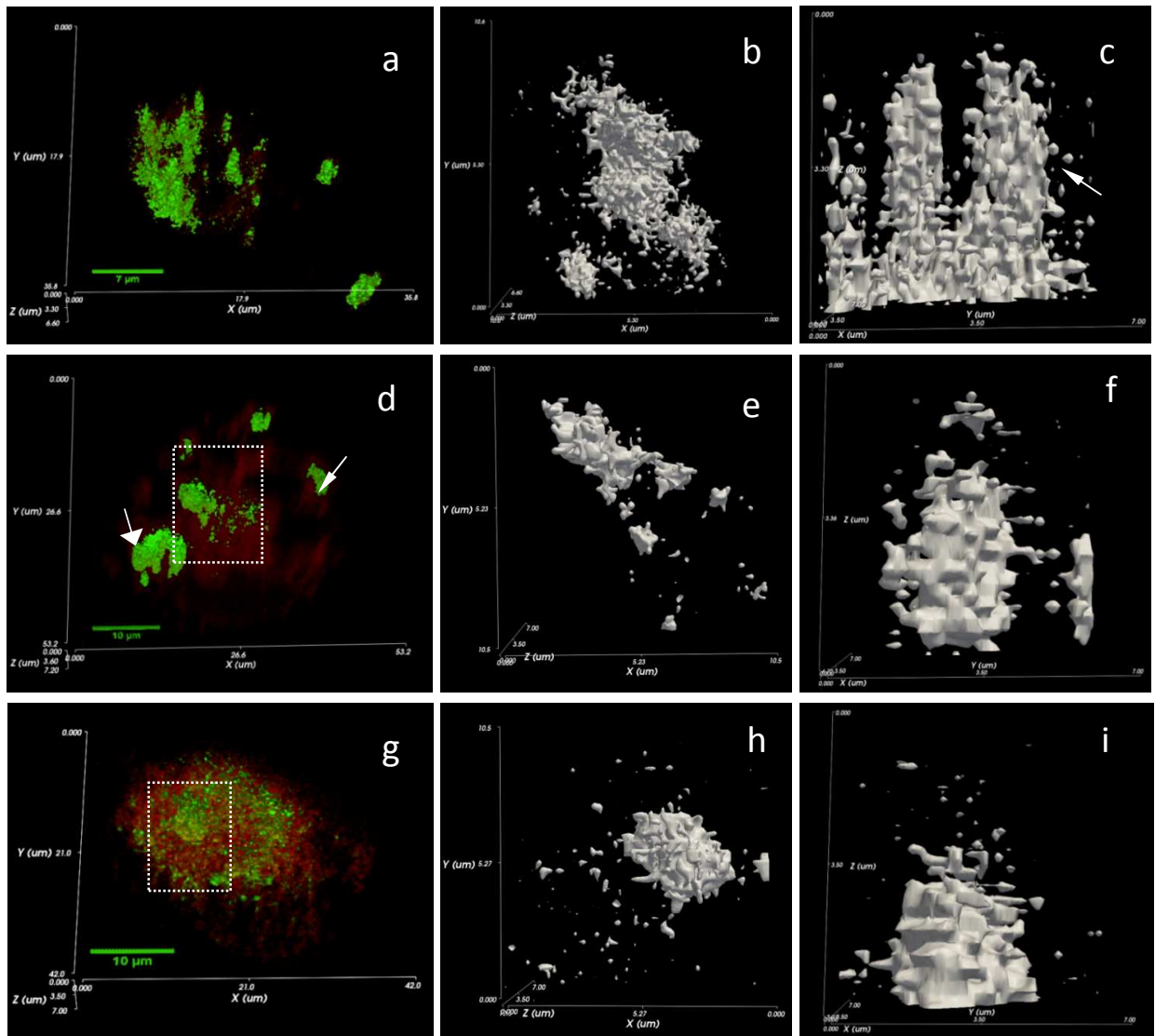


Figure 4.5. 3D reconstructions of z-stacked images of Nt8e cells stained with Golgi specific bodipy ceramide green. Volume rendered images (left panel) in top on tilted view showing regions of pronounced staining (green) and weak nonspecific staining (red) corresponding to Golgi and other cellular regions, respectively. The top view of smaller region of images (dashed rectangle) is shown as isosurface rendered images (middle and left panel). A cell representing control show intact Golgi structures (a), comprising interconnected trans cisternae (b) to form a tower like structure (c, thin arrow) with several vesicle budding out from these (thin arrow, c). A damaged cell (d) with formation of membrane bubbles (arrows) typical of necrotic death and fragmentation of Golgi (dashed

square), the leftover portion of Golgi surrounded by some remains (e) and same in side view (f). Another damaged cell with condensed Golgi in the centre (g), a close view of this region from the top (dashed square) (h) and side view of the same (i).

Apart from fragmented morphology of Golgi observed in necrotic cells, we could identify another type of morphological alterations in Golgi after PDT. The images representing one such cells are shown in Fig 4.5 g-i. The volume rendered image and 3 D isosurface model shows a single centrally located Golgi structure surrounded by several irregularly shaped Golgi fragments in the perinuclear region (fig 4.5 g & h). The close view of 3 D model from top shows a condensed trans Golgi structure in the center of the cell (fig 4.5i).

4.1.5 PDT-induced damage to lysosomes

Images of a healthy cell stained with lysotracker green are shown in Fig 4.6 a-c. In the volume rendered image lysosomes in the region of cytoplasm can be seen as discrete vesicles (fig 4.6a). The side view of isosurface rendered 3D model shows that the vesicles (thick arrow) originate from a densely packed region (thin arrow) in the centre (fig 4.6b). It is important to mention here that lysotracker also stains the acidic compartments of Golgi. Consistent with this, in the closer view of the 3D model from the side, one can note the presence of tubular structures of Golgi cisternae from which these vesicles are budding off (fig 4.6c).

In cells subjected PDT the fluorescence of lysotracker green is observed to localize mainly around the perinuclear region. The images representing on such cell are shown in fig 4.6d-f. In volume rendered image no structures similar to lysosomes could be visualized and instead the fluorescence of lysotracker was observed in a larger area around the perinuclear region (fig 4.6d) as compared to control cell (fig 4.6a). The side view of 3D model obtained by isosurface rendering clearly shows absence of lysosomes and the structures at perinuclear region resembled with Golgi/ER cisternae (fig 4.6 e). In a closer view, a swelled Golgi (thick arrow) along with ER cisternae can be seen clearly (fig 4.6f).

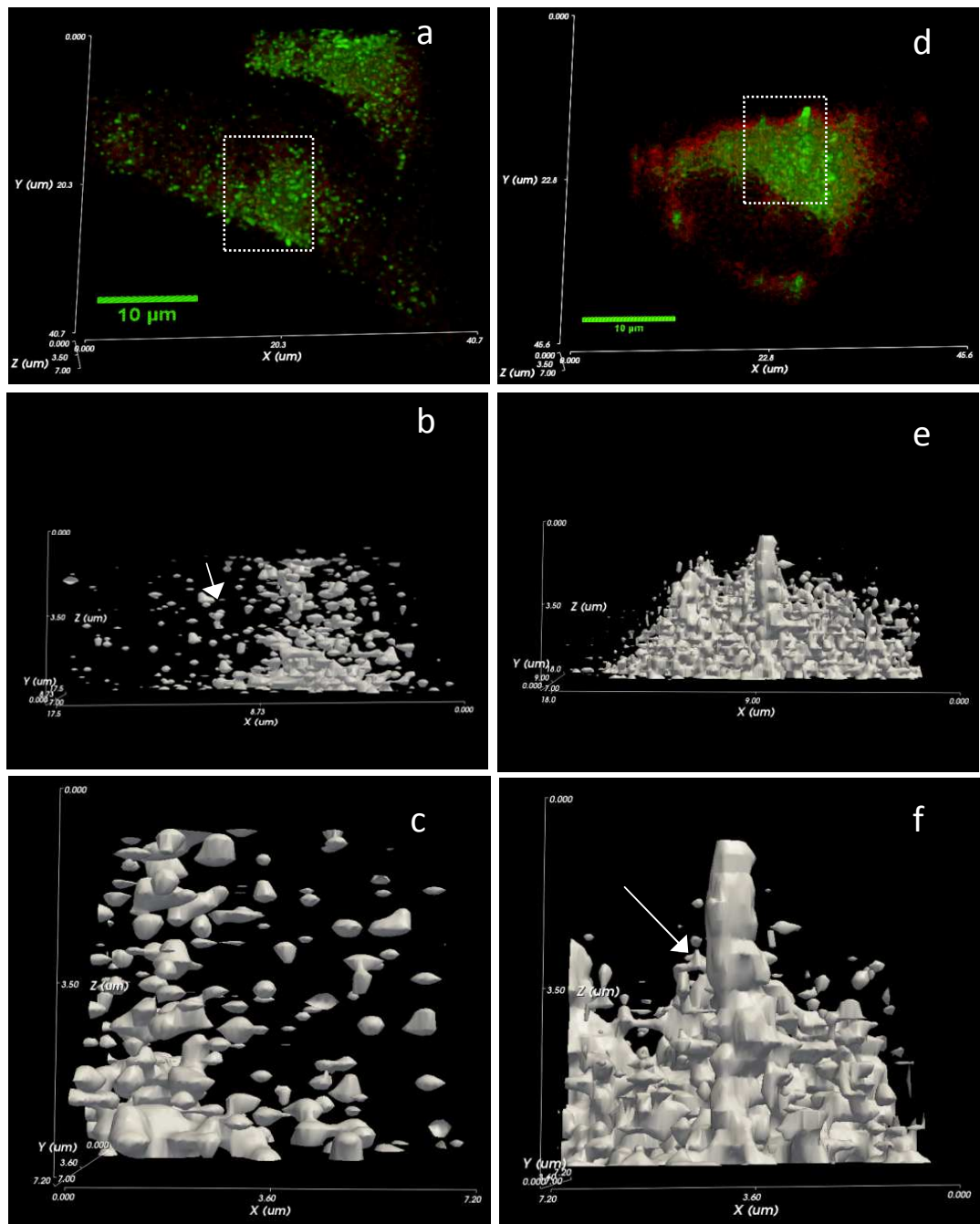


Figure 4.6. 3D reconstructions of z-stacked images of Nt8e cells stained with lysotracker green. Volume rendered images (top panel) in top tilted view showing regions of pronounced staining (green) and weak nonspecific staining (red) corresponding to acidic compartments and nearby cellular regions, respectively. The side view of a smaller region of image (dashed rectangle) is shown as isosurface rendered images (middle and bottom panel). A cell representing control show intact lysosomes in the cytoplasm (a), and a dense

perinuclear region (thin arrow) from which these vesicles (thick arrow) appear to originate (b), a much closer side view of the dense region showing many lysosomes (c). A damaged necrotic cell (d) shows the spread of lysotracker dye in a larger volume (dashed square) and same in side view (e). A closer view from side shows structures similar to a swelled Golgi (thick arrow) and portion ER in the perinuclear region (f).

4.2 Discussion:

4.2.1 Intracellular localization of Cp₆-his

Results of our study show that chlorin *p*₆-histamine conjugate localizes mainly in ER and lysosomes. In comparison, free Cp₆ was observed to localize mainly in ER and to a lesser extent in lysosomes. For Cp₆-his, localization in lysosomes was expected because of the involvement of receptor mediated mechanism in its cellular uptake as reported in our studies in chapter 3 [283]. In comparison, the absence of significant uptake of free Cp₆ is in conformity with similar observations reported by Mojziso \acute{v} a et al in human fibroblast cells for chlorin e6 [292] which is chemically similar to Cp₆ except one additional methylene (CH₂) present at meso carboxylic group in the molecule. They have observed that Ce6 at physiological pH (7.4) localized in the plasma membrane and vesicular structures but not in lysosomes and suggested that the cellular uptake of Ce6 is governed by passive diffusion or absorptive endocytosis [292].

4.2.2 PDT-induced ER damage

Although the study of sub-cellular distribution of the photosensitizer could provide knowledge of the possible intracellular target sites of the photosensitizer, it is also necessary to correlate the PDT-induced cytotoxicity with damage to various sub-cellular structures particularly for photosensitizers which localize in ER. This is due to the fact that ER is distributed in cytoplasm as a complex network of tubules and sheets comprising two distinct domains one at perinuclear regions and other in peripheral region which is physically connected to various sub-cellular compartments such as Golgi, mitochondria and plasma membrane [293]. We have applied 3D fluorescence microscopy technique to visualize and analyze the changes in the structural organization of ER, Golgi and lysosomes in human oral cancer cells following PDT with Cp_6 -histamine conjugate. The 3D model of ER constructed from the image stacks of control cell shows close similarity with the ER structure reported in mammalian cells (CHO-K1 cell line)[294]. The model shows distinct perinuclear region comprising of flat sheets surrounding the nucleus which forms smaller cisterna joined by tubules at the outer end (Fig 4.4b & C). The peripheral ER which is mostly tubular is visible in volume rendered image (Fig 4.4a) but not in iso-surface rendered 3d model. This is because the staining with ER tracker dye does not label peripheral ER as intensely as the perinuclear ER.

In PDT treated cells 3D modeling of ER gives clear view of structural alterations induced by PDT and revealed remarkable difference in the damage pattern of ER in

necrotic and apoptotic cells. In necrotic cells identifiable by the presence of large membrane bubbles extensive fragmentation of ER both at nuclear and peripheral region is detected (Fig 4.4d & e). In closer view, the loss of tubular region connecting the ER cisterna is clearly seen which suggest that tubular ER is more sensitive to PDT (fig 4.4 f). We have previously shown that both necrosis and apoptosis contributes equally to the percent cell death in Nt8e cells after PDT with Cp_6 -his at 90% phototoxicity level [283]. Consistent with these results, cells with completely different type of ER structural alterations than described above could also be identified. In these cells ER fragmentation was less obvious and instead, formation of clumps or small aggregates of ER was noticed (Fig 4.4 g, h & i). The aggregates of ER appeared to have originated from both peripheral ER and ER at nuclear region. Similar structural alterations in ER due to PDT have not been reported earlier. In a recent study, using fluorescence microscopy Ferrari et al have shown that treatment of HeLa cells with C2-ceramide, a lipid second messenger of intrinsic apoptotic pathway lead to formation of 'large round aggregates' of ER which also accompany release Ca^{2+} from ER and subsequent loss of mitochondrial membrane potential (MMP) [295]. The ER structural alternation induced by PDT with Cp_6 -his are consistent with this report and in addition we have also found that PDT with Cp_6 -his led to loss of MMP (Fig 4.3). These results therefore suggest that induction of apoptosis in Nt8e cells after PDT with Cp_6 -his could be similar to intrinsic apoptotic pathway mediated by C2-ceramide.

4.2.3 PDT induced Indirect Damage to Golgi apparatus

The 3D model of Golgi in control cell appeared as interconnected tubular structure with spherical ending surrounded by secretory vesicle (fig 4.5). The Golgi tracker 'Bodipy ceramide' is known to accumulate in the trans-Golgi portion [296]. The modeled structure shows close similarity with the structure of trans-Golgi reported in epithelial cells [297]. The 3D image reconstruction of Golgi allowed a clear visualization of PDT induced structural changes which can be seen as fragmentation of Golgi and the fragment appeared displaced from its main location at the perinuclear region (fig 4.5). In lateral view, the loss of connecting regions of the Golgi from its base can be seen clearly and the damaged portion of Golgi appear dilated and floating as compared to the structure of Golgi in control cell which appear intact and adhered to the base (fig 4.5c & f). Since Cp_6 -his did not localize in Golgi the direct damage to Golgi after PDT is less likely. It is known that ER form close association with Golgi around domains of its trans-cisternae [298]. Thus we believed that the structural damage to Golgi apparatus observed after PDT involve loss of its contact sites with ER due to the fragmentation of later. Since the cell under observation showed presence of membrane bubbles the fragmentation of Golgi structure appeared to be associated with necrosis. Studies have shown that the structure of Golgi complex is altered differently during necrotic and apoptotic cell death induced by staurosporine (STS) treatment in HEP-2 cells [299]. These authors reported fragmentation of Golgi in necrosis and swelling of Golgi followed by condensation and vesicle formation during early and late stages of apoptosis [299]. We also observed that apart from fragmented morphology,

the cells treated with PDT also displayed alterations in Golgi structures as formation of single condensed body around the nuclear region and several small vesicular structures at perinuclear region. Since fluorescence imaging was performed 1 h after PDT, these structural changes in Golgi could be associated with early stage apoptosis as reported by Nozawa et al [299].

4.2.4 PDT induced damage to lysosomes

Cp_6 -his conjugate showed significant localization in lysosomes also. 3D imaging of cells stained with lysotracker dye revealed several intact vesicles in the cytoplasm and a part of Golgi region from where these vesicles appear to originate (fig 4.6a-c). In cells subjected to PDT, presence of less number of intact vesicles and some distorted or swelled vesicles suggested disruption of lysosomes after PDT (fig 4.6 d-f). In a previous study on PDT of murin hepatoma cells with N-aspartyl chlorin e6, the disruption of lysosomes has been judged by rapid disappearance of acridine orange fluorescence in cells [300]. In 3D model, we show that 3 D fluorescence imaging provided direct visualization of the damage to lysosomes represented by less number of intact lysosomes in treated cells. Further, as compared to the control the fluorescence of lysotracker dye in treated cells was observed to re-distributed and localize in larger portions around the perinuclear region. These structures were clearly identifiable based on 3D model which revealed dilated or swelled structures resembling part of Golgi apparatus and ER cisternae (fig 4.6f). These

observations suggest that PDT-induced lysosomal damage leads to re-localization of the lysotracker dye in parts of Golgi and ER network.

4.3 Conclusion

In conclusion, our results show that ER and lysosomes are the major intracellular sites of Cp_6 -his localization in oral cancer cells and 3D fluorescence imaging not only allowed direct visualization of structural damage to these organelles but could also differentiate changes related to necrotic and apoptotic cell death. The observations suggest that ER fermentation leads to indirect damage to Golgi apparatus due to loss of its contact site which could also play a role in necrotic death. As compared to alterations in ER and Golgi structure in necrotic cells, the distinctly different pattern of damage in ER network and Golgi appeared to be associated with apoptotic cell death. Further, the damage to lysosomes was observed to lead to relocalization of lysotracker dye in Golgi and ER. Recent study showed that diverse cell death pathways leading to apoptosis are induced in PDT depending on the sub-cellular targets [301]. By revealing structural damage to cell organelles by 3D fluorescence imaging we suggest that the close association of organelles and indirect damage apart from site of localization of photosensitizer could play an important role in induction of diverse cell death pathways.

CHAPTER 5

EVALUATION OF PDT EFFICACY OF

***Cp*₆-HISTAMINE CONJUGATE IN**

HAMSTER CHEEK POUCH MODEL.

Based on encouraging results of *in vitro* studies presented in previous chapter, we monitored the expression of histamine H2 receptors in tumors and normal mucosa of hamster cheek pouch model using immuno-histochemistry. The results showed that the expression of Histamine H2 receptor is higher in tumors as compared to normal mucosa. This was consistent with the overexpression of H2 receptors reported for other types of malignancies [212]. Motivated by these results, we evaluated the photodynamic efficacy of Cp_6 -his for the treatment of oral tumors in this animal model by monitoring accumulation of Cp_6 -his in tumors, normal tissue and skin to determine its tumor selectivity and clearance. PDT-induced tumor damage has been assessed by tissue histology and tumor volume measurements. These results are presented and discussed below.

5.1 Results:

5.1.1 Tumor selectivity of Cp_6 -his

The fluorescence spectra collected from tumors, and normal mucosa at 4 h after intraperitoneal injection (3mg/kg body weight) of Cp_6 -his and Cp_6 are shown in Fig.5.1 a & b. The fluorescence spectra collected from the tumors and normal pouch of each animal are shown as superimposed curves (dotted line) along with a representative spectrum. The fluorescence spectrum from tumor tissue shows fluorescence band of Cp_6 -his and Cp_6 at ~674 nm whereas the bands at 635 nm and 705 nm are due to the presence of endogenous porphyrin (Pp). The level of endogenous Pp varied in different tumors, therefore to determine the level of Cp_6 -his and Cp_6 , the fluorescence of endogenous Pp was

mathematically removed by subtracting each spectrum with a reference spectrum that was obtained from the tumor before photosensitizer injection. The resultant spectra are shown in fig 5.1 a& b inset and the values of peak fluorescence intensity (674 nm) thus obtained for Cp_6 -his and Cp_6 in tumors and normal pouch of each animal are presented in table 1. Since the fluorescence yield of Cp_6 -his is nearly half than that of Cp_6 , the value of fluorescence intensity of Cp_6 is divided by a factor of 2 to compare its level with that of Cp_6 -his. It can be seen that the fluorescence intensity of Cp_6 -his in tumor is much higher as compared to that for normal mucosa indicating its preferential accumulation in tumor. While Cp_6 also showed similar higher accumulation in tumor, the accumulation of Cp_6 -his in normal mucosa was much less as compared to Cp_6 ($p < 0.001$) (Table 1). The tumor to normal tissue ratio of fluorescence intensity at 674 nm was significantly higher for Cp_6 -his (9.2, $p < 0.001$) as compared to Cp_6 (2.3). These results suggest that the tumor selectivity of Cp_6 -his is better than that for Cp_6 .

5.1.2 Pharmacokinetics of Cp_6 -his in Hamster cheek pouch model

The clearance of Cp_6 -his from abdominal skin was observed to be rapid as indicated by ~50% decreases in its fluorescence within 24 hr and further decrease by ~ 90% at 72 hr after its intraperitoneal injection (circles, Fig 5.2). For Cp_6 similar trend was observed (square, Fig. 5.2). The respective fluorescence spectra of Cp_6 -his collected from the abdominal skin at different time intervals are shown in Figure 5.2 inset. The pharmacokinetics of Cp_6 -his and Cp_6 in tumor and normal mucosa was observed to follow a similar trend (Fig. 5.3).

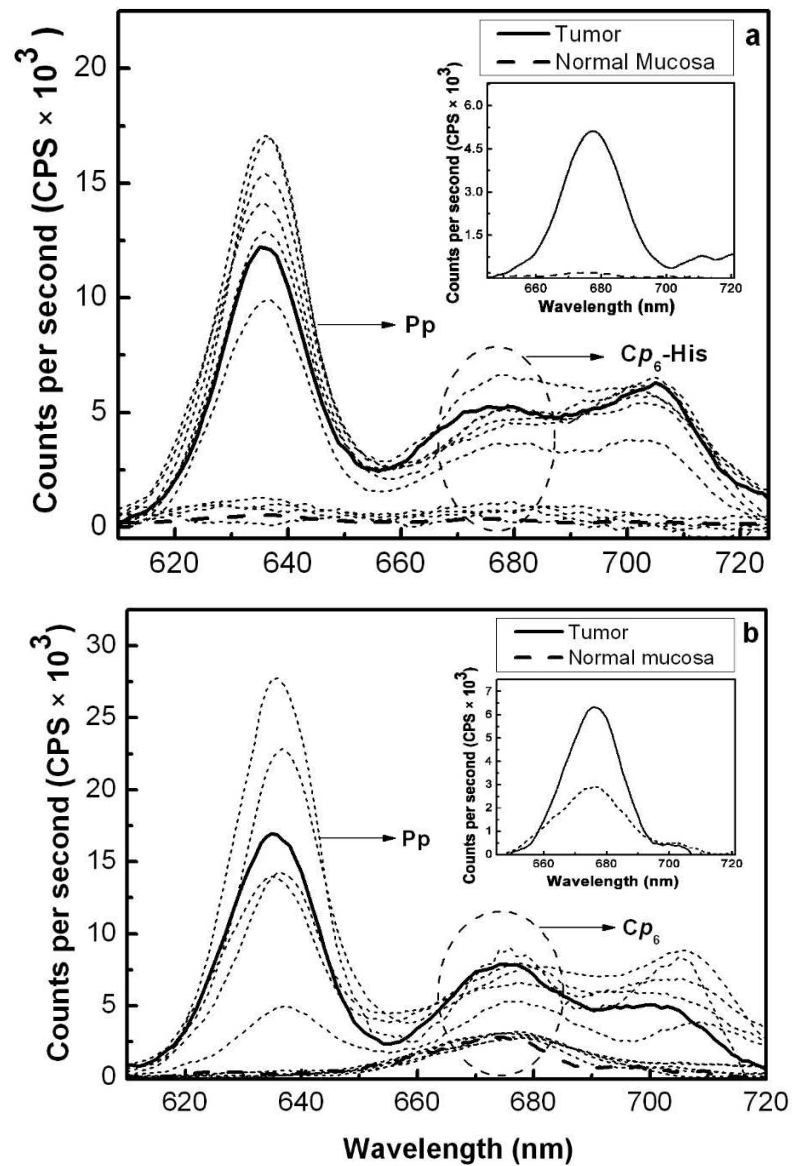


Figure 5.1: Fluorescence emission spectra collected from a tumor (solid curve) and normal pouch (dashed curve) and superimposed spectra from all other tumors and normal pouch (dotted curves) of four different hamsters are shown. *Cp₆-his* (a) and *Cp₆* (b). Measurements were done at 4 h after administration of the photosensitizer (3 mg/kg body weight). Pp – fluorescence band of endogenous porphyrin. Dashed circle shows the position of fluorescence band of *Cp₆-his* or *Cp₆*. Inset- Representative Spectrum obtained from tumor and normal pouch after subtraction of endogenous Pp auto-fluorescence.

Table 5.1. Fluorescence intensity of Cp_6 -his and Cp_6 in tumor and normal mucosa at 4hr after the administration of photosensitizer at dose of 3.0 mg/kg body weight. * - In order to compare the level of Cp_6 with Cp_6 -his, the fluorescence intensity of Cp_6 is divided by a factor of 2 considering its higher fluorescence yield. ** - In normal mucosa, the level of Cp_6 is significantly higher than that for Cp_6 -his. † - The tumor to normal ratio for Cp_6 -his is significantly higher than for Cp_6 .

Cp_6 -His				Cp_6			
Animal #	Fluorescence Intensity (Cps)			Animal #	Fluorescence Intensity (Cps)		
	Tumor	Normal	Ratio Tumor/Normal		Tumor	Normal	Ratio Tumor/Normal
1	5941	762	7.7	1	9498.2	3244.8	2.92
(2Tumors)	4651		6.1	(2Tumors)	8287.4		2.55
2	3715	320	11.6	2	6540.5		2.18
(2Tumors)	3150		9.8	(2Tumors)	6034	2988.4	2.07
3	2721.8	475	5.7	3	5227.9	2906.51	2.13
4	2047	166	12.3	4	5086	2451.5	2.074
(2Tumors)	2255		13.5				
Average ±SD	3497 ±1397	430 ±254	9.5 ±3.0	Average ±SD	6779 ±1763 (3389±881)*	2897 ±330 (1440±179)*	2.3 ±0.34
<i>P</i> value		<0.001 **	<0.001 **				

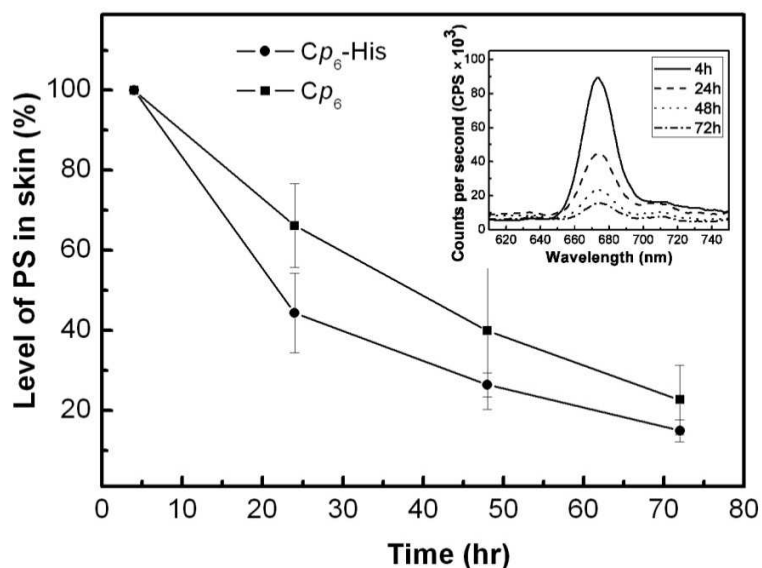


Figure 5.2: The level of Cp_6 -his (circle) and Cp_6 (square) in the abdominal skin of the hamster at different time interval after i.p injection is shown as percent of their peak fluorescence intensity at each time point with respect to fluorescence intensity at 4 hr after injection. Data are average \pm SD, n - four animals. Inset – Representative fluorescence spectra of Cp_6 -his collected from skin of the hamster at 4 h, 24h, 48h and 72h after administration of 3 mg/kg body weight. Spectra of Cp_6 were similar.

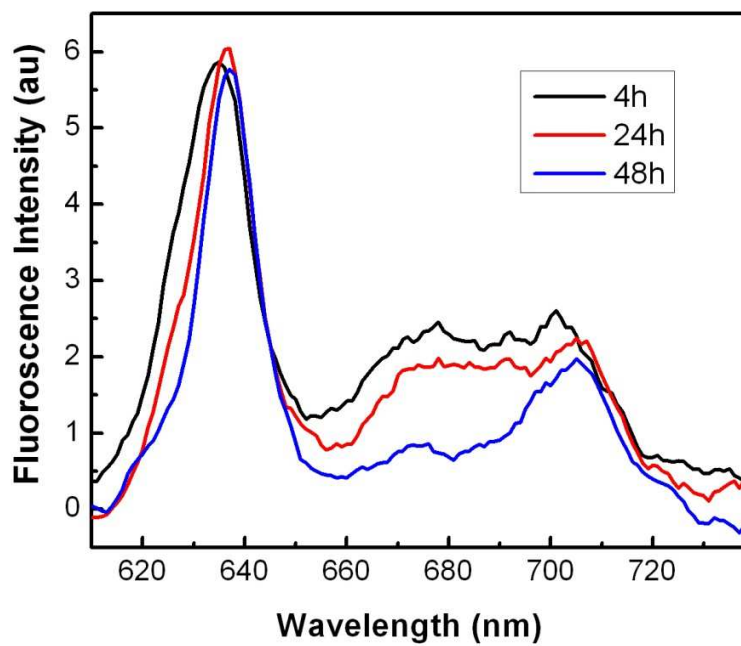


Figure 5.3: Fluorescence emission spectra collected from a tumor at different time interval after administration of the photosensitizer Cp_6 -his (3 mg/kg body weight).

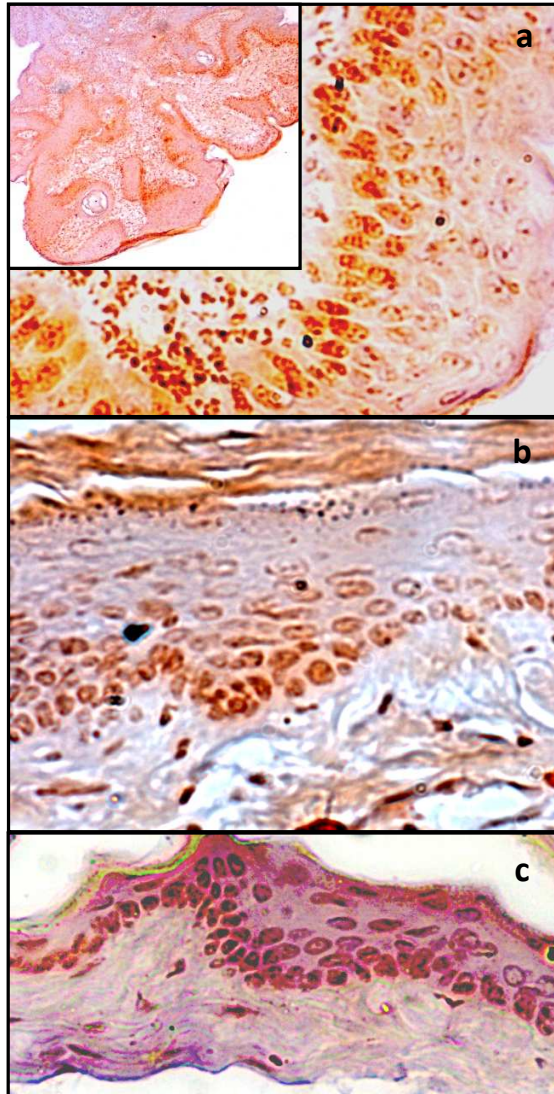


Figure 5.4: Immunohistochemical detection of H2R receptor in tumor (a) mucosa adjoining tumor (b) and normal mucosa (c). Magnification 400X, Bar-15 μm . Inset - Photomicrograph at 600X magnification, Bar-100 μm .

5.1.3 Histamine receptor expression

In order to confirm the presence of histamine receptors immunohistochemistry using H2 receptor antibody was done. Results of immunohistochemistry of tumor, tissue surrounding tumor and normal cheek pouch mucosa are shown in photomicrograph in figure 5.3. The expression of histamine receptor was found to be higher in tumor tissue (Fig 3a) compared to surrounding tissue (Fig 3b) and normal mucosa (Fig 3c). This is also confirmed by western blot shown in Fig 5.4 in which a band at 80 kDa was observed due to presence of oligomer of H2 receptor [252]. The intensity of this protein band was more in tumor (TM) and surrounding mucosa (SM) as compared to normal mucosa (NM). The expected molecular weight of H2R is ~33 KDa. It has been reported that H2R isoforms of different species (canine, rat, human, guinea pig) are closely related to each other (80%) with respect to amino acid sequence. However, immunological detection by SDS-PAGE showed differences in the migration pattern of H2R from different species [252]. For example, while human H2R showed bands corresponding to monomer, dimer and oligomers, for canine and guinea pig H2R the monomers were absent and doublet bands at ~60 kDa of differentially glycosylate H2R dimmers has been reported. The absence of monomer H2R and doublet band seen at 70-80 KDa for H2R of hamster cheek pouch is similar to migration pattern reported for H2R of canine and guinea pig [252].

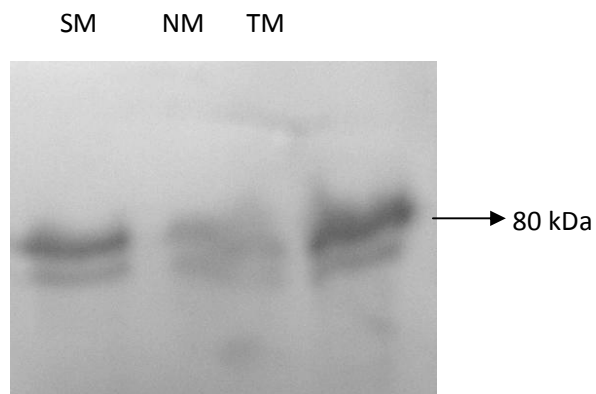


Figure 5.5: Image of nitrocellulose membrane showing presence of H2 receptor in tumor, mucosa adjoining tumor and normal mucosa of the hamster after Western blot of the protein using polyclonal rabbit anti-H2 receptor antibody and HRP conjugated Goat Anti-Rabbit IgG and detection using enhanced liquid substrate (DAB).

5.1.4 PDT induced tumor damage and regression

The extent of tumor damage at 24 h after PDT was assessed by histopathology using standard HE staining. The control tumor is stained dark with hematoxylin staining (Fig. 5.5a) due to presence of intact nucleus in tumor cells. In contrast, absence of hematoxylin staining in treated tumor (Fig. 5.5b) indicates cellular damage and necrosis. As can be seen in table 5.2, one week after PDT all the tumors of small size regressed completely and larger tumors (>500) regressed to ~95%. The photographs of tumor in a representative animal before and after PDT are shown in figure 6. The size of this tumor before PDT was ~520 mm³ and the mucosa surrounding the tumor had prominent vasculature (fig 5.6a). One week after PDT the tumor reduced to ~95% of its original size and the mucosal vasculature also attains a normal morphology. (Fig 5.6b). During follow up the regressed tumor did not show further growth and the morphology of mucosa and vasculature around the tumor was completely normal (fig. 5.6c).

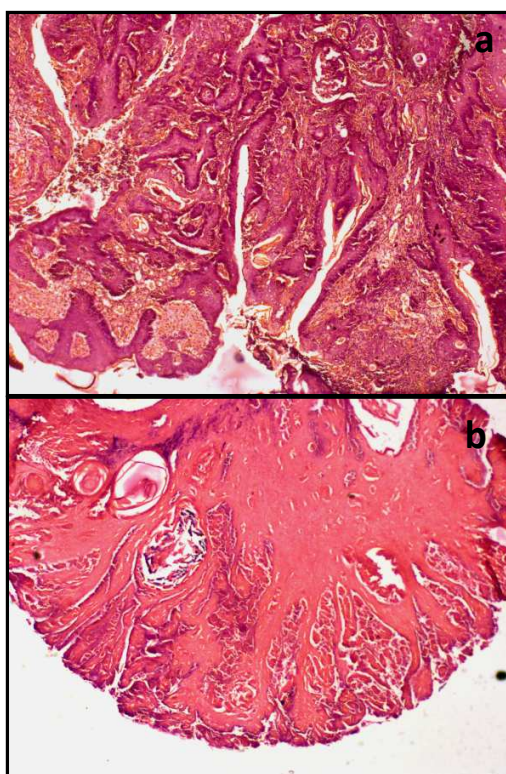


Figure 5.6: Photomicrographs showing histology of untreated tumor tissue (a) and tumor tissue subjected to PDT (b) using Cp_6 -his at 3.0 mg/kg and light dose of 100 J/cm^2 . Magnification 400X, Bar- $400 \mu\text{m}$.

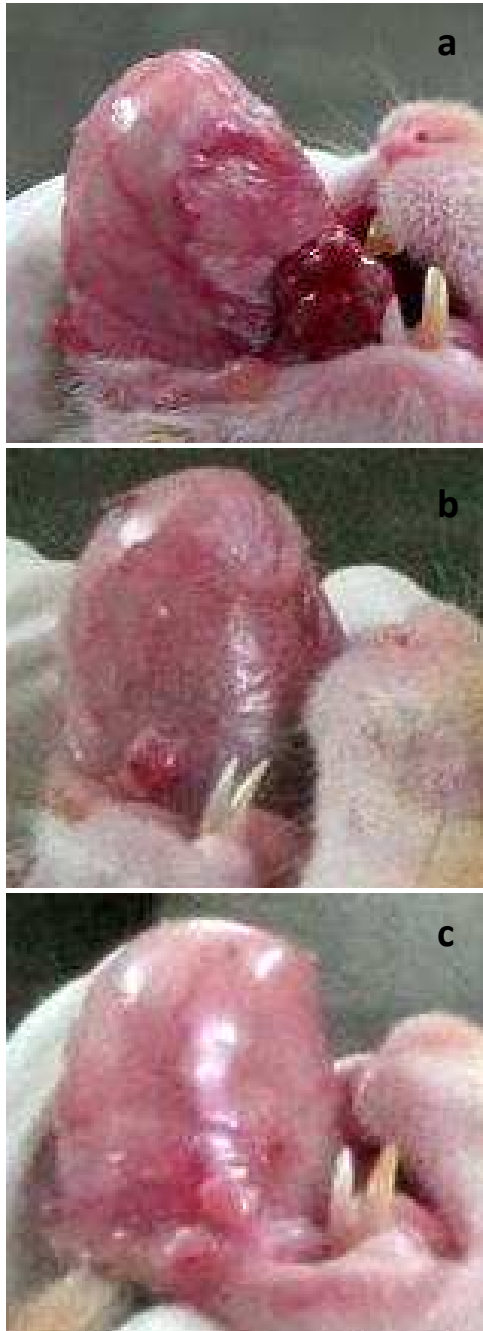


Figure 5.7: Photographs showing PDT-induced tumor regression in a representative animal. (a) Tumor before PDT and (b) one week after PDT using Cp_6 -his at 3.0 mg/kg body weight and light dose of 100 J/cm² (c) One month after PDT.

Table 5.2: Tumor volume before and one week after photodynamic treatment using Cp_6 -his at 3.0 mg/kg body weight and light dose of 100 J/cm².

Animals	Tumor	Tumor Volume (mm ³)	
		Before PDT	One week after PDT
Hamster(1)	(1)	29	— (100 % Regression)
	(2)	52	— (100 % Regression)
Hamster(2)	(1)	98	4 (95 % Regression)
	(2)	115	— (100 % Regression)
Hamster(3)	(1)	1264	68 (95 % Regression)
Hamster(4)	(1)	378	— (100 % Regression)
Hamster(5)	(1)	520	26 (95 % Regression)

5.2 Discussion

Results of our study show over-expression of histamine H2 receptor in tumors of hamster cheek pouch and therefore provide basis for use of Cp_6 -his for PDT. So far, there exists no report on status of histamine receptor expression in human oral malignancies. The hamster cheek pouch model is a well characterized oral cancer model having several features common with that of human oral cancer including structural similarity related to progression of cancer such hyperkeratosis, dysplasia, invasive carcinoma and well differentiated carcinoma [302] as well as molecular changes like expression of oncogenes, cell proliferation markers and immune-related cytokines [303]. Particularly, increased expression of several transmembrane receptors (EGFR, FGFR, erb2) has been found similar to human OSCC [303]. In this context, chlorin e6 conjugated to epidermal growth factor receptor monoclonal antibody (EGFR-MAB) has been investigated for PDT of oral pre-cancer in hamster [304]. So far no other photosensitizer conjugate has been investigated for targeted PDT of OSCC. Based on results on over-expression of histamine receptors in hamster model we investigated the use of Cp_6 -his for PDT of oral tumors.

The results on the accumulation of Cp_6 -his in tumor and normal mucosa show that while both Cp_6 -his and free Cp_6 accumulate preferentially in tumor, the accumulation of Cp_6 -his in normal mucosa is much less as compared to Cp_6 . The ratio of fluorescence intensity of Cp_6 -his at 674 nm for tumor vs. normal mucosa was significantly higher than that for Cp_6 which is primarily because of its lower accumulation in normal mucosa. Other

photosensitizers used for PDT of OSCC in hamster e.g. meta(tetrahydroxyphenyl)chlorin (mTHPC) [21] and 2-[1-hexyloxyethyl]-2-devinyl pyropheophorbide-a (HPPH) [308] have been shown to give tumor vs. normal tissue ratio ≥ 2 , which is similar to that for free Cp_6 . The clearance of Cp_6 -his from the skin was rapid similar to Cp_6 [125], whereas in case of mTHPC studies in hamster OSCC model have shown its prolonged retention in the skin for five days followed by $\sim 80\%$ elimination in 10 days after injection [306]. The lower accumulation of Cp_6 -his in normal mucosa and its rapid elimination from skin show clear advantage with respect to minimizing the side effects of PDT.

PDT with Cp_6 -his led to almost complete regression of tumors of size as large as $\sim 1264 \text{ mm}^3$. In PDT with Cp_6 complete tumor regression was seen for tumor size of $\sim 133 \text{ mm}^3$ and larger tumors regressed only partially given the same light dose and slightly higher drug dose (4.0 mg/kg) [126]. This comparison suggests that photodynamic efficacy of Cp_6 -his is significantly better than Cp_6 . We expect that the improved PDT efficacy of Cp_6 -his could be due to its better uptake in tumor cells as demonstrated earlier in oral cancer cell line [283]. We compared the levels of Cp_6 -his and Cp_6 in tumors based on their fluorescence intensity after correction with their respective fluorescence yield and found no significant difference. It is however, important to note here that the level of photosensitizer measured from tumor tissue by in vivo fluorescence measurements represents amount present in tumor cells as well as tumor microvasculature. Therefore, with these measurements it cannot be ascertained whether conjugation of Cp_6 with histamine facilitated its uptake in tumor cells *per se* in vivo.

Since our studies in oral cancer cells showed significant inhibition in the cellular uptake of the conjugate by histamine receptor antagonist and low temperature [283], we believe that the uptake of Cp_6 -his is receptor mediated and therefore its higher tumor selectivity could be because of difference in expression level of histamine receptor in normal mucosa and tumor. In addition, the change in physical properties of Cp_6 such as charge and hydrophobicity due to attachment of histamine is also expected to contribute in the tumor selective accumulation of Cp_6 -his. This is due to the fact that the hydrophobicity of the photosensitizer is largely determined by the nature of side chain in the molecule [307] which in turn is believed to play significant role in the selective accumulation of photosensitizer in tumor [308]. Since Cp_6 -his has one carboxylic group less as compared to Cp_6 , there can be significant difference in their hydrophobicity. For example, dicarboxylic duteroporphyrin is more hydrophobic and shows higher affinity for LDL as compared to chlorin e6 which has three carboxylic groups in the molecule [307]. While photosensitizer bound to LDL enter in tumor cells via receptor specific endocytosis, hydrophilic photosensitizer is carried mostly by serum albumin into the tumor vasculature and accumulate in tumor stroma due to leaky neovasculature [307]. This might be the mechanism responsible for the preferential accumulation of Cp_6 in tumors in hamster where like many other tumors higher degree of neovasculature as compared to normal tissue has been reported [309]. In case of Cp_6 -his, interaction with histamine receptor or also with LDL for the reason described above can lead to better accumulation in tumor cells. This also raises the possibility that despite preferential accumulation of both Cp_6 and Cp_6 -his in tumor, there can be differences in their relative distribution between cellular and

vascular compartment of the tumor. It needs further investigations in appropriate model system to verify these aspects.

5.3 Conclusion

In conclusion, results show that histamine receptors are over-expressed in OSCC tumors and tumor selectivity of Cp_6 can be improved by conjugating it to histamine. PDT with Cp_6 -his led to complete regression of relatively large tumors, which suggests considerable improvement in PDT efficacy also. To find whether conjugation of histamine facilitate the accumulation of Cp_6 -his in the tumor cells as observed earlier for oral cancer cells required detail studies on its intratumoral distribution by confocal microscopy. While difference in histamine receptor level might contribute to higher tumor selectivity of Cp_6 -his, it is also likely that a change in physical properties of Cp_6 due to attachment of histamine also play some role. Taken together, coupling of Cp_6 to histamine provided a promising approach to improve PDT efficacy in hamster model and open new possibility which may be worth to explore further for PDT of human OSCC.

CHAPTER 6

INTERACTION OF Cp_6 -HIS AND Cp_6

WITH BSA AND LIVER MICROSOMES

For PDT effectiveness the selective uptake of the photosensitizer in tumor and its rapid clearance from the body are the two important aspects. Our studies in human oral cancer cells substantiated that Cp_6 -conjugate as compared to free Cp_6 led to higher cellular uptake and thus enhanced phototoxicity [283]. Also, in hamster cheek pouch tumor model the tumor selectivity of the conjugate was significantly higher than free Cp_6 . Further, the conjugated Cp_6 showed rapid clearance from the skin and PDT-induced tumor regression also improved considerably with respect to free Cp_6 [310]. While studies in cancer cells confirmed that the uptake of the conjugate is receptor mediated [283], there is also possibility that the changes in the chemical characteristics such as charge and hydrophobicity as a result of the conjugation of Cp_6 to histamine may also influence the uptake and clearance of the conjugate. It is well known that the transport and preferential retention of the photosensitizer in tumor after its systemic administration is modulated by its interaction with various serum proteins such as albumin, LDL and HLD [311]. Generally, while hydrophilic photosensitizers show fast plasma clearance and non-specific or low retention in tumor due to their higher affinity with serum albumin, hydrophobic photosensitizers are likely to bind with serum LDL and can accumulate preferentially in tumor depending on the presence of LDL receptors on the tumor cells [312,313]. Further, the interaction of drug with microsomal proteins particularly Cytochrome P450 enzyme systems also depend on the lipophilicity of the drug and thus can affect its metabolic clearance [314].

In this chapter, we report results of our studies on the interaction of free Cp_6 and Cp_6 -his with bovine serum albumin and liver microsomal enzyme system. Since liver

microsomes also provide an ideal system to assess the photodynamic efficacy of the photosensitizers [315] we have monitored the extent of protein damage and lipid peroxidation in microsomes following PDT with Cp_6 and Cp_6 -histamine conjugate to compare their relative PDT efficacy.

6.1 Results

6.1.1 Interaction of Cp_6 and Cp_6 -his with BSA and liver microsomes

The absorbance spectra of Cp_6 and Cp_6 -his, with or without BSA and liver microsomes respectively are presented in fig.6.1. Addition of BSA ($1\ \mu\text{M} \sim 67\ \mu\text{g}$) to a solution of either Cp_6 or Cp_6 -his ($10\ \mu\text{M}$) resulted in a shift ($\sim 8\text{nm}$) of the absorbance band of the PS at 659 nm to 667 nm. Similarly, $\sim 13\ \text{nm}$ red shift was observed at Q band absorbance on addition of microsomes ($100\ \mu\text{g}$) in to the solution of each photosensitizer. The shift in absorbance spectra of PS shows the association of the sensitizer with the BSA and microsomes.

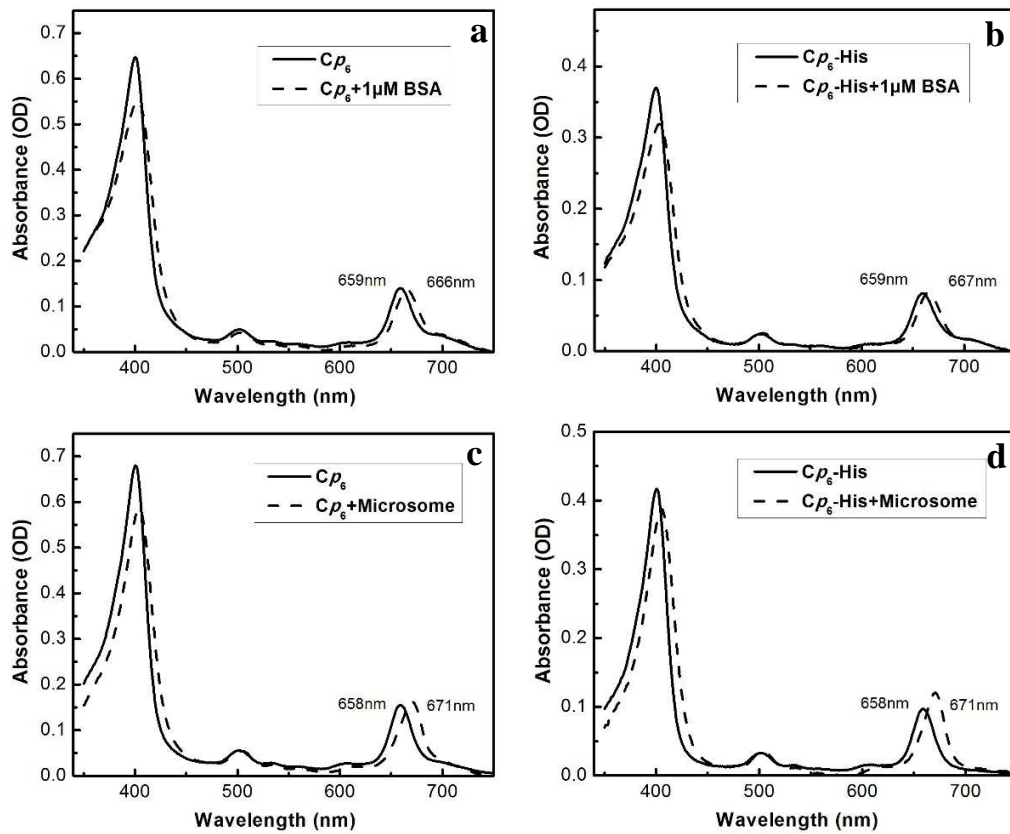


Figure 6.1: Absorption spectra of Cp_6 (a, c) and Cp_6 -his (b, d) in 25 mM phosphate buffer pH 7.4 (solid) and in presence of (dashed) either BSA (a, b) or microsome (c, d).

6.1.2 Measurement of binding parameters

The quenching of intrinsic tryptophan fluorescence of BSA and microsomal proteins by Cp_6 and Cp_6 -his was measured and plotted as Stern–Volmer plot to determine the binding parameters such as binding constant and number of binding sites. Interaction between BSA/microsomes and photosensitizers can be represented by following equation:

$$\log (F_0-F)/F = \log K + n \log [Q]$$

where F_0 and F are the fluorescence emission intensities at 338 nm in absence and presence of photosensitizers. K is the binding association constant and n is the number of binding sites. The quenching curve of Cp_6 and Cp_6 -his to BSA/microsomes shows a linear relationship (Fig.6.2 a-d) shows the linear plot for $\log (F_0-F)/F$ vs. $\log [PS]$. Results (Table 6.1) showed that the binding constant of Cp_6 -his with BSA is lower by ~ 4 order ($5.0 \pm 0.5 \times 10^2$) as compared to free Cp_6 ($2.4 \pm 0.6 \times 10^6$). Moreover, the number of binding sites for conjugate is nearly half (0.60 ± 0.05) as compared to free Cp_6 (1.23 ± 0.15). However, with microsomes the binding constant of Cp_6 -his was found to be lower by ~2 order ($1.3 \pm 0.3 \times 10^4$) then free Cp_6 ($9.1 \pm 0.4 \times 10^5$). Also, the numbers of binding sites in microsomes for conjugate was found to be slightly lower (0.87 ± 0.08) then free Cp_6 (1.17 ± 0.03).

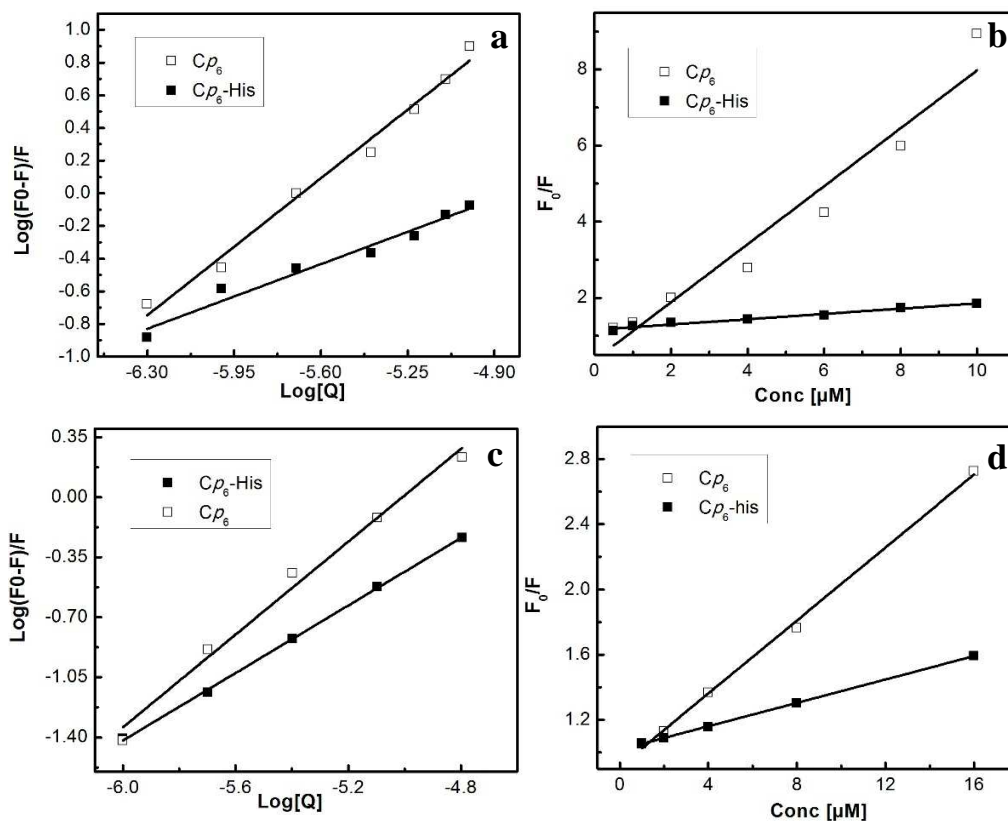


Figure 6.2: Double logarithm plot of $\log(F_0-F)/F$ vs. $\log[Cp_6/Cp_6\text{-his}]$. (a) A solution of BSA ($1 \mu\text{M}$ ~ $67 \mu\text{g}$) or (c) microsomes ($100 \mu\text{g}$) in 25 mM phosphate buffer pH 7.4 was titrated against different concentration of $Cp_6/Cp_6\text{-his}$ and fluorescence emission was measured at 338 nm with $\lambda_{\text{ex}} = 295 \text{ nm}$. Stern Volmer plot for $Cp_6/Cp_6\text{-his}$ – BSA (b) or Microsomes (d). Each data points represent mean \pm SD of three independent experiments.

Table 6.1. Binding parameters.

Protein	Photosensitizer	Binding Constant(Kb M ⁻¹)	No. of binding Sites (n)	Ksv (M ⁻¹)
Microsomes	<i>Cp₆-His</i>	1.3± 0.3×10 ⁴	0.87 ± 0.08	3.5×10 ⁴
	<i>Cp₆</i>	9.1± 0.4×10 ⁵	1.17± 0.03	1.1×10 ⁵
BSA	<i>Cp₆-His</i>	5.0± 0.5×10 ²	0.60±0.05	6.8×10 ⁴
	<i>Cp₆</i>	2.4± 0.6×10 ⁶	1.23±0.15	8.1×10 ⁵

Table6.2. Effect of *Cp₆* and *Cp₆-his* on the reduction of cytochrome c by NADPH-cytochrome P-450 and NADH-cytochrome b5 reductase

Enzyme Activity	Control	Treatment	
		<i>Cp₆-His</i>	<i>Cp₆</i>
NADPH-cytochrome P-450 reductase (nmol/min/mg protein) [Percent inhibition of cytochrome c reduction]	3.24±0.49 [100]	2.55±0.13 [21.26]	2.47±0.16 [23.64]
NADH-cytochrome b5 reductase (nmol/min/mg protein) [Percent inhibition of cytochrome c reduction]	15.73±0.29 [100]	14.69±0.68 [6.56]	13.21±.34 [16.09]

6.1.3 Effect of Cp₆ and Cp₆-his on the reduction of cytochrome c by NADPH-cytochrome P-450 and NADH-cytochrome b5 reductase

In liver microsomes cytochrome c can be reduced either by NADPH-cytochrome P450 reductase in the presence of NADPH, or by NADH-cytochrome b5 reductase in the presence of NADH. Cytochrome c reduction was dependent on the presence of NAD(P)H and microsomes. Addition of either Cp₆ or Cp₆-his to the incubation mixtures had no effect on the reduction of cytochrome c. However, when microsomes were incubated with Cp₆ prior to the addition of cytochrome c and NAD(P)H, cytochrome c reduction was inhibited. The effect of pre-incubation with either Cp₆ or Cp₆-his on the inhibition of cytochrome c reduction was shown in Table 6.2. Results shows that pre-incubation with either Cp₆-his or Cp₆ with microsomes led to similar level of NADPH-cytochrome P450 reductase mediated inhibition of cytochrome c reduction. While Cp₆ significantly ($P \geq 0.001$) inhibit the cytochrome c reduction mediated by NADH-cytochrome b5 reductase, there was no significant inhibition of cytochrome c reduction in case of Cp₆-His (Table 6.2).

6.1.4 Quenching of tryptophan fluorescence with potassium iodide

The quenching of fluorescence of membrane-bound fluorophores molecules by iodide ions is used as a tool in assessing their relative depth in the lipid bilayer [319]. By employing this methodologies, it was demonstrated that as the alkyl carboxylate side chain was made longer the tetrapyrrole core of hematoporphyrins, protoporphyrins or dithiaporphyrins is located at larger depths in the membrane [316].

The addition of the quencher iodide to the solutions of either Cp_6 or Cp_6 -his resulted in a concentration-dependent decrease in PS fluorescence. Analysis of this data using Stern-Volmer plots (which relate the decrease in fluorescence intensity (F_0/F) to the quencher concentration) showed that (Fig. 6.3) the quenching constant KQ for Cp_6 ($6.31 \pm 0.61 \times 10^6 \text{ M}^{-1}$) did not change significantly on addition of microsomes to Cp_6 solution ($KQ = 6.49 \pm 0.65 \times 10^6 \text{ M}^{-1}$). This indicates that the iodide has full accessibility to Cp_6 . However, in case of Cp_6 -his the KQ was found to decrease from $6.37 \pm 0.18 \times 10^6 \text{ M}^{-1}$ to $5.42 \pm 0.27 \times 10^6 \text{ M}^{-1}$ ($P \geq 0.01$) on addition of microsomes to the solution of Cp_6 -his.

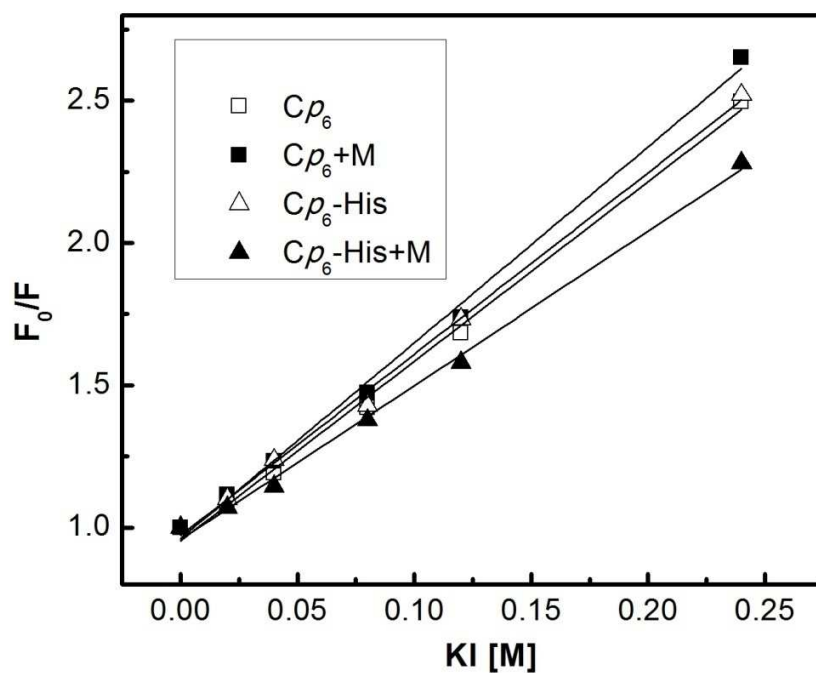


Figure 6.3: Stern–Volmer quenching plots of Cp_6 / Cp_6 -his fluorescence: The fluorescence of Cp_6 or Cp_6 -his (10 μ M) in 50 mM phosphate buffer, pH 7.4, was determined in the presence and absence of liver microsomes (10 μ g of protein/ml) (excitation 400 nm; emission 667 nm). Open and filled square represents Cp_6 in buffer ($K_Q = 6.31 \pm 0.61 \times 10^6$ M^{-1}) and on addition with microsomes ($K_Q = 6.49 \pm 0.65 \times 10^6$ M^{-1}), respectively. Open and filled triangle represents Cp_6 -his in buffer ($K_Q = 6.37 \pm 0.18 \times 10^6$ M^{-1}) and on addition with microsomes ($K_Q = 5.42 \pm 0.27 \times 10^6$ M^{-1}), respectively. K_Q represents bimolecular quenching constant.

6.1.5 Protein damage induced by PDT with Cp_6 and Cp_6 -his

The irradiation of BSA / microsomes along with either Cp_6 or Cp_6 -his with red light led to photodynamic damage to the protein residues and generation of protein carbonyls, which was measured biochemically. The amount of protein carbonyls generated directly reflects the extent of protein damage following PDT. The table 6.3 shows the magnitude of photodynamic damage to BSA/ liver microsomes induced by the Cp_6 -his and free Cp_6 as determined by estimation of protein carbonyls formation. While in case of BSA the amount of protein carbonyl generated following PDT with Cp_6 -his was half as compared to the Cp_6 (**Table 6.3**), with microsomal proteins no significant difference is observed in the magnitude of protein carbonyl formation when microsomes are subjected to PDT with either of the photosensitizer (table 6.3).

Table6.3. Estimation of Protein carbonyl following PDT with Cp_6 -his and Cp_6 .

Photosensitizer	Protein Carbonyl (nmol/mg protein)			
	BSA		Microsome	
	Control	Treatment	Control	Treatment
Cp_6 -His	29.07±4.1	70.64±5.8	30.15±1.4	118.03±25.3
Cp_6	34.75±8.9	119.5±9.2	25.30±8.2	117.42±25.7

6.1.6 Photodynamic lipid damage in presence of Cp_6 and Cp_6 -his

Apart from binding to microsomal enzyme proteins specifically, the photosensitizers can also bind with membrane lipids non-specifically depending on their relative lipophilicity and this interaction is expected to determine the extent of lipid damage following PDT. Measurements on PDT induced lipid peroxidation however showed (Table 6.4) no difference for Cp_6 -his and Cp_6 indicating that their non-specific binding with liver microsomes is also similar.

Table6.4. Lipid peroxidation in microsomes following PDT with Cp_6 -his and Cp_6 .

Photosensitizer	TBARS (nmol/mg protein)	
	Control	Treatment
Cp_6 -His	0.33±0.12	6.73±0.18
Cp_6	0.42±0.09	6.61±0.34

6.1.7 Partition coefficients

To evaluate the lipophilicity/ hydrophobicity of Cp_6 and Cp_6 -his, partition coefficients of both the PS were measured in the 1-octanol–water system. The partition coefficients measured by Eq. (1) showed Cp_6 -his is slightly more lipophilic as compared to parent Cp_6 .

6.2 Discussion

6.2.1 Interaction of Cp_6 -his and free Cp_6 with BSA

Results of our study show that as compared to Cp_6 the binding affinity of Cp_6 -his with BSA is lower by ~ 4 orders of magnitude and the number of binding site is also decreased significantly. Previous studies have shown that the binding affinity of di and monocarboxylic porphyrins to serum albumin increases with increase in the lipophilicity of the photosensitizer [317,318]. We measured Octanol: water partition coefficient of the two photosensitizers and results show that Cp_6 -his is slightly more lipophilic as compared to free Cp_6 . The increase in lipophilicity of Cp_6 -his is expected because the carboxylic group at 17th carbon position in the molecule is removed to attach the histamine. Thus, the trend with respect to relative lipophilicity and the affinity to albumin appeared to be opposite in case of Cp_6 and Cp_6 -his. In fact, for chlorin type photosensitizers the dependence of affinity to serum albumin on lipophilicity is not clearly established [312,319]. For

example, with Ce6 the binding affinity to serum albumin has been found to be similar to deuteroporphyrin and protoporphyrin in spite of the fact that later two are more hydrophobic as compared to Ce6 [312]. The reason for the similar binding affinity of the three photosensitizers was explained based on their common asymmetric structure where the carboxylic side chain is at the side of hydrophobic core [312]. It has been suggested that the side chain carboxylic group interacts with basic residues at entrance of the hydrophobic pocket in albumin and the tetrapyrrol moiety of the photosensitizer binds the hydrophobic pocket at subdomain IB and in a manner similar to heme [312]. This contention that the side chain carboxylic group provides anchor for attachment to the external, near the polar face of globular protein has been suggested by Ben et al also [317]. We therefore believe that a large decrease in the affinity of Cp_6 -his as compared to Cp_6 could also arise because of loss of side chain carboxylic group upon conjugation with histamine and also due the fact that histamine itself did not bind with serum albumin.

6.2.2 Interaction of Cp_6 -his and free Cp_6 with microsomal protein

The liver microsomes contains some key enzymes particularly NADPH-cytochrome P450 reductase and NADH-cytochrome b5 reductase for the metabolism and detoxification of various drugs [320]. Photosensitizer accumulation in liver can affect the activity of these enzymes which may result in abnormal liver function. For examples, liver toxicity has been observed as one of the most common side effects in case of PDT with ALA induced protoporphyrin [321]. Similar accumulation of protoporphyrin in case of protoporphyria is

associated with failure of liver function. It has been shown by Williams et al, using liver microsomal system that protoporphyrin inhibits the activity cytochrome P-450 system and thus affects its detoxification function [322]. We observed that both Cp_6 and Cp_6 -his led to ~ 22% inhibition of NADPH-cytochrome P450 reductase activity. For NADH-cytochrome b5 reductase activity, Cp_6 -his showed only slight inhibition as compared to 20% inhibition induced by Cp_6 . It is important to mention here that the microsomal binding of drugs can involve specific interaction with microsomal proteins and the nonspecific interaction with lipid part of the microsomes depending on the lipophilic/hydrophobic nature of the drug molecule [323]. Since there is small but significant difference in the lipophilicity to Cp_6 -his and Cp_6 , the non-specific binding to microsomal lipid is also expected to be different. It has been reported the inhibition of cytochrome P-450 by protoporphyrin could be associated with deeper localization of protoporphyrin in microsome membrane due to its lipophilic nature whereas hydrophilic urophorphyrin which remain outside did not lead to such inhibition [324]. We also studied the localization of both the photosensitizers in the microsomes by probing the quenching of photosensitizer fluorescence by iodide ion. The results show that the presence of iodide has no significant effect on fluorescence of Cp_6 in both the absence or presence of microsomes. This suggests that Cp_6 is not localized very deep in the microsome. For Cp_6 -his, the quenching of its fluorescence by iodide in the presence of microsomes was slightly lower than in the absence of microsomes which suggested that it is localized little deeper in the microsomes. It is important to note that the drug metabolizing enzyme CytP450 protein complex localize at the surface of the microsome membrane with its catalytic domain inserted shallow in the membrane [325]. We probed the intrinsic tryptophan fluorescence of the microsomal proteins to determine

the specific interaction. The results show that Cp_6 -his and Cp_6 binds with microsomal proteins and the binding constant for Cp_6 was higher than for Cp_6 -his. Whereas, the number of binding sites for both Cp_6 and Cp_6 -his is close to one. This together with the fact that the two photosensitizers inhibit the activity of microsomal enzymes to the same extent suggests that the interaction of Cp_6 -his with microsomal proteins is not significantly different from Cp_6 . In confirmation with our previous observations that the clearance of the two photosensitizers from the skin in hamster cheek pouch model was similar [326], these results suggest that the conjugation to histamine would not affect the metabolism and clearance of Cp_6 .

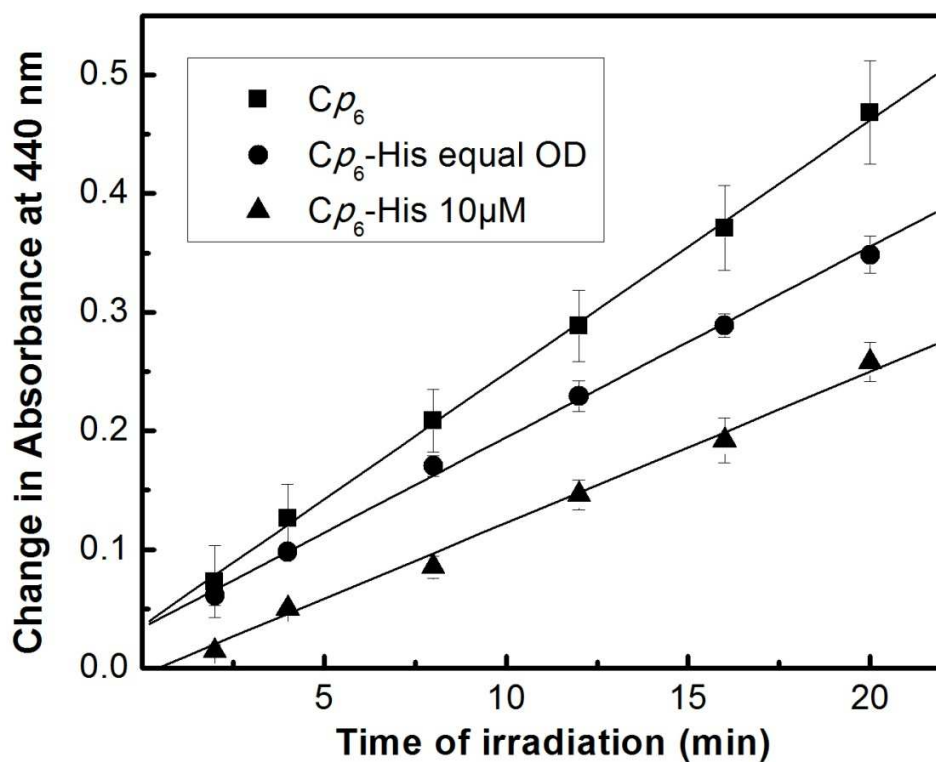


Figure 6.4: Cp_6/Cp_6 -his mediated photodynamic RNO bleaching with respect to time. A solution containing RNO ($A_{440} \sim 0.8$), 10 mM imidazole and 10 μ M of either Cp_6 or Cp_6 -his in 25 mM Na_2HPO_4 buffer of pH 7.4 was irradiated with red light (660 ± 25 nm) for different time period and at the end of each irradiation absorbance of irradiated and un-irradiated samples was measured at 440 nm. Each data points represent mean and standard deviations of three independent experiments.

6.2.3 Photodynamic damage to proteins and lipids

We also studied whether the affinity of Cp_6 -his and free Cp_6 to BSA and microsomal proteins have any influence on the PDT-induced protein damage. Results however show that while the protein carbonyl formation following PDT with Cp_6 -his was ~50 % less as compared to that for Cp_6 , the difference in the affinity of the two photosensitizers to BSA was much larger. We have previously reported that the Cp_6 -induced photodynamic damage to BSA is mediated by singlet oxygen [310]. The comparison of the singlet oxygen yield of Cp_6 and Cp_6 -his in aqueous environment showed that the singlet oxygen generation capability of Cp_6 -his is lower than that of Cp_6 and this also correlates with the difference in the amount of protein carbonyl formation induced by two photosensitizers. Earlier studies have shown that the photooxidation to protein measured by tryptophan oxidation is significantly different for various porphyrin and chlorin type photosensitizers even after normalization with respect to the small differences in singlet oxygen yield of these (fig.6.4) [317]. This was attributed to the differences in the relative proximity of the photosensitizers to tryptophan in the protein molecule [317]. In our study, the amount of carbonyl formation represents overall protein damage due to the fact that these are formed by oxidation of nearly all amino acids in the protein. Therefore the observed photodamage to protein is more dependent on singlet oxygen yield of the two photosensitizers rather on binding affinity measured by tryptophan quenching.

Interestingly, we observed that both Cp_6 -his and Cp_6 induced roughly same amount of protein damage in liver microsomes after PDT. Compared to the protein in neat buffer system, the proteins in microsomes are surrounded by lipid environment and since both Cp_6 -his and Cp_6 are amphiphilic these can also partition in the lipid region. This is evident from the larger red shift in the Q band absorption of the two photosensitizers (from 659 nm to 671 nm) when added to microsomes as compared to BSA. In addition, since Cp_6 -his might be located little deeper in the microsomal membrane and also due to the fact that the life time of singlet oxygen in lipid environment is longer than in aqueous phase [327,328], Cp_6 -his is expected to lead to higher protein damage in membrane as compared to aqueous environment. Bronshtein et al using hemato- and protoporphyrins, which have alkyl spacers of varying lengths between the tetrapyrrole ring and the carboxylate groups, have shown that the deeper localization of photosensitizer in membrane result in higher photodamage of membrane localized target molecule [218]. Thus deeper localization of Cp_6 -his would compensate for its lower singlet oxygen generation capability as compared to Cp_6 and both resulted in almost same amount of protein damage in microsomes. This observation may also explain Cp_6 -his and Cp_6 showing no significant difference in PDT induced lipid damage.

6.3 Conclusion

To summarize, it is shown that while conjugation of Cp_6 to histamine led to tremendous decrease in its binding affinity with serum albumin, the specific interaction of Cp_6 -his with

proteins in liver microsomes is similar to Cp_6 . These results have two implications, first that serum albumin less likely to play a role in the transport of Cp_6 -his as compared to free Cp_6 which may contribute to its better accumulation in tumor cells with respect to tumor vasculature. Second, the recognition of both Cp_6 and Cp_6 -his by microsomal proteins for further metabolism and clearance is not altered which are desirable features for its in vivo PDT efficacy. The use of microsomes also allowed comparison of the PDT efficacy of the two photosensitizers and results demonstrate that Cp_6 -his in spite of lower singlet oxygen generation capacity led to almost same amount of damage to membrane lipid and proteins which could arise because of better localization of Cp_6 -his in microsomal lipids due to higher lipophilicity of the conjugate. These observations are consistent with the higher cellular uptake, better tumor selectivity and enhanced photodynamic efficacy of Cp_6 -his conjugate reported in our earlier studies [283,310].

CHAPTER 7

SUMMARY AND FUTURE

PROSPECTIVES

To conclude, the results of *in-vitro* studies in oral cancer cell lines as well as breast carcinoma cell line showed that the Cp_6 -his is taken up more efficiently than free Cp_6 in cells and thus the resultant photo-toxicity is also enhanced substantially. The results also suggested that uptake of the conjugate is mediated by histamine H2 receptors. The sites of intracellular localization of Cp_6 -his has been identified as lysosomes and endoplasmic reticulum suggesting its uptake by endocytosis. Characterization of PDT-induced damage to cell organelles by 3D reconstruction revealed that tubular regions of ER are more sensitive to photodynamic damage and damage to ER also led to alterations in structure of Golgi apparatus.

Studies on evaluation of PDT efficacy of Cp_6 -his in hamster cheek pouch model showed higher tumor selectivity for Cp_6 -his as compared to Cp_6 and PDT led to complete regression of tumors of size $\leq 1000 \text{ mm}^3$. Results also showed that histamine H2 receptors are over-expressed in hamster tumor tissue. Hamster oral cancer model is well characterized which shows several biochemical and structural features similar to human oral cancer. So far, the status of histamine receptor is not reported in literature. We analyzed few histology slides of human OSCC tissue samples obtained from Choithram Hospital & Research Centre, Indore and observed strong immune-staining in various regions of tumor tissue suggesting high expression of histamine H2 receptor (Fig. 7.1 A, B, C, D). This is also consistent with our observations in oral tumors of hamster. Therefore it will be interesting to study expression of histamine receptors in human oral cancer to further exploit the clinical use of Cp_6 histamine conjugate for PDT of oral tumors.

While difference in expression of histamine receptor level might contribute to higher tumor selectivity of Cp_6 -his, it is also likely that a change in physicochemical properties of Cp_6 due to attachment of histamine also play some role in its uptake. To gain some insight on this aspect studies on interaction of Cp_6 -his and Cp_6 with serum albumin and liver microsomes has been done. Results revealed that the Cp_6 -his has lower affinity with serum albumin as compared to Cp_6 which could also be an important factor in its tumor selective uptake. Moreover, results on interaction of Cp_6 -his and Cp_6 with liver microsomes showed no difference in binding which suggest that conjugation of Cp_6 with histamine would not affect its hepatic metabolism and clearance. This is also consistent with similar time dependent rapid clearance of Cp_6 -his and Cp_6 observed in hamster model. In conclusion, Cp_6 -his showed promising results in cancer cells and hamster tumor model and thus the coupling of Cp_6 to histamine provided new possibility for targeted PDT which may be worth to explore further.

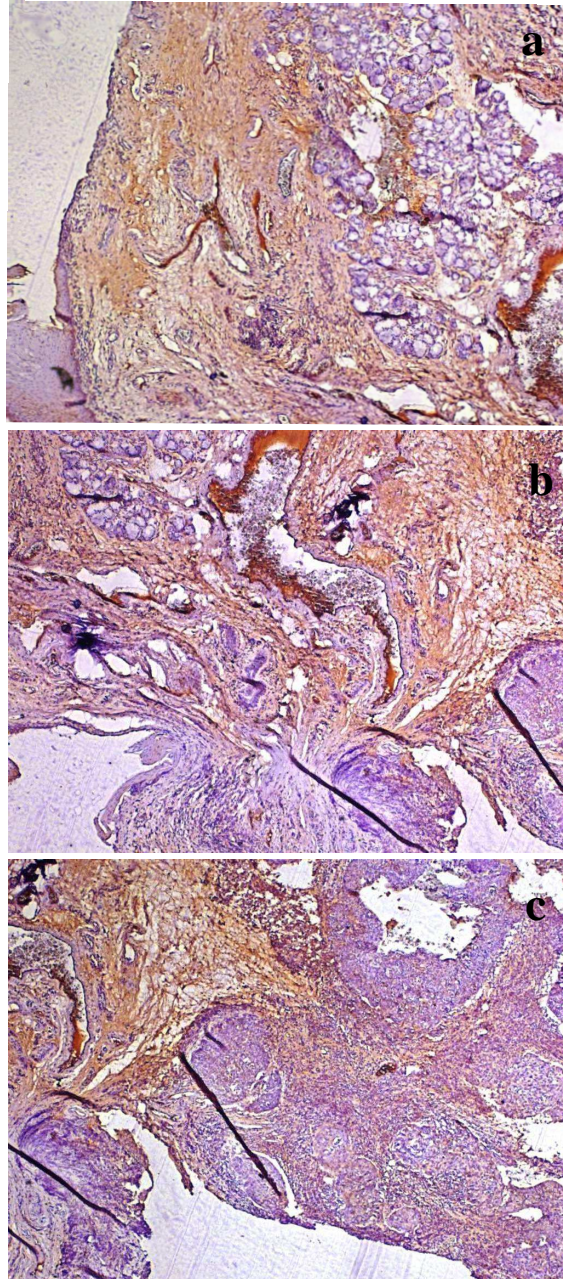


Figure 7.1 (A): H2R receptor expression in Human OSCC biopsy samples (Supraglottic region of Larynx) detected by Immunohistochemistry. Different regions of same tissue section are shown in a-c. Note the prominent staining (brown color) in tumor cells and also in tumor matrix.

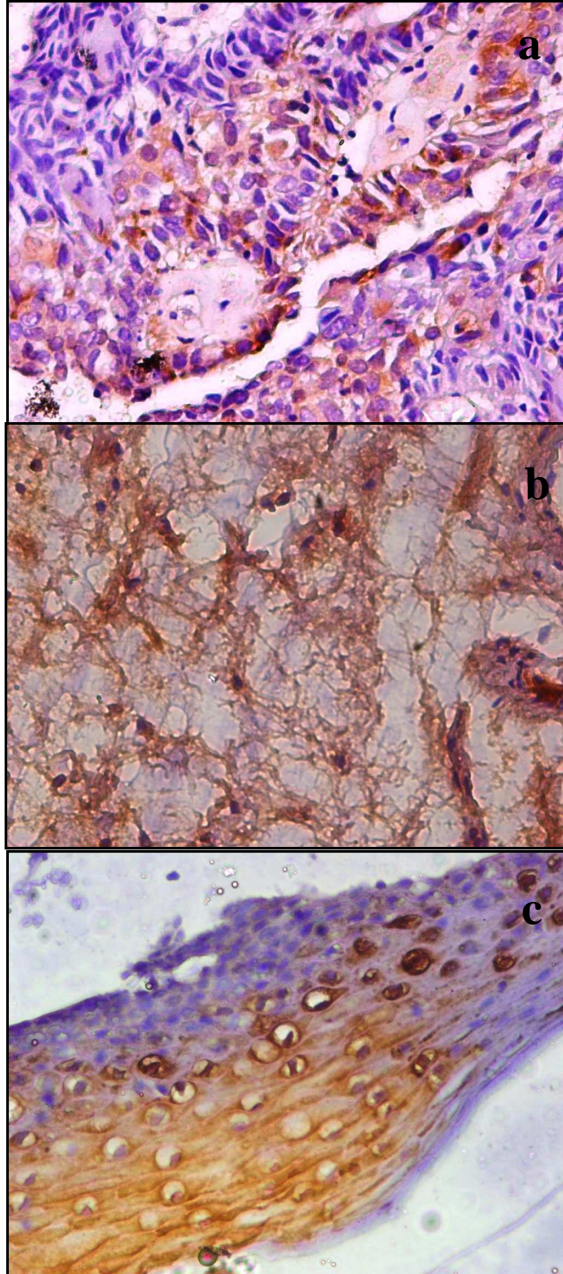


Figure 7.1 (B): H2R receptor expression in Human OSCC biopsy samples (OSCC tumor of oral cavity) detected by Immunohistochemistry. Different regions of same tissue section are shown in a-c. Note the prominent staining (brown color) in tumor cells and also in tumor matrix.

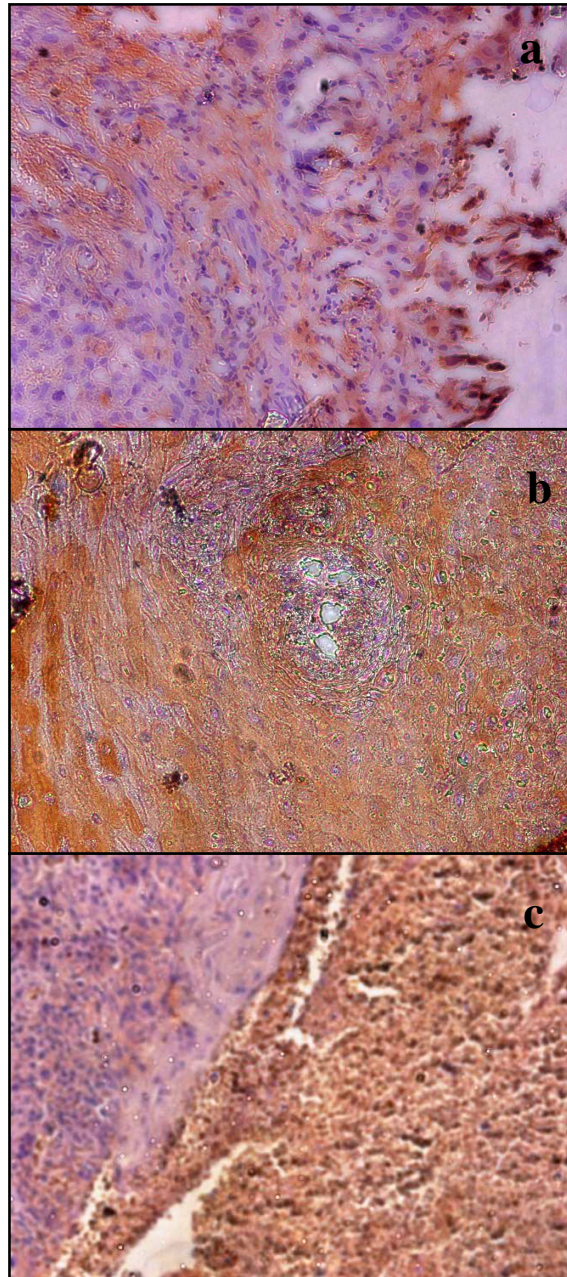


Figure 7.1 (C): H2R receptor expression in Human OSCC biopsy samples (OSCC tumor of oral cavity) detected by Immunohistochemistry. Different regions of same tissue section are shown in a-c. Note the prominent staining (brown color) in tumor cells and also in tumor matrix.

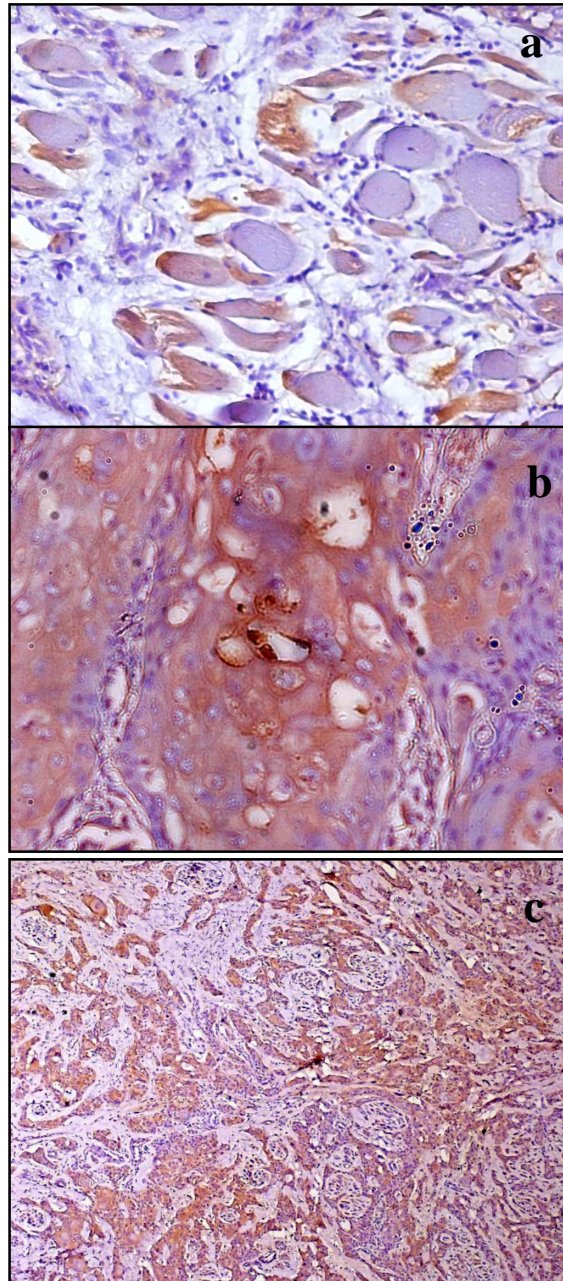


Figure 7.1 (D): H2R receptor expression in Human OSCC biopsy samples (OSCC tumor from Alveolar Region Buccal Mucosa) detected by Immunohistochemistry. Different regions of same tissue section are shown in a-c. Note the prominent staining (brown color) in tumor cells and also in tumor matrix.

REFERENCES

1. Baskar R, Lee KA, Yeo R, Yeoh KW. Cancer and radiation therapy: current advances and future directions. *Int J Med Sci.* 2012; 9(3):193-9.
2. Hanahan D, Weinberg RA. The hallmarks of cancer. *Cell.* 2000; 100(1):57-70.
3. Chaffer CL, Weinberg RA. A perspective on cancer cell metastasis. *Science.* 2011; 331(6024):1559-64.
4. Hanahan D, Weinberg RA. Hallmarks of cancer: the next generation. *Cell.* 2011; 44: 646-674.
5. <http://www.cancer.org>
6. Bergman PJ, Harris D. Radioresistance, chemoresistance, and apoptosis resistance. The past, present, and future. *Vet Clin North Am Small Anim Pract.* 1997; 27(1):47-57.
7. Weiss JF, Landauer MR. History and development of radiation-protective agents. *Int J Radiat Biol.* 2009; 85(7):539-73.
8. Kunwar A, Bansal P, Kumar SJ, Bag PP, Paul P, Reddy ND, Kumbhare LB, Jain VK, Chaubey RC, Unnikrishnan MK, Priyadarsini KI. In vivo radioprotection studies of 3,3'-diselenodipropionic acid, a selenocystine derivative. *Free Radic Biol Med.* 2010; 48(3):399-410.
9. Wilson BC, Patterson MS. The physics, biophysics and technology of photodynamic therapy. *Phys Med Biol.* 2008; 53:R61-R109.
10. Brown SB, Brown EA, Walker I. The present and future role of photodynamic therapy in cancer treatment. *Lancet Oncol* 2004; 5:497-508
11. Agostinis P, Berg K, Cengel KA, Foster TH, Girotti AW, Gollnick SO, Hahn SM, Hamblin MR, Juzeniene A, Kessel D, Korbelik M, Moan J, Mroz P, Nowis D, Piette J, Wilson BC, Golab J. Photodynamic therapy of cancer: an update. *CA Cancer J Clin.* 2011; 61:250-281.

12. Allison RR, Downie GH, Cuenca R, Hu XH, Childs CJH, Sibata CH. Photosensitizers in Clinical PDT. *Photodiag. Photodyn. Therapy* 2004; 1:27–42.
13. Detty MR, Gibson SL, Wagner SJ. Current Clinical and Preclinical Photosensitizers for Use in Photodynamic Therapy. *J. Med. Chem* 2004; 47:3897–3915.
14. Henderson, BW Dougherty TJ, How does photodynamic therapy work? *Photochem Photobiol*, 1992; 55(1): 145-57.
15. MacDonald IJ, Dougherty TJ. Basic principles of photodynamic therapy. *Journal of Porphyrins and Phthalocyanines*, 2001; 5(2):105-129.
16. Dougherty TJ, Gomer CJ, Henderson BW, Jori G, Kessel D, Korblik M, Moan J, Peng Q. Photodynamic therapy. *J Natl Cancer Inst.* 1998; 90(12):889-905.
17. Dolmans DE, Fukumura D, Jain RK. Photodynamic therapy for cancer. *Nat Rev Cancer.* 2003; 3:380-387.
18. Huang Z. A Review of Progress in Clinical Photodynamic Therapy. *Technol Cancer Res Treat.* 2005; 4(3): 283–293.
19. Ricchelli F, Jori G, Moreno G, Vincenz F, Salet C. Factors influencing the distribution pattern of porphyrins in cell membranes. *J Photochem Photobiol B.* 1990; 6(1-2):69-77.
20. G. Bock, S. Harnett (Eds.), *Photosensitizing Compounds: Their Chemistry, Biology and Clinical Use*, Ciba Foundation Symposium, vol. 146, Wiley Interscience, Chichester, 1989; 146: 4–16.
21. Wilson PC: *Photosensitizing Compounds: Their Chemistry, Biology and Clinical Use*; Ciba Foundation Symposium, vol. 73, Wiley Interscience: Chichester,; 1989.
22. Palma M, Cárdenas-Jirón GI, Menéndez Rodríguez MI. Effect of chlorin structure on theoretical electronic absorption spectra and on the energy released by porphyrin-based photosensitizers. *J Phys Chem A.* 2008; 112(51):13574-83.

23. DeRosa MC, Crutchley RJ. Photosensitized singlet oxygen and its applications. *Coordination Chemistry Reviews*. 2002; 233(234) 351-371.
24. Woodburn K, Chang CK, Sangwan L, Henderson B, Kessel D: Biodistribution and PDT efficacy of aketochlorin photosensitizer as a function of the delivery vehicle. *Photochem Photobiol* 1994; 60: 154-159.
25. Jori G. Tumor photosensitizers: approaches to enhance the selectivity and efficiency of photodynamic therapy. *J Photochem Photobiol B: Biology* 1996; 36: 87-93.
26. Hamblin MR. and Newman LE. On the mechanism of the tumor localizing effect in photodynamic therapy. *J. Photochem. Photobiol. B: Biol.*, 1994; 23: 3-8.
27. Wilson BC, Patterson MS. The physics, biophysics and technology of photodynamic therapy. *Phys Med Biol*. 2008; 53:R61-R109.
28. Henderson BW, Busch TM, Snyder JW. Fluence rate as a modulator of PDT mechanisms. *Lasers Surg Med*. 2006; 38:489-493.
29. Brancalion L, Moseley H. Laser and nonlaser light sources for photodynamic therapy. *Lasers Med Sci*. 2002; 17:173-186.
30. Juzeniene A, Juzenas P, Ma LW, Iani V, Moan J. Effectiveness of different light sources for 5-aminolevulinic acid photodynamic therapy. *Lasers Med Sci*. 2004; 19:139-149.
31. Szeimies RM, Morton CA, Sidoroff A, Braathen LR. Photodynamic therapy for non-melanoma skin cancer. *Acta Derm Venereol*. 2005; 85:483-490.
32. Beyer W. Systems for light application and dosimetry in photodynamic therapy. *J Photochem Photobiol B*. 1996; 36:153-156.
33. Plaetzer K, Krammer B, Berlanda J, Berr F, Kiesslich T. Photophysics and photochemistry of photodynamic therapy: fundamental aspects. *Lasers Med Sci*. 2009; 24:259-268.
34. Buytaert E, Dewaele M, Agostinis P. Molecular effectors of multiple cell death pathways initiated by photodynamic therapy. *Biochim Biophys Acta*. 2007; 1776: 86-107.

35. Dysart JS, Patterson MS. Characterization of Photofrin photobleaching for singlet oxygen dose estimation during photodynamic therapy of MLL cells in vitro. *Phys Med Biol.* 2005; 50:2597-2616.
36. Moan J, Berg K, Kvam E, Western A, Malik Z, Rück A, Schneckenburger H. Intracellular localization of photosensitizers. *Ciba Found Symp.* 1989; 146:95-107; discussion 107-11.
37. Kessel D, Castelli M. Evidence that bcl-2 is the target of three photosensitizers that induce a rapid apoptotic response. *Photochem Photobiol.* 2001; 74:318-322.
38. Xue LY, Chiu SM, Oleinick NL. Photochemical destruction of the Bcl-2 oncoprotein during photodynamic therapy with the phthalocyanine photosensitizer Pc 4. *Oncogene.* 2001; 20:3420-3427.
39. Berg K, Moan J. Lysosomes as photochemical targets. *Int J Cancer.* 1994; 59:814-822.
40. Reiners JJ Jr, Caruso JA, Mathieu P, Chelladurai B, Yin XM, Kessel D. Release of cytochrome c and activation of procaspase-9 following lysosomal photodamage involves Bid cleavage. *Cell Death Differ.* 2002; 9:934-944.
41. Kessel D. Relocalization of cationic porphyrins during photodynamic therapy. *Photochem Photobiol Sci.* 2002; 1:837-840.
42. Vanlangenakker N, Vanden Berghe T, Krysko DV, Festjens N, Vandenabeele P. Molecular mechanisms and pathophysiology of necrotic cell death. *Curr Mol Med.* 2008; 8:207-220.
43. Zong WX, Thompson CB. Necrotic death as a cell fate. *Genes Dev.* 2006; 20:1-15.
44. Nakagawa T, Shimizu S, Watanabe T, Yamaguchi O, Otsu K, Yamagata H, Inohara H, Kubo T, Tsujimoto Y. Cyclophilin D-dependent mitochondrial permeability transition regulates some necrotic but not apoptotic cell death. *Nature.* 2005; 434(7033):652-8.
45. Buytaert, E. Callewaert, G. Vandenheede, JR. Agostinis, P. Deficiency in apoptotic effectors Bax and Bak reveals an autophagic cell death pathway

- initiated by photodamage to the endoplasmic reticulum. *Autophagy*. 2006; 2:238-240.
46. Reiners JJ Jr, Agostinis P, Berg K, Oleinick NL, Kessel D. Assessing autophagy in the context of photodynamic therapy. *Autophagy*. 2010; 6(1):7-18.
47. Dewaele M, Maes H, Agostinis P. ROS mediated mechanisms of autophagy stimulation and their relevance in cancer therapy. *Autophagy*. 2010; 6:838-854.
48. Jain, R.K. and Carmeliet, P.F. Vessels of death or life. *Scientific American*, 2001. 285(6): 38-45.
49. Carmeliet, P. and R.K. Jain, Angiogenesis in cancer and other diseases. *Nature (London)*, 2000; 407(6801): 249-257.
50. Dolmans DE, Kadambi A, Hill JS, Waters CA, Robinson BC, Walker JP, Fukumura D, Jain RK. Vascular accumulation of a novel photosensitizer, MV6401, causes selective thrombosis in tumor vessels after photodynamic therapy. *Cancer Res*. 2002; 62(7):2151-6.
51. Fingar VH, Kik PK, Haydon PS, Cerrito PB, Tseng M, Abang E, Wieman TJ. Analysis of acute vascular damage after photodynamic therapy using benzoporphyrin derivative (BPD). *Br J Cancer*. 1999; 79(11-12):1702-8.
52. Star WM, Marijnissen HP, van den Berg-Blok AE, Versteeg JA, Franken KA, Reinhold HS. Destruction of rat mammary tumor and normal tissue microcirculation by hematoporphyrin derivative photoradiation observed in vivo in sandwich observation chambers. *Cancer Res*, 1986. 46(5): p. 2532-40.
53. Henderson BW, Fingar VH. Oxygen limitation of direct tumor cell kill during photodynamic treatment of a murine tumor model. *Photochem Photobiol*, 1989; 49(3): 299-304.
54. Ferrario A, von Tiehl KF, Rucker N, Schwarz MA, Gill PS, Gomer CJ. Antiangiogenic treatment enhances photodynamic therapy responsiveness in a mouse mammary carcinoma. *Cancer Res*. 2000; 60(15):4066-9.

55. Shumaker BP, Hetzel FW. Clinical laser photodynamic therapy in the treatment of bladder carcinoma. *Photochem Photobiol*, 1987; 46(5): p. 899-901.
56. Henderson BW, Dougherty T.J. How does photodynamic therapy work? *Photochem Photobiol*, 1992; 55(1): p. 145-57.
57. Gollnick SO, Liu X, Owczarczak B, Musser DA, Henderson BW. Altered expression of interleukin 6 and interleukin 10 as a result of photodynamic therapy in vivo. *Cancer Res.* 1997; 57(18):3904-9.
58. de Vree WJ, Essers MC, de Bruijn HS, Star WM, Koster JF, Sluiter W. Evidence for an important role of neutrophils in the efficacy of photodynamic therapy in vivo. *Cancer Res.* 1996; 56(13):2908-11.
59. Korbelik M, Cecic I. Contribution of myeloid and lymphoid host cells to the curative outcome of mouse sarcoma treatment by photodynamic therapy. *Cancer Lett.* 1999; 137:91-98.
60. Abdel-Hady ES, Martin-Hirsch P, Duggan-Keen M, Stern PL, Moore JV, Corbitt G, Kitchener HC, Hampson IN. Immunological and viral factors associated with the response of vulval intraepithelial neoplasia to photodynamic therapy. *Cancer Res.* 2001; 61(1):192-6.
61. Kabingu E, Vaughan L, Owczarczak B, Ramsey KD, Gollnick SO. CD8 β T cell mediated control of distant tumours following local photodynamic therapy is independent of CD4 β T cells and dependent on natural killer cells. *Br J Cancer.* 2007; 96:1839-1848.
62. Henderson BW, Gollnick SO, Snyder JW, Busch TM, Kousis PC, Cheney RT, Morgan J. Choice of oxygen-conserving treatment regimen determines the inflammatory response and outcome of photodynamic therapy of tumors. *Cancer Res.* 2004; 64(6):2120-6.
63. Reis e Sousa C. Activation of dendritic cells: translating innate into adaptive immunity. *Curr Opin Immunol.* 2004; 16: 21-25.
64. Gollnick SO, Evans SS, Baumann H, Owczarczak B, Maier P, Vaughan L, Wang WC, Unger E, Henderson BW. Role of cytokines in photodynamic

- therapy-induced local and systemic inflammation. *Br J Cancer*. 2003; 88(11):1772-9.
65. Sur BW, Nguyen P, Sun CH, Tromberg BJ, Nelson EL. Immunophototherapy using PDT combined with rapid intratumoral dendritic cell injection. *Photochem Photobiol*. 2008; 84:1257-1264.
 66. Castellino F, Germain RN. Cooperation between CD4 β and CD8 β T cells: when, where, and how. *Annu Rev Immunol*. 2006; 24:519-540.
 67. Gollnick SO, Vaughan L, Henderson BW. Generation of effective antitumor vaccines using photodynamic therapy. *Cancer Res*. 2002; 62:1604-1608.
 68. Korbelyik M, Cecic I. Mechanism of tumor destruction by photodynamic therapy. In: Nalwa HS, ed. *Handbook of Photochemistry and Photobiology*. Stevenson Ranch, CA: American Scientific Publishers; 2003; 65:39-77.
 69. Korbelyik M, Sun J. Photodynamic therapy-generated vaccine for cancer therapy. *Cancer Immunol Immunother*. 2006; 55: 900-909.
 70. Korbelyik M, Merchant S, Huang N. Exploitation of immune response-eliciting properties of hypocrellin photosensitizer SL052-based photodynamic therapy for eradication of malignant tumors. *Photochem Photobiol*. 2009; 85:1418-1424.
 71. Spikes, J.D., The historical development of ideas on applications of photosensitized reactions in the health sciences. *NATO ASI Series, Series A: Life Sciences*, 1985; 85(Primary Photo-Processes Biol. Med.): p. 209-27.
 72. Raab, O., Action of fluorescent materials on infusorial substances. *Zeitschrift fuer Biologie (Munich)*, 1900; 39: 524-546.
 73. Finsen, N.R., The red light treatment of small-pox: A reply. *Lancet*, 1904; 2: 1272-1272.
 74. Finsen, N.R., The red-light treatment of smallpox. *Journal of the American Medical Association*, 1903; 41: 1207-1208.
 75. von Tappeiner H, Jodlbauer A, Lehmann H., Photodynamic and optical behaviour of anthraquinones. *Arch. klin. Med*. 1903; 82: 217-22.

76. Meyer-Betz, F., Untersuchungen über die biologische (photodynamische) Wirkungdes Hämatoporphyrins und anderer derivate des Blut- und Gallenfarbstoffs. *Dtsch Arch Klin Med*, 1913; 112: 476–503.
77. Lipson RL, Baldes EJ. The Photodynamic Properties of a Particular Hematoporphyrin Derivative. *Archives of Dermatology*, 1960; 82(4): 508-516.
78. Dougherty TJ, Kaufman JE, Goldfarb A, Weishaupt KR, Boyle D, Mittleman A. Photoradiation therapy for the treatment of malignant tumors. *Cancer Res*. 1978; 38(8):2628-35.
79. Moser, JG. Definitions and General Properties of 2nd & 3rd Generation Photosensitizers. In: Moser, JG., editor. *Photodynamic Tumor Therapy-2nd & 3rd Generation Photosensitizers*. Harwood Academic Publishers; London: 1997; 56: 3-8.
80. Lipson RL, Baldes E.J. The Photodynamic Properties of a Particular Hematoporphyrin Derivative. *Archives of Dermatology*, 1960; 82(4): 508-516.
81. Nyman ES, Hynninen PH, Research advances in the use of tetrapyrrolic photosensitizers for photodynamic therapy *J Photochem Photobiol B. Biol*. 2004; 73:1-28.
82. Allison RR. Photosensitizers in clinical PDT. *Photodiagnosis and Photodynamic Therapy*, 2004; 1(1): 27-42.
83. Dougherty, TJ, Gomer, CJ, Henderson BW, Jori, G, Kessel D, Korbelik M, Moan J, Peng QJ, Photodynamic therapy. *Natl. Cancer Inst*. 1998; 90: 889-905.
84. Husain D, Miller JW, Michaud N, Connolly E, Flotte TJ, Gragoudas ES,. Intravenous infusion of liposomal benzoporphyrin derivative for photodynamic therapy of experimental choroidal neovascularization. *Archives of Ophthalmology* 1996; 114: 978-985.
85. Allison BA, Crespo MT, Jain AK, Richter AM, Hsiang YN, Levy JG. Delivery of benzoporphyrin derivative, a photosensitizer, into atherosclerotic

- plaque of Watanabe heritable hyperlipidemic rabbits and balloon-injured New Zealand rabbits. *Photochemistry and Photobiology*, 1997; 65:877-883.
86. Taylor CR, Kwangstith C, Wimberly J, Kollias N, Anderson RR. Turbo PUVA: dihydroxyacetone-enhanced photochemotherapy for psoriasis: a pilot study. *Archives of Dermatology*, 1999; 135: 540-544.
87. Tanew A, Radakovic-Fijan S, Schemper M, Honigsmann H, Narrowband UVB phototherapy vs photochemotherapy in the treatment of chronic plaque-type psoriasis: a paired comparison study. *Archives of Dermatology*, 1999; 135: 519-524.
88. Razum N, Snyder A, Doiron D, SnEt2: Clinical update. *Proceedings of SPIE (Society for Photo-optical International Engineering)*, 1996; 2675: 43-46.
89. Oleinick NL, Antunez AR, Clay ME, Rihter BD, Kenney ME. New phthalocyanine photosensitizers for photodynamic therapy. *Photochemistry and Photobiology*, 1993; 57: 243-247.
90. Separovic D, He J, Oleinick NL. Ceramide generation in response to photodynamic treatment of L5178Y mouse lymphoma cells. *Cancer Research*, 1997; 57:1717-1721.
91. Anderson CY, Freye K, Tubesing KA, Li YS, Kenney ME, Mukhtar H, Elmets CA. A comparative analysis of silicon phthalocyanine photosensitizers for in vivo photodynamic therapy of RIF-1 tumors in C3H mice. *Photochemistry and Photobiology*, 1998; 67: 332-336.
92. V. Král, J. Králová, R. Kaplánek, T. Bříza, P. Martásek. Quo vadis porphyrin chemistry? *Physiol.2006 Res. 55 (Suppl. 2): S3-S26*.
93. Spikes JD, Bommer JC. Chlorophylls and related pigments as photosensitizers in biology and medicine, in: H. Scheer (Ed.), *Chlorophylls*, CRC Press, Boca Raton, FL, 1991; 1181–1204.
94. Kraljic, N. Barboy, J.-P. Leicknam, Photosensitized formation of singlet oxygen by chlorophyll a in neutral aqueous micellar solutions with Triton X-100, *Photochem. Photobiol.* 1979; 30: 631–633.

95. C. Tanielian, C. Wolff, Porphyrin-sensitized generation of singlet molecular oxygen: comparison of steady state and time-resolved methods, *J. Phys. Chem.* 1995; 99: 9825–9830.
96. S.Y. Egorov, A.A. Krasnovsky Jr., Laser-induced luminescence of singlet molecular oxygen. Generation by drugs and pigments of biological importance, *Proc. SPIE – Int. Soc. Opt. Eng.* 1990; 1403: 611–621.
97. Jakubowska M, Szczygieł M, Michalczyk- DW, Susz A, Stochel G, Elas M, Fiedor L, Urbanska K. Zinc-pheophorbide a—Highly efficient low-cost photosensitizer against human adenocarcinoma in cellular and animal models. *Photodiagnosis and Photodynamic Therapy* - 11 February 2013 (10.1016/j.pdpdt.2012.12.004) Article in press.
98. Pandey RK, Goswami LN, Chen Y, Gryshuk A, Missert JR, Oseroff A, Dougherty TJ, Nature: a rich source for developing multifunctional agents. Tumor-imaging and photodynamic therapy. *Lasers Surg Med.* 2006; 38:445-67.
99. Bellnier DA, Greco WR, Nava H, Loewen GM, Oseroff AR, Dougherty TJ, Mild skin photosensitivity in cancer patients following injection of Photochlor (2-[1-hexyloxyethyl]- 2-devinyl pyropheophorbide-a; HPPH) for photodynamic therapy. *Cancer Chemother Pharmacol.* 2006; 57:40-5.
100. Busch T, Cengel KA, Finlay J. Pheophorbide a as a photosensitizer in photodynamic therapy: in vivo considerations. *Cancer Biol Ther.* 2009 Mar 15;8(6):540-2.
101. You H, Yoon HE, Yoon JH, Ko H, Kim YC. Synthesis of pheophorbide-a conjugates with anticancer drugs as potential cancer diagnostic and therapeutic agents. *Bioorg Med Chem.* 2011; 19(18):5383-91.
102. Lijuan Jiao. Synthesis and functionalizations of tetrapyrrole derivatives. 2007, PhD Thesis, Louisiana State University, United States.
103. Juzeniene A. Chlorin e6-based photosensitizers for photodynamic therapy and photodiagnosis. *Photodiagnosis Photodyn Ther.* 2009; 6(2):94-6.
104. Tsukagoshi S, Development of a novel photosensitizer, talaporfin sodium, for the photodynamic therapy (PDT) *Gan To Kagaku Ryoho,* 2004; 31:979-85.

105. Stewart F, Baas P, Star W. What does photodynamic therapy have to offer radiation oncologists (or their cancer patients)? *Radiother Oncol.* 1998; 48(3):233-48.
106. Isakau HA, Trukhacheva TV, Petrov PT. Isolation and identification of impurities in chlorin e6. *J Pharm Biomed Anal* 2007; 45(1):20-9.
107. Abakumova OY, Baum RP, Ermakova NY, et al. Novel drug form of chlorin e6. *Proc SPIE* 1999;4059:130-8.
108. Moss RW. Patient responses to Cytoluminescent Therapy for cancer: an investigative report of early experiences and adverse effects of an unconventional form of photodynamic therapy. *Integr Cancer Ther* 2003; 2(4):371-89.
109. Uzdensky AB, Dergacheva OY, Zhavoronkova AA, Reshetnikov AV, Ponomarev GV. Photodynamic effect of novel chlorine e6 derivatives on a single nerve cell. *Life Sci* 2004; 74(17):2185-97.
110. Isakau HA, Parkhats MV, Knyukshto VN, Dzhagarov BM, Petrov EP, Petrov PT. Toward understanding the high PDT efficacy of chlorin e6-polyvinylpyrrolidone formulations: photophysical and molecular aspects of photosensitizer—polymer interaction in vitro. *J Photochem Photobiol B* 2008; 92(3):165-74.
111. Vargas FD, Yartsev Y, Marcano A, Lappa A. Photophysical properties of novel PDT photosensitizer Radachlorin in different media. *Ciencia (Maracaibo)* 2004; 12(1), 70.
112. <http://www.radapharma.ru/main> Internet Communication 2-6-2009.
113. <http://belmedpreparaty.com/product/anot.php?anotid=187> Internet Communication 29-5-2009.
114. <http://www.naturalhealthfoundation.com/medicines.php?langchange=ru> Internet Communication 29-5-2009.
115. Stranadko EP, Ponomarev GV, Mechkov VM, et al. The first experience of Photodithazine clinical application for photodynamic therapy of malignant tumors. *Proc SPIE* 2000; 3909:138-44.

116. E. Zenkevich, E. Sagun, V. Knyukshto, A. Shulga, A. Mironov, O. Efremova, R. Bonnett, S.P. Songca, M. Kassem, Photophysical and photochemical properties of potential porphyrin and chlorin photosensitizers for PDT, *J. Photochem. Photobiol. B.*, 1996; 33: 171–180.
117. J.K. Hooper, T.W. Sery, N. Yamamoto, Photodynamic sensitizers from chlorophyll: purpurin-18 and chlorin p6, *Photochem. Photobiol.* 1988; 48, 579–582.
118. Feofanov, A., A. Grichine, T. Karmakova, A. Pljutinskaya, V. Lebedeva, A. Filyasova, R. Yakubovskaya, A. Mironov, M. Egret-Charlier and P. Vigny Near-infrared photosensitizer on the basis of cycloimide derivative of chlorin p6: 13,15-N-(3'-hydroxypropyl)cycloimide chlorin p6. *Photochem. Photobiol.* (2002) 74, 633-643.
119. Grichine, A, A. Feofanov, T. Karmakova, N. Kazdchkina, E. Pecherskih, R. Yakubovskaya, A. Mironov, M. Egret-Charlier and P. Vigny. Influence of the substitution of 3-vinyl by 3-formyl group on the photodynamic properties of chlorin p6: molecular, cellular and in vivo studies. *Photochem. Photobiol.* 2001; 73:267-277.
120. Feofanov A, Sharonov G, Grichine A, Karmakova T, Pljutinskaya A, Lebedeva V, Ruziyev R, Yakubovskaya R, Mironov A, Refregier M, Maurizot JC, Vigny P. Comparative study of photodynamic properties of 13,15-N-cycloimide derivatives of chlorin p6. *Photochem Photobiol.* 2004; 79(2):172-88.
121. Michael W. Leach, Robert J. Higgins, James E. Boggan, Shwn-Ji Lee, Susan Autry, and Kevin M. Smith Effectiveness of a Lysyl Chlorin p6/Chlorin p6 Mixture in Photodynamic Therapy of the Subcutaneous 9L Glioma in the Rat. *cancer research* 1992; 52:1235-1239.
122. Datta, A. Dube, B. Jain, A. Tiwari, P.K. Gupta, The effect of pH and surfactant on aggregation behavior of chlorin p6: A fluorescence spectroscopic study, *Photochem. Photobiol.*, 2002; 75: 488–494.

123. Das, K Jain, B. A. Dube, P.K. Gupta, pH dependent binding of chlorin-p6 with phosphatidyl choline liposomes. *Chemical Physics Letters* 2005; 401: 185–188.
124. Sharma, M Dube, A. Bansal, H. Gupta, P.K. Effect of pH on uptake and photodynamic action of chlorin p6 on human colon and breast adenocarcinoma cell lines. *Photochem. Photobiol. Sci.* 2004; 3: 231-235.
125. Dube A, Sharma S, Gupta PK. Evaluation of chlorin p6 for photodynamic treatment of squamous cell carcinoma in the hamster cheek pouch model. *Oral Oncol* 2006; 42(1):77–82.
126. Dube A, Sharma S, Gupta PK. Tumor regression induced by photodynamic treatment with chlorin p6 in hamster cheek pouch model of oral carcinogenesis: Dependence of mode of tumor cell death on the applied drug dose. *Oral Oncol.* 2011; 47: 467–471.
127. James T.C. Wojtyk, Rebecca Goyan, Eva Gudgin-Dickson, Roy Pottier. Exploiting tumour biology to develop novel drug delivery strategies for PDT. *Medical Laser Application* 2006; 21: 225–238
128. Hudson, R and Boyle, RW. Strategies for selective delivery of photodynamic sensitizers to biological targets, *J. Porphyrins Phthalocyanines*, 2004; 8: 954–975.
129. Richter,A.M. Waterfield, E. Jain, A.K. Canaan, J Allison, B.A. and Levy,J.G. Liposomal, delivery of a photosensitizer, benzoporphyrin derivative monoacid ring A (BPD), to tumor tissue in a mouse tumor model, *Photochem. Photobiol.*, 1993; 57:1000–1006.
130. Kurohane, K. Tominaga, Sato, A.K. North, J.R. Namba, Y and Oku, N. Photodynamic therapy targeted to tumor-induced angiogenic vessels, *Cancer Lett.*, 2001; 167: 49–56.
131. Allemann, E. Rousseau, Brasseur, J.N. Kudrevich, S.V. Lewis, K. and van Lier, J.E. Photodynamic therapy of tumours with hexadecafluoro zinc phthalocynine formulated in PEG-coated poly(lactic acid) nanoparticles, *Int. J. Cancer*, 1996; 66: 821–824.

132. Swamy, N. James, D.A. Mohr, S.C. Hanson, R.N. and Ray, R. An estradiol-porphyrin conjugate selectively localizes into estrogen receptor-positive breast cancer cells, *Bioorg. Med. Chem.*, 2002; 10: 3237–3243.
133. Damle NK, Frost P. Antibody-targeted chemotherapy with immunoconjugates of calicheamicin. *Curr Opin Pharmacol* 2003; 3:386–90.
134. Kosmas C, Linardou H, Epenetos AA. Review: advances in monoclonal antibody tumour targeting. *J Drug Target* 1993; 1:81–91.
135. Pietersz GA, Krauer K. Antibody-targeted drugs for the therapy of cancer. *J Drug Target* 1994; 2:183–215.
136. Mew D., Wat C., Towers G. & Levy J. Photoimmunotherapy: treatment of animal tumors with tumor-specific monoclonal antibody-hematoporphyrin conjugates. *J. Immunol*, 1983; 130:1473-1477.
137. Mew D, Lum V, Wat CK, Towers GH, Sun CH, Walter RJ, Wright W, Berns MW, Levy JG. Ability of specific monoclonal antibodies and conventional antisera conjugated to hematoporphyrin to label and kill selected cell lines subsequent to light activation. *Cancer Res.* 1985; 45: 4380-6.
138. Savellano M. D. & Hasan T. Targeting Cells That Overexpress the Epidermal Growth Factor Receptor with Polyethylene Glycolated BPD Verteporfin Photosensitizer Immunoconjugates. *Photochem. Photobiol.* 2003; 77: 431-439.
139. Savellano MD, Hasan T. Photochemical targeting of epidermal growth factor receptor: a mechanistic study. *Clin Cancer Res.* 2005; 11: 1658-68.
140. Hemming AW, Davis NL, Dubois B, Quenville NF, Finley RJ. Photodynamic therapy of squamous cell carcinoma. An evaluation of a new photosensitizing agent, benzoporphyrin derivative and new photoimmunoconjugate. *Surg Oncol.*1993; 2:187-96.
141. Oseroff AR, Ohuoha D, Hasan T, Bommer JC, Yarmush ML. Antibodytargeted photolysis: selective photodestruction of human T-cell leukemia cells using monoclonal antibody-chlorin e6 conjugates. *Proc Natl Acad Sci USA* 1986; 83: 8744-8

142. Soukos NS, Hamblin MR, Keel S, Fabian RL, Deutsch TF, Hasan T. Epidermal growth factor receptor-targeted immunophotodiagnosis and photoimmunotherapy of oral precancer in vivo. *Cancer Res.* 2001; 61: 4490-6
143. Hamblin M. R., Miller J. L. & Hasan T. Effect of Charge on the Interaction of site-specific photoimmunoconjugates with human ovarian cancer cells. *Cancer Res.* 1996; 56: 5205-5210.
144. Yarmush ML, Thorpe WP, Strong L, Rakestraw SL, Toner M, Tompkins RG (1993) *Crit. Rev. Ther. Drug Carriers.* 1993; 10: 197-252. Antibody-targeted photolysis.
145. Savellano M. D., Pogue B. W., Hoopes P. J., Vitetta E. S. & Paulsen K. D. (2005). Multiepitope HER2 Targeting Enhances Photoimmunotherapy of HER2-Overexpressing Cancer Cells with Pyropheophorbide-a Immunoconjugates. *Cancer Res.* 2005; 65: 6371-6379.
146. Serebrovskaya EO, Edelweiss EF, Stremovskiy OA, Lukyanov KA, Chudakov DM, Deyev SM (2009). Targeting cancer cells by using an antireceptor antibody photosensitizer fusion protein. *Proc Natl Acad Sci USA.* 2009; 106: 9221-5.
147. Hudson R, Carcenac M, Smith K, Madden L, Clarke OJ, Pelegrin A, et al. The development and characterization of porphyrin isothiocyanate-mono-clonal antibody conjugates for photoimmunotherapy. *Br J Cancer* 2005; 92:1442-9.
148. Duan WB, Smith KA, Savoie H, Greenman J, Boyle RW. Near IR emitting isothiocyanato-substituted fluorophores: their synthesis and bioconjugation to monoclonal antibodies. *Org Biomol Chem.* 2005; 3: 2384-2386.
149. Morgan J, Lottman H, Abbou C, Chopin DK. Comparison of direct and liposomal antibody conjugates of sulfonated aluminum phthalocyanines for selective photoimmunotherapy of human bladder-carcinoma. *Photochem Photobiol.* 1994; 60: 486-496.

150. Birchler M, Viti F, Zardi L, Spiess B, Neri D (1999). Selective targeting and photocoagulation of ocular angiogenesis mediated by a phage-derived human antibody fragment. *Nat Biotechnol.* 1999; 17: 984-8.
151. Fabbrini M., Trachsel E., Soldani P., Bindi S., Alessi P., Bracci L., Kosmehl H., Zardi L., Neri D. & Neri P. (2006). Selective occlusion of tumor blood vessels by targeted delivery of an antibody-photosensitizer conjugate. *Int. J. Cancer*, 2006; 118: 1805-1813.
152. Vrouenraets, M. B. Visser, G.M.W. and Loup, C. et al., Targeting of a hydrophilic photosensitizer by use of internalizing monoclonal antibodies: a new possibility for use in photodynamic therapy, *Int. J.Cancer*, 2000; 8: 108–114.
153. Bhatti, M. Yahiolu, G. Milgrom, L.R. Garcia-Maya, M. Chester, K.A. and Deonarain, M. P. Targeted photodynamic therapy with multiply-loaded recombinant antibody fragments, *Int. J. Cancer*, 2007; 122: 1155–1163.
154. Jiang FN, Jiang S, Liu D, Richter A, Levy JG. Development of technology for linking photosensitizers to a model monoclonal antibody. *J Immunol Methods* 1990; 134:139–49.
155. Krinick NL. Soluble polymers as targetable drug carriers. In: Juliano RL, editor. *Targeted drug delivery*. Berlin: Springer; 1991; () : 105–66.
156. Illum L, Jones PD. Attachment of monoclonal antibodies to microspheres. *Methods Enzymol* 1985; 112:67–84.
157. Cobb PW, LeMaistre CF. Therapeutic use of immunotoxins. *Semin Hematol* 1992;29:6–13.
158. Oldham RK. Monoclonal antibodies in cancer therapy. *J Clin Oncol* 1983; 1:582–90.
159. Moolten FL, Schreiber BM, Zajdel SH. Antibodies conjugated to potent cytotoxins as specific antitumour agents. *Immunol Rev* 1982; 62:47–73.
160. Jain RK. Physiological barriers to delivery of monoclonal antibodies and other macromolecules in tumours. *Cancer Res* 1990; 50:814-9.
161. Jain RK. Delivery of molecular and cellular medicine to solid tumours. *J Control Release* 1998; 53:49–67.

162. Sharman WM, van Lier JE, Allen CM., Targeted photodynamic therapy via receptor mediated delivery systems. *Adv Drug Delv Rev* 2004; 56:53-76
163. Chen B, Pogue BW, Hoopes PJ, Hasan T (2006) Vascular and Cellular Targeting for Photodynamic Therapy. *Crit Rev Eukaryot Gene Expr* 2006; 16:279-305
164. Torchilin VP. Recent advances with liposomes as pharmaceutical carriers. *Nat Rev Drug Discov* 2005; 4:145–60.
165. Lombardi P, Norata G, Maggi FM, Canti G, Franco P, Nicolini A, et al. Assimilation of LDL by experimental tumours in mice. *Biochim Biophys Acta* 1989; 1003: 301–6.
166. West CM, West DC, Moore JV. Low-density lipoprotein uptake and the sensitivity to photodynamic treatment of cultured endothelial cells. *Int J Radiat Biol* 1991; 60:25–8.
167. Kongshaug M. Distribution of tetrapyrrole photosensitizers among human plasma proteins. *Int J Biochem* 1992; 34:1239–65.
168. Jori G, Beltramini E, Reddi B, Salvato A, Pagnan L, Ziron L, et al. Evidence for a major role of plasma lipoproteins as hematoporphyrin carriers in vivo. *Cancer Lett* 1987; 24: 291–7.
169. Polo L, Valduga G, Jori G, Reddi E. Low-density lipoprotein receptors in the uptake of tumour photosensitizers by human and rat transformed fibroblasts. *Int J Biochem Cell Biol.* 2002; 34(1):10-23.
170. Schmidt-Erfurth U, Diddens H, Birngruber R, Hasan T. Photodynamic targeting of human retinoblastoma cells using covalent low-density lipoprotein conjugates. *Br J Cancer.* 1997; 75(1):54-61.
171. Hopkinson, H.J. Vernon, D.I. and Brown, S.B. Identification and partial characterization of an unusual distribution of the photosensitizer meta-tetrahydroxyphenyl chlorin (temoporfin) in human plasma, *Photochem. Photobiol.*, 1999; 69: 482–488.
172. Laskin, J.J. and Sandler, A.B. Epidermal growth factor receptor: a promising target in solid tumours, *Cancer Treat. Rev.*, 2004; 30: 1–17.

173. Levitzki and S. Klein, Signal transduction therapy of cancer, *Mol. Aspects Med.*, 2010; 31: 287–329.
174. Lutsenko SV, Feldman NB, Finakova GV, Posypanova GA, Severin SE, Skryabin KG, Kirpichnikov MP, Lukyanets EA, Vorozhtsov GN. Targeting phthalocyanines to tumor cells using epidermal growth factor conjugates. *Tumour Biol.* 1999; 20: 218-224.
175. Gijssens A, De Witte P. Targeting of chlorine E6 by EGF increasing its photodynamic activity in selective ways. *Verh K Acad Geneesk Belg.* 2000; 62(4):329-52.
176. Gijssens A, Missiaen L, Merlevede W, de Witte P. Epidermal growth factor-mediated targeting of chlorin e6 selectively potentiates its photodynamic activity. *Cancer Res.* 2000; 15:60(8):2197-202.
177. Slastnikova TA, Rosenkranz AA, Gulak PV, Schiffelers RM, Lupanova TN, Khramtsov YV, Zalutsky MR, Sobolev AS. Modular nanotransporters: a multipurpose in vivo working platform for targeted drug delivery. *Int J Nanomedicine.* 2012; 7:467-82.
178. Leanne B. Josefsen and Ross W. Boyle. Unique Diagnostic and Therapeutic Roles of Porphyrins and Phthalocyanines in Photodynamic Therapy, Imaging and Theranostics. *Theranostics* 2012, 2(9) :916-966.
179. Goslinski T, Piskorz J. Fluorinated porphyrinoids and their biomedical applications. *J. Photochem Photobio C: Photochem Rev.* 2011; 12: 304-321.
180. Chen X, Hui L, Foster DA, Drain CM. Efficient synthesis and photodynamic activity of porphyrin-saccharide conjugates: targeting and incapacitating cancer cells. *Biochemistry.* 2004; 43: 10918-10929.
181. Hirohara S, Nishida M, Sharyo K, Obata M, Ando T, Tanihara M. Synthesis, photophysical properties and photocytotoxicity of mono-, di-, tri- and tetra-glucosylated fluorophenylporphyrins. *Bioorg Med Chem.* 2010; 18: 1526-1535.
182. Vedachalam S, Choi B-H, Pasunooti KK, Ching KM, Lee K, Yoon HS, Liu X-W. Glycosylated porphyrin derivatives and their photodynamic activity in cancer cells. *Med Chem Commun.* 2011; 2: 371-377.

183. Yang RY, Liu FT. Galectins in cell growth and apoptosis. *Cell Mol Life Sci* 2003;60:267–76.
184. Brewer CF, Miceli MC, Baum LG. Clusters, bundles, arrays and lattices: novel mechanisms for lectin–saccharide-mediated cellular interactions. *Curr Opin Struct Biol* 2002;12:616–23.
185. Rabinovich GA, Baum LG, Tinari N, Paganelli R, Natoli C, Liu FT, Iacobelli S. Galectins and their ligands: amplifiers, silencers or tuners of the inflammatory response? *Trends Immunol.* 2002; 23(6):313-20.
186. Riss D, Jin L, Qian X, Bayliss J, Scheithauer BW, Young WF Jr, Vidal S, Kovacs K, Raz A, Lloyd RV. Differential expression of galectin-3 in pituitary tumors. *Cancer Res.* 2003; 63(9):2251-5.
187. Rini JM. Lectin structure. *Annu Rev Biophys Biomol Struct* 1995; 24:551–77.
188. Fujimoto K, Miyata T, Aoyama Y. Saccharide-directed cell recognition and molecular delivery using macrocyclic saccharide clusters: masking of hydrophobicity to enhance the saccharide specificity. *J Am Chem Soc* 2000; 122:3558–9.
189. Garin-Chesa P, Campbell I, Saigo PE, Lewis Jr JL, Old LJ, Rettig WJ. Trophoblast and ovarian cancer antigen LK26. Sensitivity and specificity in immunopathology and molecular identification as a folate-binding protein. *Am J Pathol* 1993; 142:557–6.
190. Sudimack J, Lee RJ. Targeted drug delivery via the folate receptor. *Adv Drug Deliv Rev* 2000; 41:147–62.
191. Reddy JA, Low PS. Folate-mediated targeting of therapeutic and imaging agents to cancers. *Crit Rev Ther Drug Carrier Syst* 1998; 15:587–627.
192. Schneider R, Schmitt F, Frochot C, Fort Y, Lourette N, Guillemin F, Müller JF, Barberi-Heyob M. Design, synthesis, and biological evaluation of folic acid targeted tetraphenylporphyrin as novel photosensitizers for selective photodynamic therapy. *Bioorg Med Chem.* 2005; 13(8):2799-808.

193. Stevens, P.J. Sekido, M. and Lee, R.J. Synthesis and evaluation of a hematoporphyrin derivative in a folate receptor-targeted solid-lipid nanoparticle formulation, *Anticancer Res.*, 2004; 24: 161–166.
194. Stefflova K, Li H, Chen J, Zheng G. Peptide-based pharmacomodulation of a cancer-targeted optical imaging and photodynamic therapy agent. *Bioconjug Chem.* 2007; 18(2):379-88.
195. Syu WJ, Yu HP, Hsu CY, Rajan YC, Hsu YH, Chang YC, Hsieh WY, Wang CH, Lai PS. Improved photodynamic cancer treatment by folate-conjugated polymeric micelles in a KB xenografted animal model. *Small.* 2012; 8(13):2060-9.
196. García-Díaz M, Nonell S, Villanueva A, Stockert JC, Cañete M, Casadó A, Mora M, Sagristá ML. Do folate-receptor targeted liposomal photosensitizers enhance photodynamic therapy selectivity? *Biochim Biophys Acta.* 2011;1808(4):1063-71.
197. Tamara V. Akhlynina, Andrey A. Rosenkranz, David A. Jans, and Alexander S. Sobolev, Insulin-mediated Intracellular Targeting Enhances the Photodynamic Activity of Chlorin e6. *Cancer Research* 1995; 55: 1014-1019.
198. Derycke AS, Kamuhabwa A, Gijssens A, Roskams T, De Vos D, Kasran A, Huwyler J, Missiaen L, de Witte PA. Transferrin-conjugated liposome targeting of photosensitizer ALPcS4 to rat bladder carcinoma cells. *J Natl Cancer Inst.* 2004; 96(21):1620-30.
199. Gijssens, A. Derycke, A. Missiaen, L. De Vos, D. Huwyler, J. Eberle, A. and DeWitte, P. Targeting of the photocytotoxic compound ALPcS4 to HeLa cells by transferrin conjugated PEG-liposomes, *Int. J. Cancer*, 2002; 101: 78–85.
200. Derycke AS, De Witte PA. Transferrin-mediated targeting of hypericin embedded in sterically stabilized PEG-liposomes. *Int J Oncol.* 2002; 20(1):181-7.
201. Paszko E, Vaz GM, Ehrhardt C, Senge MO. Transferrin conjugation does not increase the efficiency of liposomal Foscan during in vitro

- photodynamic therapy of oesophageal cancer. *Eur J Pharm Sci.* 2013; 23;48(1-2):202-10.
202. Schneider E, Rolli-Derkinderen M, Arock M, Dy M. Trends in histamine research: new functions during immune responses and hematopoiesis. *Trends Immunol* 2002; 23:255-263
203. Bartholeyns J, Fozard JR. Role of histamine in tumor development. *Trends Pharmacol Sci* 1985; 6:123-125
204. Medina MA, Quesada AR, Núñez de Castro I, Sánchez-Jiménez F (1999) Histamine, polyamines, and cancer. *Biochem Pharmacol* 1999; 57:1341-1344.
205. Mitsuhashi M, Payan DG (1992) Functional diversity of histamine and histamine receptors. *J Invest Dermatol* 1992; 98:8S–11S
206. Leurs R, Traiffort E, Arrang JM, Tardivel-Lacombe J, Ruat M, Schwartz JC (1994) Guinea pig histamine H1 receptor: II. Stable expression in chinese hamster ovary cells reveals the interaction with three major signal transduction pathways. *J. Neurochem* 62:519–527
207. Del Valle J, Wang L, Gantz I, Yamada T (1992) Characterization of H2 histamine receptor: linkage to both adenylate cyclase and $[Ca^{2+}]_i$ signaling systems. *Am J Physiol* 263:G967–G972
208. Leurs R, Smit MJ, Timmerman H (1995) Molecular pharmacological aspects of histamine receptors. *Pharmacol Ther* 1995; 66:413–463
209. Del Valle J, Gantz I (1997) Novel insights into histamine H2 receptor biology. *Am J Physiol* 273:G987–G996.
210. Medina MA, Quesada AR, Nunez de Castro I, Sanchez-Jimenez F. Histamine, polyamines and cancer. *Biochem Pharmacol* 1999; 57:1341-44.
211. Pos Z, Hegyesi H, Rivera ES. Histamine and cell proliferation. In: Falus A, ed. *Histamine: biology and medical aspects*. Budapest, Hungary: SpringMed publishing, 2004:199-217
212. Rivera ES, Cricco GP, Engel NI, Fitzsimons CP, Martin GA, Bergoc RM. Histamine as an autocrine growth factor: an unusual role for a widespread mediator. *Semin Cancer Biol* 2000; 10:15-23.

213. Cricco G, Martín G, Medina V, Núñez M, Gutiérrez A, Cocca C, Bergoc R, Rivera E. Histamine regulates the MAPK pathway via the receptor in PANC-1 human cells. *Inflamm Res* 2004; 53:S65-6.
214. Medina V, Croci M, Crescenti E, Mohamad N, Sanchez-Jimenez F, Massari N, Nune M, Cricco G, Martin G, Bergoc R, Rivera E. The role of histamine in human mammary carcinogenesis:H3 and H4 receptors as potential therapeutic targets for breast cancer treatment. *Cancer Biol Ther* 2008; This issue.
215. Kahlson G, Rosengren E. New approaches to the physiology of histamine. *Annu Rev Physiol* 1965; 48:155-96.
216. Hegyesi H, Somlai B, Varga VL, Toth G, Kovacs P, Molnar EL, Laszlo V, Karpati S, Rivera E, Falus A, Darvas Z. Suppression of melanoma cell proliferation by histidine decarboxylase specific antisense oligonucleotides. *J Invest Dermatol.* 2001; 117(1):151-3.
217. Graff L, Frungieri M, Zanner R, Pohlinger A, Prinz C, Gratzl M. Expression of histidine decarboxylase and synthesis of histamine by human small cell lung carcinoma. *Am J Pathol* 2002; 160:1561-5.
218. Garcia-Caballero M, Neugebauer E, Rodriguez F, Nunez de Castro I, Vara-Thorbeck C. Histamine synthesis and content in benign and malignant breast tumours. Its effects on other host tissues. *Surg Oncol* 1994; 3:167-73.
219. Chanda R, Ganguly AK. Diamine-oxidase activity and tissue di- and poly-amine contents of human ovarian, cervical and endometrial carcinoma. *Cancer Lett* 2001; 89:23-8.
220. Garcia-Caballero M, Neugebauer E, Campos R, Nunez de Castro I, Vara-Thorbeck C. Increased histidine decarboxylase (HDC) activity in human colorectal cancer: results of a study on ten patients. *Agents Actions* 1988; 23:357-60.
221. Cianchi F, Vinci MC and Masini E. Histamine in cancer. *Cancer Biology & Therapy* 2008; 7(1), 36-37.
222. Nielsen HJ Histamine-2 receptor antagonists as immunomodulators: New therapeutic views? *Ann Med* 1996; 28:107–113

223. Hirohata M, Sasaguri Y, Shigemori M, Maruiwa H, Morimatsu M(1995) A role of histamine in human malignant glioma cells. *Int J Oncol* 7:1109–1115
224. Nielsen HJ, Kikuchi Y Histamine H₂-antagonists as potential adjuvant treatment of malignant disease, in *Histamine in Normal and Cancer Cell Proliferation, Advances in the Bioscience* (Garcia-Caballero M, Brandes L, Hosoda S, eds) 1993; pp. 319–334. Pergamon Press, Oxford
225. Burtin C, Noiro C, Scheinmann P, Gallopin L, Sabolovic D, Bernard P Clinical improvement in advanced cancer disease after treatment combining histamine and H₂-antihistaminics (ranitidine or cimetidine). *Eur J Cancer Clin Oncol* 1988;24:161–167
226. Adams WJ, Lawson JA and Morris DL: Cimetidine inhibits in vivo growth of human colon cancer and reverses histamine stimulated in vitro and in vivo growth. *Gut*. 1994; 35: 1632-1636.
227. Reynolds JL, Akhter J and Morris DL: In vitro effect of histamine and histamine H₁ and H₂RAs on cellular proliferation of human malignant melanoma cell lines. *Melanoma Res*. 1996; 6: 95-99.
228. Morris DL and Adams WJ: Cimetidine and colorectal cancer – old drug, new use? *Nat Med* 1995;1: 1243-1244.
229. Natori T, Sata M, Nagai R and Makuuchi M: Cimetidine inhibits angiogenesis and suppresses tumor growth. *Biomed Pharmacother*. 2005 59: 56-60.
230. Osband ME, Hamilton D, Shen YJ, Cohen E, Shlesinger M, Lavin P, Brown A and McCaffrey R: Successful tumour immunotherapy with cimetidine in mice. *Lancet* 1981;1: 636-638.
231. Hellstrand K and Hermodsson S: Histamine H₂-receptor-mediated regulation of human natural killer cell activity. *J Immunol* 1986;137:656-660.
232. Gifford RR and Tilberg AF: Histamine type-2 receptor antagonist immune modulation. II. Cimetidine and ranitidine increase interleukin-2 production. *Surgery* 1987; 102: 242-247.

233. Lefranc F, James S, Camby I, Gaussin JF, Darro F, Brotchi J, Gabius J and Kiss R: Combined cimetidine and temozolomide, compared with temozolomide alone: significant increases in survival in nude mice bearing U373 human glioblastoma multiforme orthotopic xenografts. *J Neurosurg* 2005;102: 706-714.
234. Kobayashi K, Matsumoto S, Morishima T, Kawabe T and Okamoto T: Cimetidine inhibits cancer cell adhesion to endothelial cells and prevents metastasis by blocking E-selectin expression. *Cancer Res* 2000;60: 3978-3984.
235. Pócs Z, Sáfrány G, Müller K, Tóth S, Falus A, Hegyesi H, Phenotypic profiling of engineered mouse melanomas with manipulated histamine production identifies histamine H₂ receptor and rho-C as histamine-regulated melanoma progression markers. *Cancer Res* 2005; 65:4458-4466
236. Medina VA, Rivera ES, Histamine receptors and cancer pharmacology. *Br J Pharmacol* 2010;161:755-767.
237. Szabó PM, Wiener Z, Tömböl Z, Kovács A, Pócza P, Horányi J, Kulka J, Riesz P, Tóth M, Patócs A, Gaillard RC, Falus A, Rácz K, Igaz P Differences in the expression of histamine-related genes and proteins in normal human adrenal cortex and adrenocortical tumors. *Virchows Arch* 2009; 455:133-142.
238. Vesuna and Raman, Histamine: A Potential Therapeutic Agent for Breast Cancer Treatment. *Cancer Biol Ther.* 2006; 5(11): 1472–1473
239. Kavekos M. Site specific therapy: An integrative approach to treating melanoma. *Medical Hypotheses* 2005;64:1097–1099.
240. Hooper JK, Sery TW, Yamamoto N, Photodynamic sensitizers from chlorophyll: purpurin-18 and chlorin p6. *Photochem Photobiol* 1988;48:579–582.
241. Lowry OH, Rosebrough NJ, Farr AL, Randall RJ. Protein measurement with the Folin phenol reagent. *J Biol Chem.* 1951; 193(1):265-75.
242. Mosman T, Rapid colorimetric assay for cellular growth and survival application and cytotoxicity assays. *J Immunol Methods.* 1983; 65:55–63

243. Kraljic I, El-Mohsni S, A new method for detection of singlet oxygen in aqueous solution, *Photochem. Photobiol.* 1978; 28: 577–581.
244. Levine RL, Williams J, Stadtman E.R., Shacter E, Carbonyl assays for determination of oxidatively modified proteins, *Method. Enzymol.* 1994;233: 346–357.
245. Placer ZA, Cushman LL, Johnson BC, Estimation of product of lipid peroxidation (malonyl dialdehyde) in biochemical systems, *Anal. Biochem.* 1966;16: 359–364.
246. Strobel HW, Dignam JD. Purification and properties of NADPH-cytochrome P-450 reductase. *Methods Enzymol.* 1978; 52:89-96.
247. Gupte MD, Ramachandran V, Mutatkar RK. Epidemiological profile of India: historical and contemporary perspectives. *J Biosci* 2001; 26:437–64.
248. Biel MA. Photodynamic Therapy Treatment of Early Oral and Laryngeal Cancers. *Photochem Photobiol.* 2007; 83:1063–1068
249. Soukos NS, Hamblin MR, Keel S, Fabian RL, Deutsch TF, Hasan T. Epidermal growth factor receptor-targeted immunophotodiagnosis and photoimmunotherapy of oral precancer in vivo. *Cancer Res.* 2001; 61:4490-4496.
250. Gupta S, Dwarakanath BS, Muralidhar K, Jain V, Cellular uptake, localization and photodynamic effects of haematoporphyrin derivative in human glioma and squamous carcinoma cell lines. *J Photochem Photobiol B Biol* 2003;69:107–120
251. Mulherkar R, Goud AP, Wagle AS, Naresh KN, Mahimkar MB, Thomas SM, Pradhan SA, Deo MG Establishment of a human squamous cell carcinoma cell line of the upper aero-digestive tract. *Cancer Lett* 1997;118:115-121.
252. Preuss H, Ghorai P, Kraus A, Dove S, Buschauer A, Seifert R. Constitutive activity and ligand selectivity of human, guinea pig, rat, and canine histamine H₂ receptors. *J Pharmacol Exp Ther.* 2007;321:983-995.
253. Van der Goot H, Timmerman H, Selective ligands as tools to study histamine receptors. *Eur J Med Chem* 2000;35:5–20

254. Osawa S, Kajimura M, Yamamoto S, Ikuma M, Mochizuki C, Iwasaki H, Hishida A, Terakawa S. Alteration of intracellular histamine H₂ receptor cycling precedes antagonist-induced upregulation. *Am J Physiol Gastrointest Liver Physiol*. 2005;289(5):G880-9.
255. Morissette G, Lodge R, Bouthillier J, Marceau F, Receptor-independent, vacuolar ATPase-mediated cellular uptake of histamine receptor-1 ligands: Possible origin of pharmacological distortions and side effects. *Toxicol App Pharmacol* 2008; 229:320–331.
256. Mojzisova H, Bonneau S, Vever-Bizet C, Brault D, Cellular uptake and subcellular distribution of chlorin e6 as functions of pH and interactions with membranes and lipoproteins. *Biochim Biophys Acta*. 2007; 1768:2748-56.
257. Ogasawara M, Yamauchi K, Satoh Y, Yamaji R, Inui K, Jonker J., Schinkel A, and Maeyama K, Recent Advances in Molecular Pharmacology of the Histamine Systems: Organic Cation Transporters as a Histamine Transporter and Histamine Metabolism. *J Pharmacol Sci* 2006;101: 24 – 30
258. Corbel S, Traiffort E, Stark H, Schunack W, Dy M, Binding of histamine H₃-receptor antagonists to hematopoietic progenitor cells - Evidence for a histamine transporter unrelated to histamine H₃ receptors. *FEBS Letters*, 1997;404:289-293
259. Schneider E , Machavoine F, Pléau J , Bertron A , Thurmond R , Ohtsu H , Watanabe T, . Schinkel A, and Dy M ,Organic cation transporter 3 modulates murine basophil functions by controlling intracellular histamine levels. *JEM* 2005;202:387-393.
260. Kessel, D, Determinants of photosensitization by mono-L-aspartyl Chlorin e6. *Photochemistry and Photobiology*, 1989;49: 447–452.
261. Csaba G, Kova'cs P, Perinuclear localization of biogenic amines (serotonin and histamine) in rat immune cells. *Cell Biol Int* 2006;30:861-865
262. Begum G, Dube A, Joshi PG, Gupta PK, Joshi NB, Chlorin p6 preferentially localizes in endoplasmic reticulum and Golgi apparatus and inhibits Ca²⁺ release from intracellular store. *J. Photochem Photobiol B Biol* 2009;95:177–184

263. Fernandez N, Monczor F, Baldi A, Davio C and Shayo C (2008), Histamine H2 Receptor Trafficking: Role of Arrestin, Dynamin, and Clathrin in Histamine H2 Receptor Internalization. *Mol Pharmacol* 2008; 74:1109–1118
264. Osawa S, Kajimura M, Yamamoto S, Ikuma M, Mochizuki C, Iwasaki H, Hishida A, and Terakawa S, Alteration of intracellular histamine H2 receptor cycling precedes antagonist-induced upregulation *Am J Physiol Gastrointest Liver Physiol* 2005; 289:G880-G889.
265. Jennifer A Koenig, Signal reception: G protein-coupled receptors, in *Molecular Biology of neurons*, second edition (eds: R.Wayne Davies and Brian J.Morris), 2004; pp-237 ISBN 0-19-850998-(Hbk)
266. LaBella S. F and Brandes J. L (2000), Interaction of histamine and other bioamines with cytochromes P450: implications for cell growth modulation and chemopotentialization by drugs. *Semin Cancer Biol*, 10: 47–53
267. Plaetzer K, Kiesslich T, Verwanger T, Krammer B (2003) The Modes of Cell Death Induced by PDT: An Overview. *Med Laser Appl* 18:7–19
268. Burns TF, El-Deiry WS (1999) The p53 pathway and apoptosis, *J Cell Physiol* 181:231–239
269. Sax JK, El-Deiry WS (2003) p53 downstream targets and chemosensitivity, *Cell Death Differ* 10:413–417
270. Plaetzer K, Krammer B, Berlanda J, Berr F, Kiesslich T. Photophysics and photochemistry of photodynamic therapy: fundamental aspects. *Lasers Med Sci.* 2009, 24:259-68.
271. Mojzisova H, Bonneau S, Brault D. Structural and physico-chemical determinants of the interactions of macrocyclic photosensitizers with cells. *Eur Biophys J.* 2007, 36:943-953.
272. Buytaert E, Dewaele M, Agostinis P. Molecular effectors of multiple cell death pathways initiated by photodynamic therapy. *Biochim Biophys Acta.* 2007, 1776:86-107.
273. Moor AC. Signaling pathways in cell death and survival after photodynamic therapy. *J Photochem Photobiol B.* 2000, 57:1-13.

274. Malik Z, Faraggi A, Savion N. Ultrastructural damage in photosensitized endothelial cells: dependence on hematoporphyrin delivery pathways. *J Photochem Photobiol B. Biol.* 1992, 14:359-368.
275. Hsieh YJ, Wu CC, Chang CJ, Yu JS. Subcellular localization of Photofrin determines the death phenotype of human epidermoid carcinoma A431 cells triggered by photodynamic therapy: when plasma membranes are the main targets. *J Cell Physiol.* 2003, 194:363-375.
276. Nazarova A, Ignatova A, Feofanov A, Karmakova T, Pljutinskaya A, Mass O, Grin M, Yakubovskaya R, Mironov A, Maurizot JC. 13,15-N-cycloimide derivatives of chlorin p6 with isonicotinyl substituent are photosensitizers targeted to lysosomes. *Photochem Photobiol Sci.*, 2007, 6:1184-1196.
277. Tamietti BF, Machado AH, Maftoum-Costa M, Da Silva NS, Tedesco AC, Pacheco-Soares C. Analysis of mitochondrial activity related to cell death after PDT with AIPCS(4). *Photomed Laser Surg.*, 2007, 25:175-179.
278. Hilf R. Mitochondria are targets of photodynamic therapy. *J Bioenerg Biomembr.* 2007 39:85-89.
279. Nagata S, Obana A, Gohto Y, Nakajima S. Necrotic and apoptotic cell death of human malignant melanoma cells following photodynamic therapy using an amphiphilic photosensitizer, ATX-S10(Na). *Lasers Surg Med.* 2003;33(1):64-70.
280. Ali-Seyed M, Bhuvanewari R, Soo KC, Olivo M. Photolon™-photosensitization induces apoptosis via ROS-mediated cross-talk between mitochondria and lysosomes. *Int J Oncol.* 2011, 39:821-831.
281. Mak NK, Li KM, Leung WN, Wong RN, Huang DP, Lung ML, Lau YK, Chang CK. Involvement of both endoplasmic reticulum and mitochondria in photokilling of nasopharyngeal carcinoma cells by the photosensitizer Zn-BC-AM. *Biochem Pharmacol.* 2004 Dec 15;68(12):2387-96.

282. Matroule JY, Carthy CM, Granville DJ, Jolois O, Hunt DW, Piette J. Mechanism of colon cancer cell apoptosis mediated by pyropheophorbide-a methylester photosensitization. *Oncogene*. 2001, 20:4070-4084.
283. Parihar A, Dube A, Gupta PK. Conjugation of chlorin p6 to histamine enhances its cellular uptake and phototoxicity in oral cancer cells. *Cancer Chemother Pharmacol.*, 2011, 68:359-369.
284. Fedorenko GM, Fedorenko YP, Fedorenko AG, Uzdensky AB. Dynamics of ultrastructural alterations in photosensitized crayfish glial and neuronal cells: Structures involved in transport processes and neuroglial interactions. *J Neurosci Res*. 2011, 89:341-351.
285. Leach MW, Higgins RJ, Autry SA, Boggan JE, Lee SJ, Smith KM. In vitro photodynamic effects of lysyl chlorin p6: cell survival, localization and ultrastructural changes. *Photochem Photobiol*. 1993, 58:653-660.
286. Weizman E, Rothmann C, Greenbaum L, Shainberg A, Adamek M, Ehrenberg B, Malik Z. Mitochondrial localization and photodamage during photodynamic therapy with tetraphenylporphines. *J Photochem Photobiol B*. 2000, 59:92-102.
287. C. Soldani, A. C. Croce, M. G. Bottone, A. Fraschini, M. Biggiogera, G Bottioli, C. Pellicciari Apoptosis in tumour cells photosensitized with Rose Bengal acetate is induced by multiple organelle photodamage. *Histochemistry and Cell Biology*, 2007, 128:485-495.
288. Strohmaier AR, Porwol T, Acker H, Spiess E. Three-dimensional organization of microtubules in tumor cells studied by confocal laser scanning microscopy and computer-assisted deconvolution and image reconstruction. *Cells Tissues Organs*. 2000;167(1):1-8.
289. Queisser G, Wittmann M, Bading H, Wittum G. Filtering, reconstruction, and measurement of the geometry of nuclei from hippocampal neurons based on confocal microscopy data. *J Biomed Opt.*, 2008, 13:014009.
290. Hamacher-Brady A, Brady NR, Logue SE, Sayen MR, Jinno M, Kirshenbaum LA, Gottlieb RA, Gustafsson AB. Response to myocardial

- ischemia/reperfusion injury involves Bnip3 and autophagy. *Cell Death Differ.*, 2007, 14:146-157.
291. Cortez BA, Machado-Santelli GM. Chrysotile effects on human lung cell carcinoma in culture: 3-D reconstruction and DNA quantification by image analysis. *BMC Cancer*. 2008, 8:181.
292. Mojzisova H, Bonneau S, Vever-Bizet C, Brault D. Cellular uptake and subcellular distribution of chlorin e6 as functions of pH and interactions with membranes and lipoproteins. *Biochim Biophys Acta.*, 2007, 1768:2748-2756.
293. English AR, Zurek N, Voeltz GK. Peripheral ER structure and function. *Curr Opin Cell Biol.*, 2009, 21:596-602.
294. Puhka M, Vihinen H, Joensuu M, Jokitalo E. Endoplasmic reticulum remains continuous and undergoes sheet-to-tubule transformation during cell division in mammalian cells. *J Cell Biol.*, 2007, 179:895-909.
295. Ferrari D, Pinton P, Campanella M, Callegari MG, Pizzirani C, Rimessi A, Di Virgilio F, Pozzan T, Rizzuto R. Functional and structural alterations in the endoplasmic reticulum and mitochondria during apoptosis triggered by C2-ceramide and CD95/APO-1/FAS receptor stimulation. *Biochem Biophys Res Commun.*, 2010, 391:575-581.
296. Pagano RE, Martin OC, Kang HC, Haugland RP. A novel fluorescent ceramide analogue for studying membrane traffic in animal cells: accumulation at the Golgi apparatus results in altered spectral properties of the sphingolipid precursor. *J. Cell Biol.*, 1991 113:1267-1279.
297. Koga D, Ushiki T. Three-dimensional ultrastructure of the Golgi apparatus in different cells: high-resolution scanning electron microscopy of osmium-macerated tissues. *Arch Histol Cytol.* 2006 Dec;69(5):357-74.
298. Ladinsky MS, Wu CC, McIntosh S, McIntosh JR, Howell KE. Structure of the Golgi and distribution of reporter molecules at 20 degrees C reveals the complexity of the exit compartments. *Mol Biol Cell.*, 2002, 13:2810-2825.

299. Nozawa K, Casiano CA, Hamel JC, Molinaro C, Fritzler MJ, Chan EK. Fragmentation of Golgi complex and Golgi autoantigens during apoptosis and necrosis. *Arthritis Res.* 2002, 4:R3.
300. Reiners JJ Jr, Caruso JA, Mathieu P, Chelladurai B, Yin XM, Kessel D. Release of cytochrome c and activation of pro-caspase-9 following lysosomal photodamage involves Bid cleavage. *Cell Death Differ.*, 2002, 9:934-944.
301. Moserova I, Kralova J. Role of ER stress response in photodynamic therapy: ROS generated in different subcellular compartments trigger diverse cell death pathways. *PLoS One.* 2012, 7:e32972.
302. Andrejevic S, Savary JF, Fontolliet C, Monnier P, van Den Bergh H. 7,12-dimethylbenz[a]anthracene-induced 'early' squamous cell carcinoma in the Golden Syrian hamster: evaluation of an animal model and comparison with 'early' forms of human squamous cell carcinoma in the upper aerodigestive tract. *Int J Exp Pathol.* 1996; 77:7-14.
303. Vairaktaris E, Spyridonidou S, Papakosta V, Vylliotis A, Lazaris A, Perrea D, Yapijakis C, Patsouris E. The hamster model of sequential oral oncogenesis. *Oral Oncol.* 2008; 44:315-24.
304. Soukos NS, Hamblin MR, Keel S, Fabian RL, Deutsch TF, Hasan T. Epidermal growth factor receptor-targeted immunophotodiagnosis and photoimmunotherapy of oral precancer in vivo. *Cancer Res.* 2001; 61:4490-4496.
305. Furukawa K, Yamamoto H, Crean DH, Kato H, Mang TS. Localization and treatment of transformed tissues using the photodynamic sensitizer 2-[1-hexyloxyethyl]-2 devinyl pyropheophorbide-a. *Lasers Surg Med.* 1996;18:157-166.
306. Andrejevic S, Savary JF, Monnier P, Fontolliet C, Braichotte D, Wagnières G, van den Bergh H. Measurements by fluorescence microscopy of the time-dependent distribution of meso-tetra-hydroxyphenylchlorin in healthy tissues and chemically induced "early" squamous cell carcinoma of

- the Syrian hamster cheek pouch. *J Photochem Photobiol B*. 1996; 36:143-151.
307. Mojzisova H, Bonneau S, Vever-Bizet C, Brault D. The pH-dependent distribution of the photosensitizer chlorin e6 among plasma proteins and membranes: a physico-chemical approach. *Biochim Biophys Acta*. 2007; 1768:366-374.
308. Mojzisova H, Bonneau S, Brault D. Structural and physico-chemical determinants of the interactions of macrocyclic photosensitizers with cells. *Eur Biophys J*. 2007; 36:943-953.
309. Lurie A, Tatematsu M, Nakatsuka T, Rippey R, Ito N (1983) Anatomical and functional vascular changes in hamster cheek pouch during carcinogenesis induced by 7,12-dimethylbenz(a)anthracene. *Cancer Res*. 1983; 43:5986-5994.
310. Parihar A, Dube A, Gupta PK.. Photodynamic treatment of oral squamous cell carcinoma in hamster cheek pouch model using chlorin p6-histamine conjugate. *Photodiagnosis and Photodynamic Therapy*, 2013, 10:79-86.
311. Cunderlíková B, Gangeskar L, Moan J. Acid-base properties of chlorin e6: relation to cellular uptake. *J Photochem Photobiol B*. 1999 53:81-90.
312. Mojzisova H, Bonneau S, Vever-Bizet C, Brault D. The pH-dependent distribution of the photosensitizer chlorin e6 among plasma proteins and membranes: a physico-chemical approach. *Biochim Biophys Acta*. 2007; 1768:366-374.
313. Mojzisova H, Bonneau S, Brault D. Structural and physico-chemical determinants of the interactions of macrocyclic photosensitizers with cells. *Eur Biophys J*. 2007; 36:943-953.
314. Lewis DF. Quantitative structure-activity relationships (QSARs) for substrates of human cytochromes P450 CYP2 family enzymes. *Toxicol In Vitro*. 2004 Feb;18(1):89-97.
315. Chatterjee SR, Srivastava TS, Kamat JP, Devasagayam TP. Lipid peroxidation induced by meso-tetrakis[3,4-

- bis(carboxymethyleneoxy)phenyl] porphyrin on photosensitization in hepatic and tumor microsomes. *Chem Biol Interact.* 1997 Dec 12;108(1-2):27-37.
316. Bronshtein I, Afri M, Weitman H, Frimer AA, Smith KM, Ehrenberg B. Porphyrin depth in lipid bilayers as determined by iodide and parallax fluorescence quenching methods and its effect on photosensitizing efficiency. *Biophys J.* 2004 Aug;87(2):1155-64.
317. Ben Dror S, Bronshtein I, Weitman H, Smith KM, O'Neal WG, Jacobi PA, Ehrenberg B. The binding of analogs of porphyrins and chlorins with elongated side chains to albumin. *Eur Biophys J.* 2009 Sep;38(7):847-55.
318. Kongshaug M. Distribution of tetrapyrrole photosensitizers among human plasma proteins. *Int J Biochem.* 1992 Aug;24(8):1239-65.
319. Ben Dror S, Bronshtein I, Weitman H, Smith KM, O'Neal WG, Jacobi PA, Ehrenberg B. The binding of analogs of porphyrins and chlorins with elongated side chains to albumin. *Eur Biophys J.* 2009 Sep;38(7):847-55.
320. D.K. Badyal, A.P. Dadhich, Cytochrome p450 and drug interactions. *Indian Journal of Pharmacology* 2001; 33: 248-259
321. Mojzisoava H, Bonneau S, Vever-Bizet C, Brault D. The pH-dependent distribution of the photosensitizer chlorin e6 among plasma proteins and membranes: a physico-chemical approach. *Biochim Biophys Acta.* 2007 Feb;1768(2):366-74.
322. Ackroyd R, Brown N, Vernon D, Roberts D, Stephenson T, Marcus S, Stoddard C, Reed M. 5-Aminolevulinic acid photosensitization of dysplastic Barrett's esophagus: a pharmacokinetic study. *Photochem Photobiol.* 1999, 70:656-662.
323. Williams M, Van der Zee J, Van Steveninck J. Toxic dark effects of protoporphyrin on the cytochrome P-450 system in rat liver microsomes. *Biochem J.* 1992 Nov 15;288 (Pt 1):155-9.
324. Rupert p. Austin, Patrick Barton, Scott L. Cockroft, Mark C. Wenlock, and Robert J. Riley. The influence of nonspecific microsomal binding on apparent intrinsic clearance, and its prediction from physicochemical properties. *Drug Metabolism and Disposition* 2002,30:1497–1503.

325. Bayburt TH, Sligar SG. Single-molecule height measurements on microsomal cytochrome P450 in nanometer-scale phospholipid bilayer disks. *Proc Natl Acad Sci U S A*. 2002 May 14;99(10):6725-30.
326. Vlad Cojocaru, Kia Balali-Mood, Mark S. P. Sansom, Rebecca C. Wade. Structure and Dynamics of the Membrane-Bound Cytochrome P450 2C9. *PLoS Computational Biology*, 2011, 7:e1002152.
327. Bose B, Dube A. Interaction of chlorin p6 with bovine serum albumin and photodynamic oxidation of protein. *J Photochem Photobiol B*. 2006 Oct 2;85(1):49-55. Epub 2006 Jun 9.
328. Baier J, Maier M, Engl R, Landthaler M, Bäuml W. Time-resolved investigations of singlet oxygen luminescence in water, in phosphatidylcholine, and in aqueous suspensions of phosphatidylcholine or HT29 cells. *J Phys Chem B*. 2005 Feb 24;109(7):3041-6.